Ecologically Based Systems Management (EBSM)

The Snake River - Palisades Dam to Henrys Fork

Final Report
U.S. Bureau of Reclamation
Boise, Idaho

by

F. Richard Hauer
Mark S. Lorang
Diane Whited
and
Phil Matson

Flathead Lake Biological Station[1]
The University of Montana
311 Bio Station Lane
Polson, MT 59860-9659

OPEN FILE REPORT
183-04

[1] Division of Biological Sciences
The University of Montana

April 15, 2004

Citation: Hauer, F. R., M. S. Lorang, D. Whited, and P.Matson. 2004. Ecologically Based Systems Management: the Snake River - Palisades Dam to Henrys Fork. Final Report to U.S Bureau of Reclamation, Boise, Idaho. Flathead Lake Biological Station, Division of Biological Sciences, The University of Montana, Polson, Montana. pp. 133.

INTRODUCTION

Policy Background

Major U.S. federal legislation governs the requirement that our freshwater ecosystems be restored where degraded and/or maintained to meet their designated use. For example, the objective of the Federal Clean Water Act (CWA) is…… "to restore and maintain the chemical, physical and biological integrity of the Nation's waters" [Sec. 101(a)]. The Interim Goal for Aquatic Life *(protection & propagation)* [Sec. 101(a)(2)] states; "It is the national goal that wherever attainable, an interim goal of water quality which provides for the protection and propagation of fish, shellfish and wildlife and recreation in and on the water..."

The U.S. Bureau of Reclamation (Reclamation) initiated a Snake River Resources Review (SR^3) in 1995 to "seek the best way to make decisions about operating the Snake River system while incorporating the many concerns, interests and voices dependent on the Snake River" and to "maintain the health of the Snake River without violating contractual obligations and state water law." The goal of SR^3 was to incorporate credible information into a decision support system (DSS) for use in system-wide trade-off analysis related to water management. After review of existing information, it was determined that the information was not sufficient to credibly determine the relationship between river flow and reservoir storage/elevations and aquatic resources.

In 2001, Reclamation sought assistance from Flathead Lake Biological Station (FLBS) in the development of concept, data acquisition, and management approach for a DSS that would meet the objectives of SR^3. Herein, we present an Ecologically Based System Management information and decision support system, which provides a link between system management and the ecological conditions on which aquatic resources depend. These data will be used to

inform system operations and may be used in responding to the Endangered Species Act, Clean Water Act, or other system operating constraints.

Study Rationale and the Importance of Floodplains

Reclamation and other federal, state, and tribal agencies have made, and will continue to make, very large financial and human resource investments in the restoration of rivers throughout the western USA. Historically, restoration has focused on fisheries as the most widely and easily recognized aquatic resource to be impacted by human induced stressors of river resources. Unfortunately, the history of river restoration, and indeed most ecological restoration both aquatic and terrestrial, is largely fraught with ineffectual attempts directed at the wrong spatial scale (see Kershner 1997). Indeed, efforts have typically been oriented toward site-specific projects with small spatial contexts (e.g., a few hundred meters of stream length) or with single, narrowly defined objectives confined to a specific species that may be threatened-endangered or of sport or commercial interest (e.g., bull trout, Ute Ladies Tress orchid). These strategies have generally not worked effectively, in part, because they do not integrate the full range of ecosystem scale structural variation or the ecological processes that are necessary to provide the range of life cycle, habitat, or physiological requirements of species dependant on natural river processes (e.g., fishes, aquatic food webs, riparian vegetation)s. Indeed, the nature of ecological problems in rivers that are regulated by dams, diversions and geomorphic change (as is the river in the study area of this report) are primarily manifest at ecosystem levels of organization requiring landscape scale solutions affecting riverine structure and function (Hauer et al. 2003).

In the research presented herein, we have focused our efforts on floodplain reaches along the longitudinal gradient of the Snake River immediately below Palisades Dam to the confluence with the Henrys Fork. We have taken this approach because large alluvial floodplains of gravel-bed rivers throughout the West are the focal points of biological complexity and productivity of both plants and animals. River scientists have known for over a decade that system organization and complexity is maximized on unconfined (i.e., floodplain) reaches compared to confined (i.e., canyon or geomorphically constrained) river reaches (Gregory et al. 1991, Stanford and Ward 1993). Under natural conditions, biodiversity and bioproduction are highest on the expansive floodplains for both aquatic and terrestrial biotic assemblages (Hutto and Young 2002, Pepin and Hauer 2002, Mouw and Alaback 2003, Harner and Stanford 2003). At multiple spatial and temporal scales the biophysical linkages that characterize the natural, high-function floodplains of the pre-settlement Snake River Basin were critical to the sustained and highly complex vegetation, fish, amphibian, bird and mammalian populations found throughout the basin in the early 1800's.

Although there are many competing interests for the water and aquatic resources of the Snake River that will likely continue to impinge on the ecological attributes of the system; ecological integrity (Karr and Chu 1989) as specified by the US Federal Clean Water Act sets the "benchmark" and thus the target condition for restoration. This is our goal in establishing the criteria needed for an operational Ecologically Based System Management.

The Shifting Habitat Mosaic - Hydrologic and Geomorphic Variation

The floodplains of the northern Rocky Mountains encompass a wide array of habitat types associated with the magnitude, frequency and duration of flooding. Floodplains may be

expansive or narrow. The porosity of these bed sediments in unconfined river reaches facilitates strong groundwater – surface water interactions and rapid exchange between the channel and the subsurface flow of river-derived water. This hyporheic (*hypo* = under; *rheic* = river) zone of gravel-bed sediment (Figure 1) has been shown to extend as much as 10m in depth and hundreds of meters laterally across expansive western floodplains (Stanford and Ward 1988). The habitats, both on the surface and within the substratum, shift from one place to another in a dynamic mosaic mediated by the interaction between flooding, the generation of stream power, and the supply of sediment. River floodplains are constantly modified by erosion deposition and channel avulsion processes. These fluvial geomorphic processes lead to the destruction of old habitats and the development of new habitats in a spatially and temporally dynamic fashion referred to as a Shifting Habitat Mosaic (Stanford et al. 2001). The SHM is composed of habitats, ecotones, and gradients that cycle nutrients and possess biotic distributions that experience change through the forces associated with fundamental fluvial processes. Features reflecting the legacy of cut and fill alluviation (e.g., flood channels, springbrooks, scour pools, oxbows, wetland rills) may be present on young (i.e., regularly scoured channels) to very old surfaces (i.e., abandoned flood channels among the various forest stands) (Figure 2).

Flooding, geomorphic change resulting from cut and fill alluviation, and subsequent succession of the floodplain vegetation, continually transform the SHM. Development and long-term successional patterns of riparian vegetation are determined, to a large degree, by the type and relative stability of the various floodplain surfaces. For example, the dynamics of cottonwood (*Populus spp.*) and willow (*Salix spp.*) reflect both the legacy of flooding and the frequent exposure of new surfaces of the SHM. Several studies from across western North America have revealed progressive declines in the extent and health of riparian cottonwood

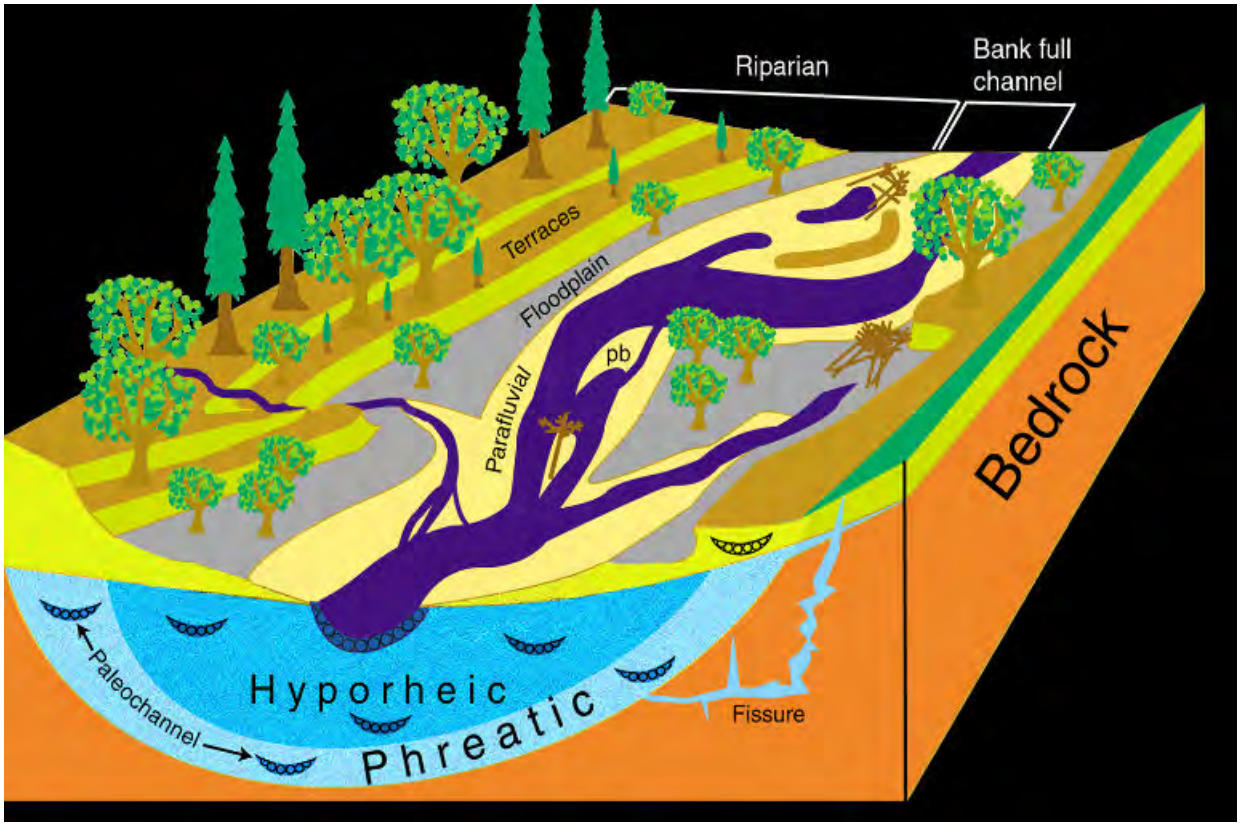

Figure 1. Three-dimensional illustration of gravel-bed river floodplains showing major surface features and the vertical and lateral extent of surface and ground water and spatial dimensions of the subsurface hyporheic zone (after Stanford 1998).

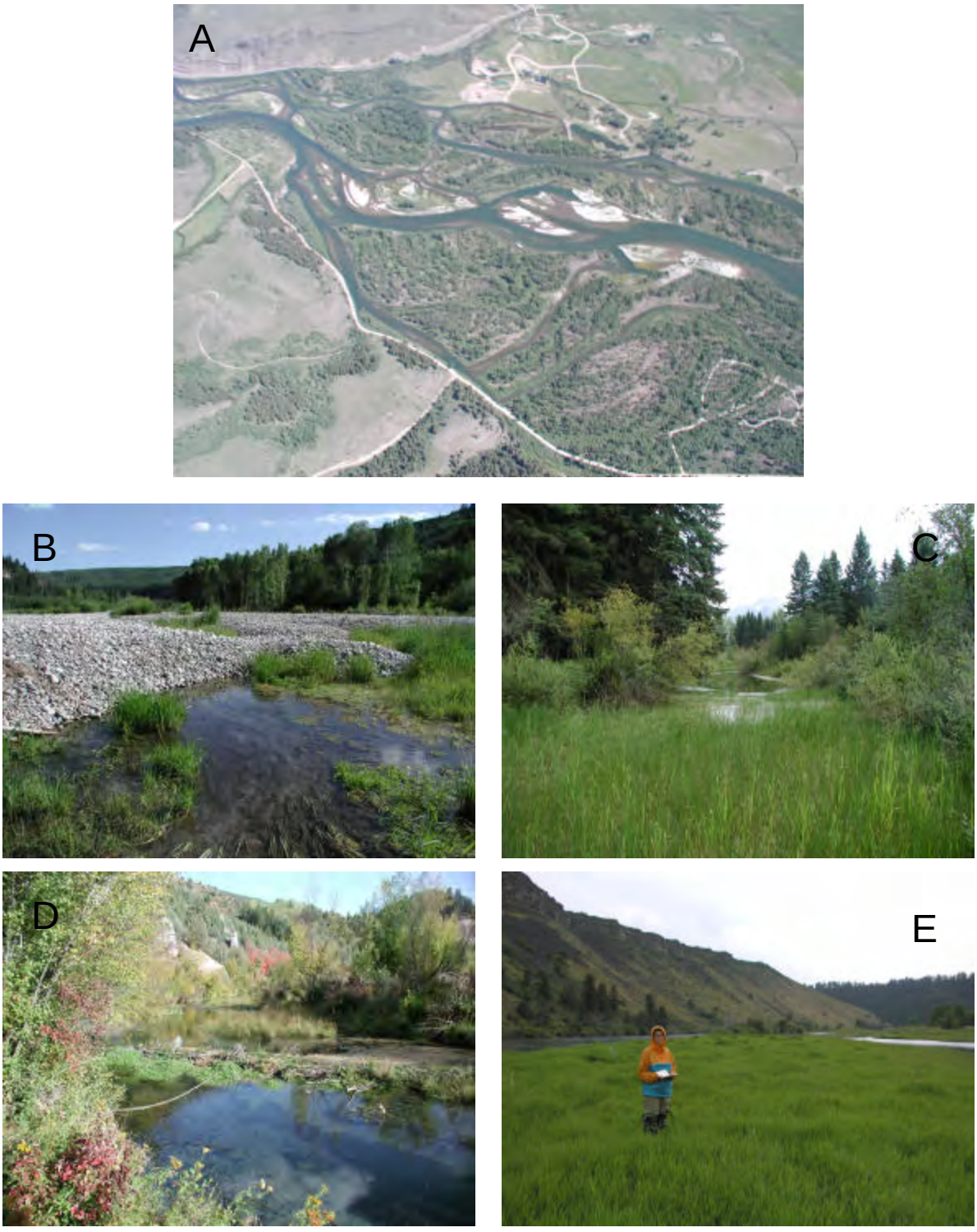

Figure 2. (A) aerial photo of the lower segment of the Swan Valley floodplain; (B) upwelling zone of groundwater through cobble bar; (C) is a backwater pond; (D) is a springbrook originating from hyporheic groundwater return flow; (E) is an island covered with vegetation.

ecosystems (Bradley et al. 1991, Braatne et al. 1996, Mahoney and Rood 1998, Rood et al. 1998). The primary causes of these declines have been impacts related to damming, water diversions and the clearing of floodplain habitats for agricultural use and livestock grazing (Braatne et al. 1996). Studies conducted in the 1990's on vegetation of the Snake River floodplains within our study area concluded that declines in riparian cottonwoods are related to the suppression of seedling recruitment (Merigliano 1996). Since cottonwoods are a relatively short-lived tree (100-200 years), declines in seedling recruitment over the past 50 years have lead to the widespread restructuring of the age structure of the communities to old individuals, which if left unchecked will eventually lead to loss of the riparian cottonwood ecosystems along the alluvial floodplain reaches of the Snake River in the study area.

Further examples of cut and fill alluviation and floodplain processes affecting the SHM is seen in the variation in thermal regime. While the change in temperature is particularly striking along the longitudinal gradient of a river (Hauer et al. 2000), there are surprising departures from this general pattern in which there may be extensive variation in temperature correlated with increased complexity of floodplain systems. Since the spatial dimension of the river landscape is three dimensional (see Figure 1 above), incorporating the river channel, surface riparian and hyporheic habitats into a river corridor as an integrated ecological unit, river floodplains are segments along the river corridor where not only is spatial complexity maximized; but also thermal complexity is maximized. This is very evident in comparing thermal regimes of the main channel with backwater or side channel habitats, but just as profound in its ecological implications in floodplain reaches affected by hyporheic return flows to the surface.

Recent study has shown that pond and springbrook habitats located on large river floodplains may have steep thermal gradients exceeding 10^{o}C over less than 2 m in vertical

strata. Thus, thermal complexity, associated with spatial complexity on large river floodplains, provide an increased abundance of riverine habitats and regimes (Stanford 1998). Thus, the hydrologic and geomorphic processes that so profoundly affect the easily observed habitat mosaic of surface features on the floodplain are equally influential upon a subsurface habitat mosaic.

The three principal concepts to grasp that underpin this work are: 1) that the Shifting Habitat Mosaic of river floodplains is spatially and temporally dynamic, 2) that the SHM is the essential template that supports the biodiversity, complexity and production of the river system, and 3) the SHM is sustainable only through geomorphic change which is driven by river hydraulics. In other words, the SHM is driven by a dynamic process that may be fast or slow and results in biotic responses that reflect the temporal and spatial heterogeneity that is a legacy of past geomorphic work and change. A fundamental feature of the SHM is that it principally functions at the landscape spatial scale and is profoundly influenced by the frequency and intensity of flooding and the ability of the river "to do work" through the processes of cut and fill alluviation. Finally, these three principle concepts are not solely affected in the Snake River study area by hydrologic patterns and regimes under the control of the Reclamation and Palisades Dam Operations. The US Army Corps of Engineers (CoE) also plays at least two very important roles that directly affect the SHM. a) The CoE is responsible for flood control throughout the Columbia River Basin and thus greatly influence dam withdrawal schedules during snowmelt, and b) through the Section 404 permitting and regulatory process affect floodplain levee and river bank hardening. Indeed, floodplains may be dramatically constrained by encroachment from levee systems that limit the extent of flooding and natural geomorphic processes.

Ecologically Based Systems Management – Research Objectives

The overarching objective of an Ecologically Based Systems Management information system is to provide managers with the fundamental knowledge and data necessary to engage the physical, biogeochemical, and biological components that result in the long term sustainability and ecological integrity of the river and the native flora and fauna. Within the context of these EBSM objectives, we organized the research to address a series of research questions. Questions were based on the literature, our experience in river ecology and understanding the Shifting Habitat Mosaic, and on how the SHM may be affected by regulation of river discharge by Palisades Dam Operations.

Specific questions addressed:

- What discharge volumes and regimes are necessary to produce sufficient power to realize cut and fill alluviation and sustain the geomorphic template of the SHM over time? Can these be achieved within the constraints of climatic water supply? Are these attainable and still meet the contractual obligations of the Reclamation and the Palisades project?
- What discharge regimes optimize the regeneration of cottonwood? Can these be achieved within the operational constraints of current operations? How might these be modified?
- What are the ranges of historic winter flows? How might these be coordinated with over-winter fish habitats to optimize native species?
- What discharge volumes and regimes are necessary during late summer and fall to sustain the regeneration of the cottonwood gallery forest and optimize variation of river habitats for the native fish and other aquatic species? Are these regimes attainable and still able to meet the contractual obligations of the Reclamation and the Palisades project?

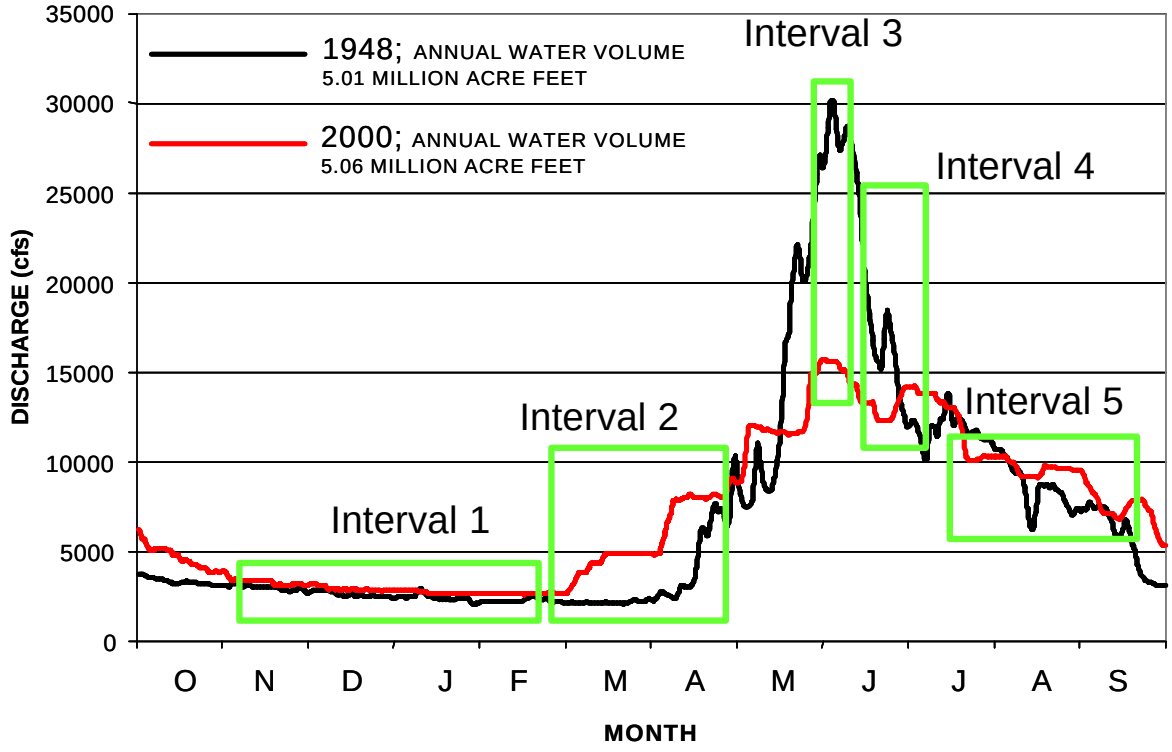

Figure 3. Two hydrographs of average water years over the period of record from 1911 to 2002. 1948 is representative of pre-dam hydrograph regime. 2000 is representative of post-dam hydrographic regime. Both years had approximately the same total water volume discharged from the Snake River at Heise. Temporal intervals 1-5 are explained in text.

Each of these research objectives and the questions that are derived above are illustrated here distributed across both a typical water year discharge regime from before and after Palisades dam construction and operations (Figure 3). The water years illustrated here are daily mean discharges for water years 1948 and 2000. (Note that in the US, water years begin on October 1 of the preceding year and end September 30 of the expressed year.)

There are five primary time intervals distributed throughout the water year that have very specific ecologically-based constraints. Interval 1 is directed toward winter flows and the habitats, particularly fish habitat that would favor native Yellowstone cutthroat trout over non-native rainbow trout or other non-natives. This issue also directly affects storage of water in Palisades reservoir. Interval 2 affects the initiation of spring snowmelt flows. In high discharge volume water years as illustrated in Figure 3, discharge has often been increased early in post-dam years to release stored water in Palisades reservoir in preparation of capturing the snowmelt and to reduce the risk of flooding. This directly affects aquatic habitats, fish life histories and the ability of fishes to physiologically respond to the increased discharge during a time interval that is not natural. Interval 3 is directed toward maximum discharges historically associated with spring snowmelt and the power that is generated by the river to do geomorphic work. We know that this is essential to the long term sustainability of the Shifting Habitat Mosaic and is a fundamental feature in the analysis below. Interval 4 affects the rate of the declining hydrograph after the spring snowmelt. The rate of the decline in the falling limb of the hydrograph (sometimes referred to as a ramping rate), directly affects the regeneration and sustainability of the cottonwood gallery forest. It also affects the rate of change in fish habitat. Interval 5 focuses on the summer flow duration, the rate of water table decline and also affects the contractual obligations and the operation of Palisades Dam and the supply of irrigation water.

STUDY AREA

Study Area Background

This study was conducted on the river reaches of the Upper Snake River between Palisades Dam in southeastern Idaho and the confluence of the Upper Snake with the Henry's Fork near Ririe ID (Figure 4). This river segment is referred to locally in eastern Idaho as the "South Fork". The Upper Snake River (6^{th} order), located in northwest Wyoming and southeastern Idaho, has a drainage basin of 5,810 mi^2 (15,048 km^2) above Lorenzo ID. The Upper Snake River regulation and diversion projects including Palisades Dam are collectively referred to as the Minidoka Project, which furnishes irrigation water to more than 1 million acres of lands from five reservoirs. With origin in Yellowstone National Park, the Upper Snake River flows south through Grand Teton National Park and Jackson Lake. A combined concrete gravity and zoned earth-fill dam regulate the outlet of Jackson Lake. A temporary dam was built in 1906 and reconstructed 1910-11. Jackson Lake Dam impounds approx. 624,400 acre feet (770 million m^3) and draws from a drainage area at the dam site of 1,824 mi^2 (4,724 km^2). The principle purposes of the dam are irrigation storage and flood control. The Snake River then flows approximately 110 km to Palisades Reservoir. The Palisades Dam was constructed at Calamity Point in eastern Idaho about 11 miles west of the Idaho-Wyoming state line. The dam provides a supplemental water supply to about 670,000 acres of irrigated land in the Minidoka and Michaud Flats Projects. The Snake River has a drainage basin at Palisades Dam of 5,150 mi^2 (13,338 km^2). The 176,600 kilowatt hydroelectric power plant furnishes energy to the Western US power grid, but the stated purpose of the power is to serve irrigation pumping units, municipalities, and

Figure 4, Study area showing geographic location in Idaho and the position of the six study floodplain distributed on the Snake River between Palisades dam and the confluence with the Henrys Fork.

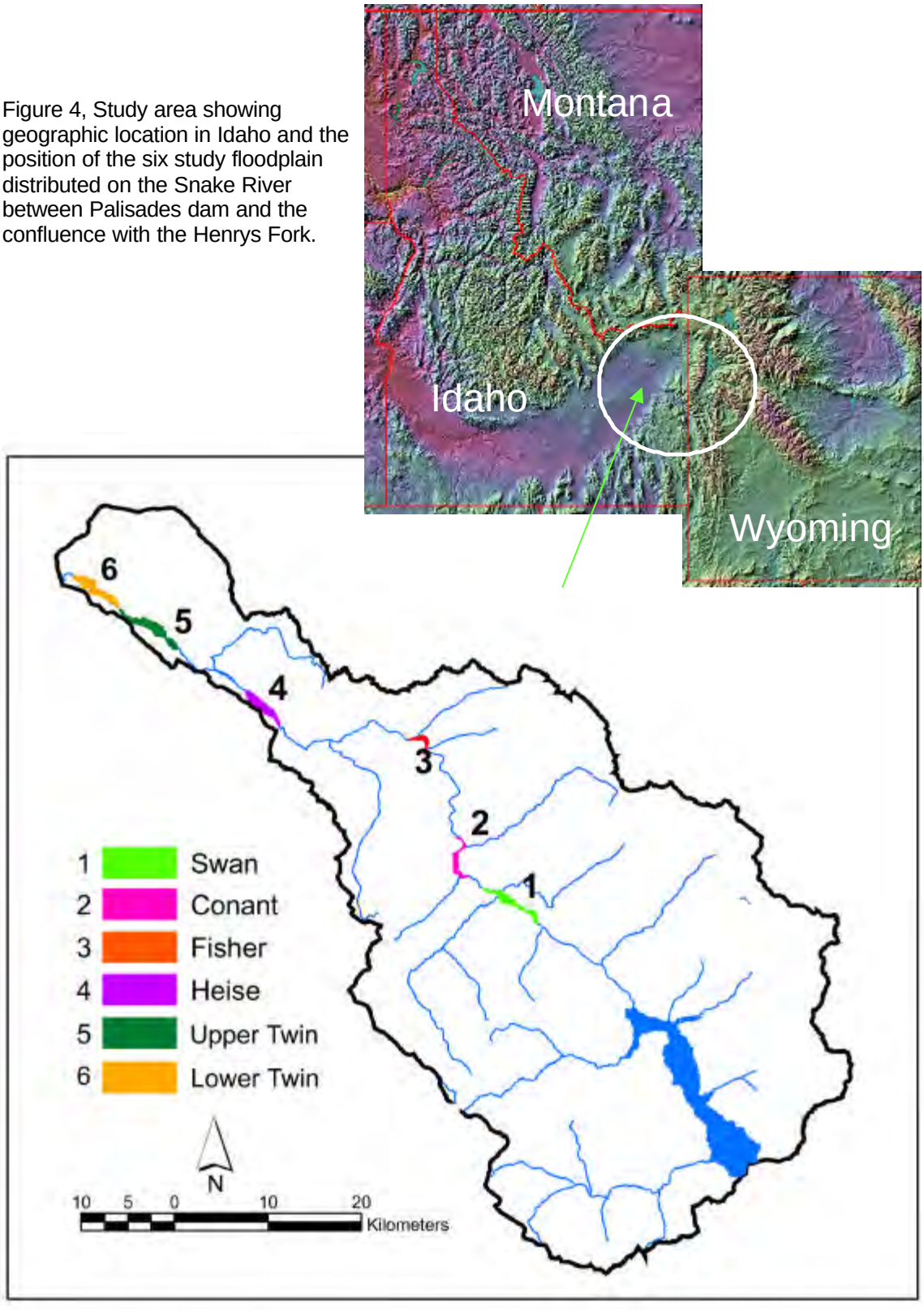

rural cooperatives in the project area. Power not needed for Reclamation project purposes is marketed in the Federal Southern Idaho Power System administered by the Bonneville Power Administration. The Upper Snake River drains the primarily montane landscape of western Wyoming and eastern Idaho. The river corridor is typical of the interior West, where the river sequentially alternates between confined and unconfined reaches.

The management of the public land below the Dam to Heise is primarily administered by the Bureau of Land Management (BLM) and US Forest Service (USFS). Management actions for these public lands are under the guidance of the Snake River Plan (BLM and USFS), the Medicine Lodge Resource Management Plan (BLM), and the Targhee Forest Management Plan (USFS).

The information on Palisades Dam and Reservoir provided here has been summarized from the Reclamation website http://dataweb.usbr.gov/html/palisades.html. Palisades Dam is a large zoned earth-fill structure 270 feet high and has a crest length of 2,100 feet. The spillway is a 28-foot-diameter tunnel through the left abutment, with a capacity of 48,500 cfs (1373.4 cms). The outlet works and power inlet structures are controlled by a fixed-wheel gate at the entrances of the inclined shafts leading to 26-foot-diameter tunnels. The outlet tunnel conveys the water to the steel manifold transition section, where it is released to the stilling basin by regulating gates. At the lower end of the power tunnel, the water may be released to the stilling basin or to four penstocks and conveyed to the turbines for power generation. The capacity of the outlet works is 33,000 cfs (934.5 cms). The dam creates a reservoir of 1,401,000 acre-feet capacity. The preconstruction phase of the Palisades Dam project was started early in 1945. Construction was delayed until the close of World War II. Actual construction of the project was initiated in 1951 and completed in 1957. The project was initially authorized by the Secretary of the Interior on

December 9, 1941, under the provisions of Section 9 of the Reclamation Project Act of August 4, 1939 (53 Stat. 1187, Public Law 76-260). Reauthorization of the project by the Congress occurred on September 30, 1950 (64 Stat. 1083, Public Law 81- 864), substantially in accordance with a supplemental report approved by the Secretary of the Interior on July 1, 1949. The authorized purposes of the Palisades Project are flood control, irrigation, power, and fish and wildlife habitat.

Palisades Dam provides holdover storage during years of average or above average precipitation for release in ensuing dry years to lands served by diversions from the river above Milner Diversion Dam. In 1994, the United States entered into a contract with Mitigation, Inc., which provided that entity with non-contracted irrigation storage space in Palisades (18,980 acre-feet) and Ririe (80,500 acre-feet) Reservoirs. This agreement was made in order to protect existing non-Indian water users from adverse effects that might result from implementation of the 1990 Fort Hall Indian Water Rights Agreement and Fort Hall Indian Water Rights Act of 1990 (104 Stat. 3061, Public Law 101-602). In 1991, the State of Wyoming entered into a contract with Reclamation for the purchase of 33,000 acre-feet of "joint use" space in Palisades Reservoir. All Palisades Reservoir spaceholder contracts provide: 1) for use of a proportionate share of the water accruing to the Palisades Reservoir water rights, 2) for keeping unused stored water for use in subsequent years, and 3) the option of participating in the Water District 1 Rental Pool. Wyoming also has the option of making exchanges to allow the use of their Palisades Reservoir space to retain water in Jackson Lake or to increase winter flows in the Snake River to benefit cutthroat trout. The Palisades Reservoir space also insures Wyoming's ability to fulfill Snake River Compact obligations. It is also important to recognize that the flow regimes throughout the Upper Snake are operationally interconnected. Thus, recommended

flows from Palisades will affect discharge regimes from Jackson Lake. However, those impacts have not been addressed through this effort. In contrast, such an effort is currently in progress on the river reaches between the Henrys Fork and American Falls Reservoir.

Study Area Floodplains

We identified six major floodplain reaches in the Snake River between Palisades Dam and the confluence with the Henrys Fork (Figure 4). These floodplains are referred throughout this report, beginning with the floodplain closest to the dam as: Swan, Conant, Fisher, Heise, Upper Twin and Lower Twin.

Within each of these floodplains there are several morphological and vegetative features that are important characteristics and will be referred to throughout this report. The near channel portion of the floodplain that is regularly inundated above base flow and is frequently scoured by the regular gravel and cobble-bed movement of the substratum is referred to as the Parafluvial. Next to the Parafluvial region of the channel-floodplain complex is that portion of the floodplain that may be regularly inundated, but generally there is insufficient power to scour the floodplain sediments. This region of the floodplain is characterized by riparian vegetation, particularly a mature or maturing gallery forest. This region is referred to as the Orthofluvial. Both the Parafluvial and the Orthofluvial contain a variety of aquatic habitats (e.g., springbrooks, ponds, inundation channels) that are a function of the legacy of past geomorphic processes on the floodplain.

METHODS

Hydrographic Regimes

We conducted a review and synthesis of hydrologic data of the Upper Snake River that was published as a technical report to the Reclamation, Boise, Idaho. This report titled: "Review and Synthesis of Riverine Databases and Ecological Studies in the Upper Snake River, Idaho" (Hauer et al 2002), provides important background data and analysis used in the interpretation of the data presented herein. We refer the reader to that report; however, we have included essential duplicative data here. We have also conducted additional analyses that are specific to the questions addressed in this report and play a significant role in the interpretations and recommendations appearing below.

The discharge data presented throughout this report are based on the daily discharge records obtained from the United States Geological Survey stream flow database for Idaho, http://id.water.usgs.gov/ and Wyoming, http://wy-water.usgs.gov/.

Temperature and Groundwater-Surface Water Interactions

Temperature data were obtained in selected regions of the Fisher floodplain to examine thermal variation and its distribution across unconfined river reaches that showed strong affinities for groundwater – surface water interactions. Temperature loggers were placed in hydrogeomorphic locations showing groundwater return to selected off-channel aquatic habitats. Loggers were placed in the study habitats and secured with iron rebar and plastic coated wire. Each logger collected temperature data ^{o}C at 2hr intervals from mid-August 2001 to mid November 2002.

Groundwater – surface water interactions on the Fisher floodplain were documented by placing piezometers into the floodplain substratum at various locations along the river gradient of the floodplain. Piezometers were installed using the methods described in Baxter et al. (2003) and were analyzed for vertical hydraulic gradient (VHG) which as a correlative measure of the piezometric surface and position of "upwelling" (+VHG) and "downwelling" (-VHG) zones on the floodplain.

Remotely Sensed Hyperspectral Data

Airborne remotely sensed data were collected with an AISA hyperspectral imagery system from Spectral Imaging, Oulu, Finland. The AISA system consists of a compact hyperspectral sensor head, miniature GPS/INS sensor, and system control and data acquisition unit. The AISA hyperspectral sensor is operated from the aircraft at the height (1000m) and speed (87kts) required to generate a 1x1m pixel resolution. Waveband configuration for digital data acquisition is from 256 individual spectral wavebands (400 to 950 nm) arrayed into 20 aggregate bands. The system also requires an aircraft top-mount of a real-time fiber-optic downwelling irradiance sensor (FODIS) that provides radiometric correction data for post-processing of surface reflectance. The GPS/INS is a Systron-Donner C-MIGITS III with Digital Quartz Inertial measurement unit (DQI) which tags each image line from the AISA sensor. The GPS coordinates are derived from 10 to 12 GPS satellites depending on satellite positions. The GPS data are linked with the inertial referencing of the C-MIGITS III to correct for pitch, roll and yaw of the aircraft during data acquisition. Data are stored during acquisition on a hot-swap removable U160 SCSI drive.

The remote sensing data were collected along predetermined flight lines oriented along the long axis of the study floodplains and having flight line overlaps of 40-50%. All data were collected within a time period of 1.5 hrs either side of solar noon. We selected the clearest days possible during a sampling interval spanning several weeks to capture flow and vegetation attributes that were targeted for the particular season and to maximize the quality of the imagery data.

Individual flight lines were cross-referenced with existing Digital Ortho Photo Quadrangles (DOQs) to examine the spatial positioning of each flight line. If an individual flight line needed further geo-rectification, then additional GCPs (ground control points) were added to improve the rectification in a given flight line. All geo-rectified flight lines had a mean RMS (root mean square) error of less than 4 meters (Table 1). The RMS error is an estimate of how close a given pixel is to its true location. Once all flight lines were geo-rectified for a given reach they were then stitched together to create a final mosaic. Minor color-balancing between flight lines were applied during the mosaiking process. All geo-rectification and mosaiking were completed in Erdas Imagine 8.5.

In addition to rectification errors, rapid turbulence experienced during data acquisition occasionally caused the aircraft to roll at a rate faster than the GPS/IMU data stream. Turbulence Induced Error (TIE) during image acquisition resulted in image distortion for some areas. These distortions were highly localized and appear as waves in the imagery. Rectification errors as well as errors caused by aircraft turbulence affect accuracy assessments causing portions of the image to be spatially offset from the true location. Rectification errors are inherent in virtually all remotely sensed data. The rectification errors we encountered represent variation generally less than 5% for all reaches.

Table 1. Mean RMS errors generated for each reach. The RMS error provides an estimate of how far off a given pixel is from its true location.

	Mean RMS error
Swan	3.3
Conant	3.8
Fisher	3.3
Heise	3
Twin	2.8

Water Depth and Velocity Ground-truth

A Sontek RS3000 Acoustic Doppler velocity-Profiler (ADP) was used to acquire detailed water depth and vertical profile measurements of flow velocity along channel reaches within the study floodplains. The ADP uses 3 transducers to generate a 3 MHz sound pulse into the water. As the sound travels through the water, it is reflected in all directions by particulate matter (e.g., sediment, biological matter) carried with the flow. The sonar signal is most strongly reflected from the bottom substrate providing a measure of water depth. Some portion of the reflected energy travels back toward the transducer where the processing electronics measure the change in frequency as a Doppler shift. The Doppler shift is correlated to the velocity of the water. The ADP operates using three transducers generating beams with different orientations relative to the flow of water. The velocity measured by each ADP transducer is along the axis of its acoustic beam. These beam velocities are converted to XYZ (Cartesian) velocities using the relative orientation of the acoustic beams, giving a 3-D velocity field relative to the orientation of the ADP. Since it is not always possible to control instrument orientation, the ADP includes an internal compass and tilt sensor to report 3-D velocity data in Earth (East-North-Up or ENU) coordinates, independent of instrument orientation. Hence, it is possible to determine the mean flow velocity in separate cells through the water column oriented perpendicular to the flow field.

By measuring the return signal at different times following the transmit pulse, the ADP measures water velocity at different distances from the transducer beginning just below the water surface and continuing to the bottom. The water velocity profile is measured and displayed as a series of separate 15 cm deep cells from top to bottom. Each recorded cell measurement is the average of several hundred measures over a 5 second time intervals.

We deployed the ADP from the front of a small jet-boat with both velocity profile data and depth data correlated spatially by linking a GPS (Global Positioning System) receiver co-located with the position of the ADP (Figure 5). During data acquisition the ADP was maneuvered back and forth across the channel to obtain data from as full an array of aquatic habitats, depths and velocities as possible. Both the ADP and GPS data were recorded simultaneously on a field laptop computer. The ADP data were then processed to create an integrated velocity value (average velocity for an individual ADP profile), as well as a depth value for each GPS location.

Four ADP surveys were collected in summer and fall of 2002 for each floodplain reach (June 20-22, August 17-20, September 24–26, November 25-26). The Heise reach was excluded from the November ADP survey due to technical difficulties with the ADP. The ADP data were obtained for base flow discharge at 1,500 cfs, and at discharges of 5,000, 8,000 and 11,500 cfs (Figure 6). Over 25,000 discrete measures of depth and flow velocity were recorded during the ADP surveys (Table 2).

Initial Depth and Velocity Classification

The integrated velocity and depth data from the ADP were combined with the September hyperspectral data for all reaches in a GIS to classify the variance in spectral reflectance of water

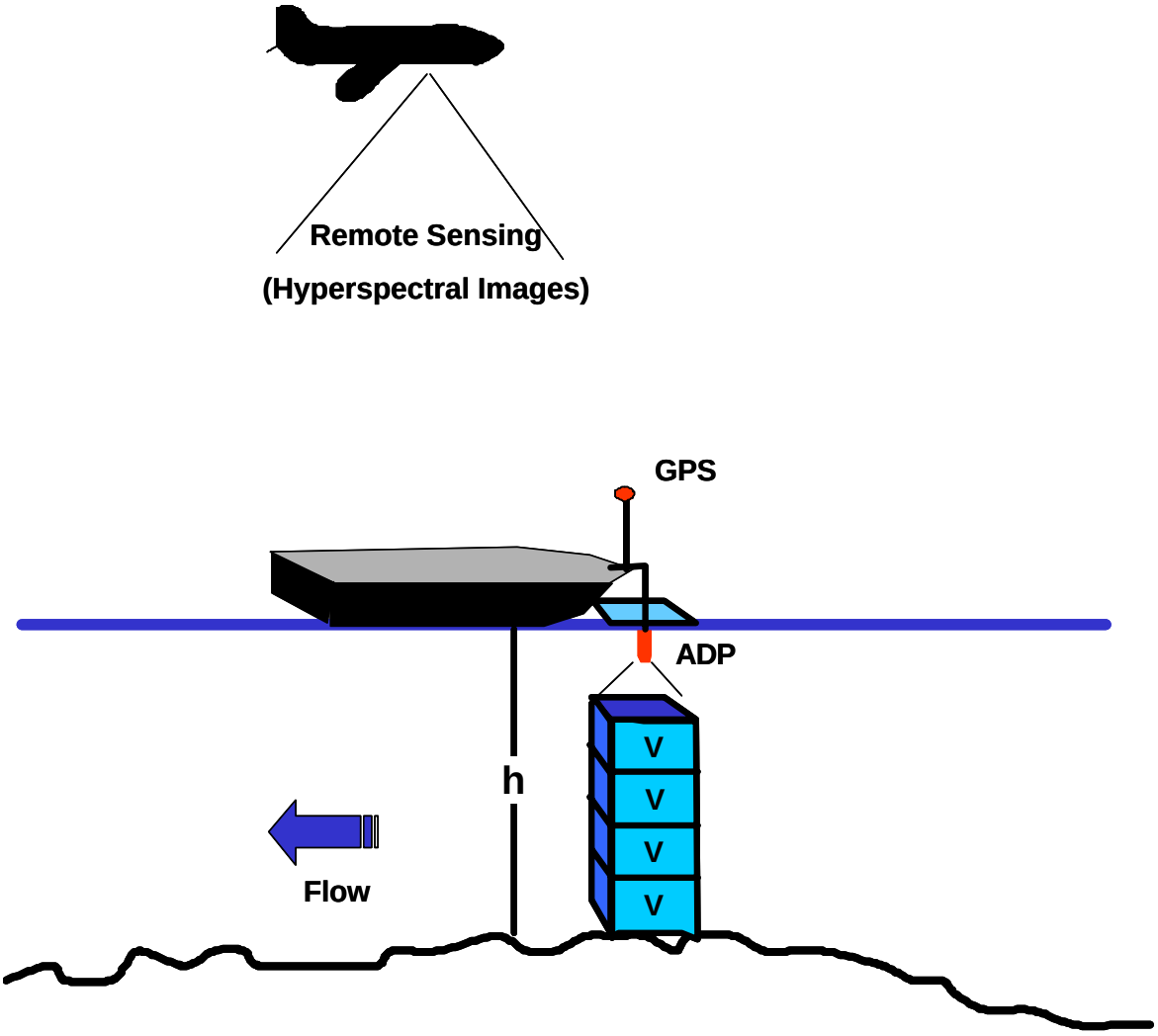

Figure 5. Illustration of linkage between remotely sensed hyperspectral data, which is geospatially explicit and the field data collection of depth (h) and velocity (V) using a boat mounted **A**coustic **D**oppler Velocity **P**rofiler (ADP) in conjunction with a Global Positioning System (GPS). All ADP data were GPS tagged to relate directly with the hyperspectral data.

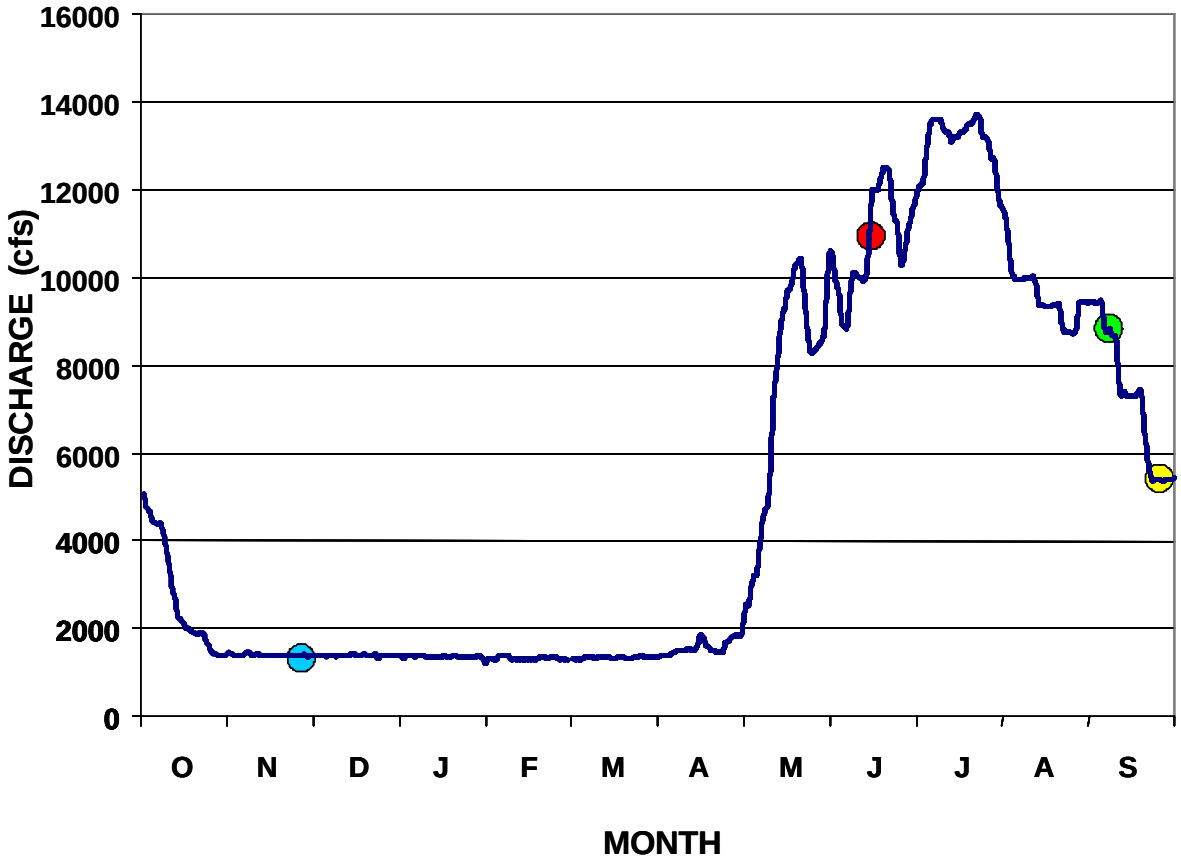

Figure 6. Annual hydrograph of Water Year 2002 illustrating the discharge and times of the year that ADP data were collected from the study floodplains of the Snake River .

Table 2. Total number of measures taken with the ADP of water depth and integrated flow velocities for each sample date shown in Figure 6.

Date	Total number of profiles
June 20 -22	8,654
August 17- 20	9,449
September 24 - 26	5,571
November 25-26	1,434
	25,108

depth and flow velocity. An unsupervised classification approach (ISODATA, Iterative Self-Ordering Data Analysis, Tou and Gonzalez 1977) was used to generate similar categories of spectral reflectance (Figure 7). Once an unsupervised classification of spectral reflectance was generated, the ADP data were distributed in the GIS environment to aggregate classes and assign unique depth and velocity categories. All reaches were classified into five depth categories (<0.5, 0.5 – 1, 1 – 1.5 , 1.5 – 2.0 , and > 2.0 m) and five velocity categories (< 0.5, 0.5 – 1.0, 1.0 – 1.5, 1.5 – 2, and > 2.0 m/s). These initial classifications of water depth and flow velocity (Figure 8) provided the basis for modeling depths and velocities at both higher and lower river stages. The ranges for each category were a function of the range of depths and flow velocity obtained with the ADP and the resolution that can be achieved from the hyperspectral imagery.

Two methods were used to assess the accuracy of the depth and velocity classifications. Traditionally, the accuracy of a classification is assessed by comparing the reference data (e.g., ADP survey data) with values on the classification map. This method is generally referred to as the 'pure' accuracy assessment. However, in spatial representations of continuous data (e.g., depth and velocity data) where sharp boundaries between classes rarely occur, it is preferable to apply a 'fuzzy' assessment of classification accuracy (Gopal and Woodcock 1994, Muller et al. 1998). The 'fuzzy' assessment allows determination of variance within the reference data and its departure from that classified in adjacent classes (i.e., one class above or one class below the depth or velocity classification being tested). Error matrices were generated for each floodplain, and include both the 'pure' and 'fuzzy' assessments (Table 3).

Some of the error between measured and classified depths and velocities are undoubtedly related to the rectification errors and the distortions discussed above caused by TIE, as well as error associated with the relative accuracy of the GPS. The accuracy of real time GPS data

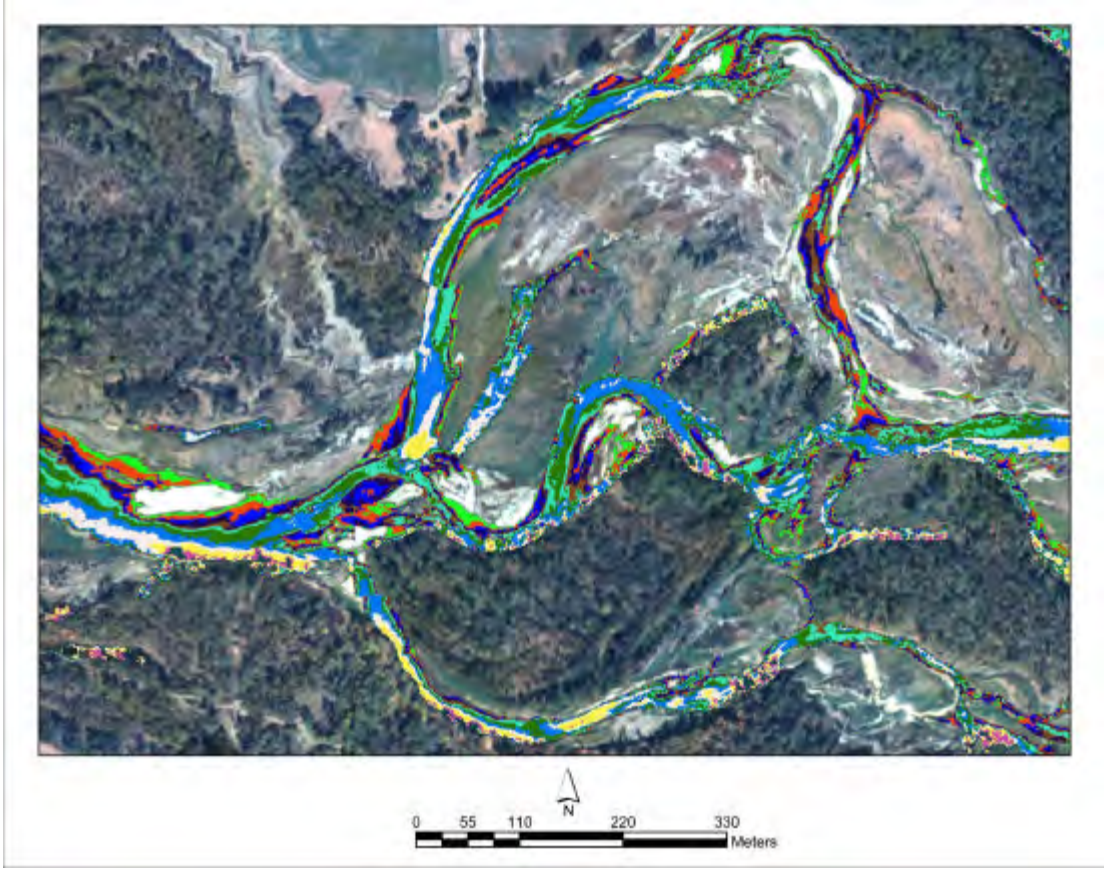

Figure 7. Unsupervised classification of hyperspectral data extracting spectral reflectance characteristics of water. These data illustrate the variation in spectral reflectance used to classify hydraulic characteristics.

Table 3. Accuracy assessment for all reaches at 5000 cfs; summarized as pure and fuzzy percentages.

	Depth		Velocity	
Flood Plain	**Pure(%)**	**Fuzzy(%)**	**Pure(%)**	**Fuzzy(%)**
Swan	60	97	33	74
Conant	53	89	43	85
Fisher	61	91	62	88
Heise	72	94	52	90
Twin	47	86	50	87

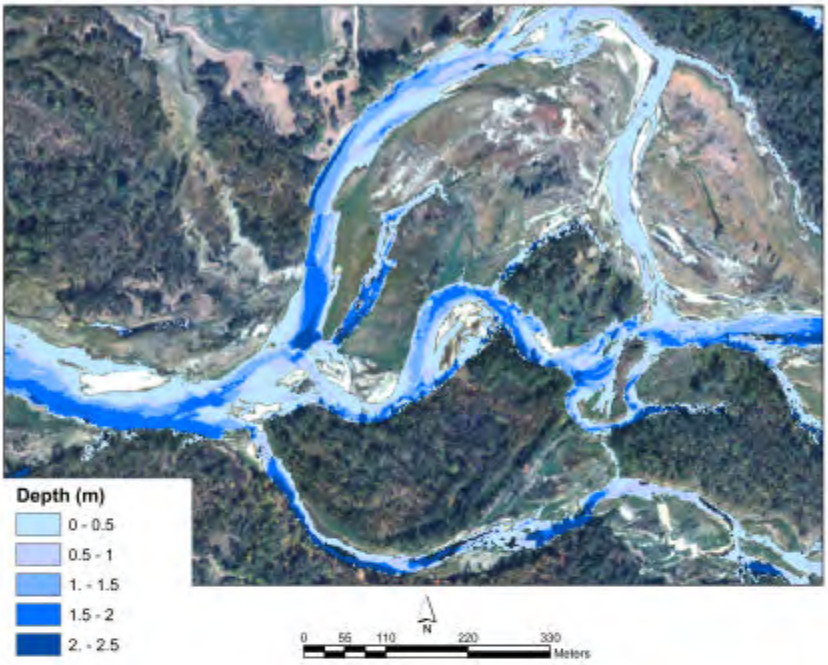

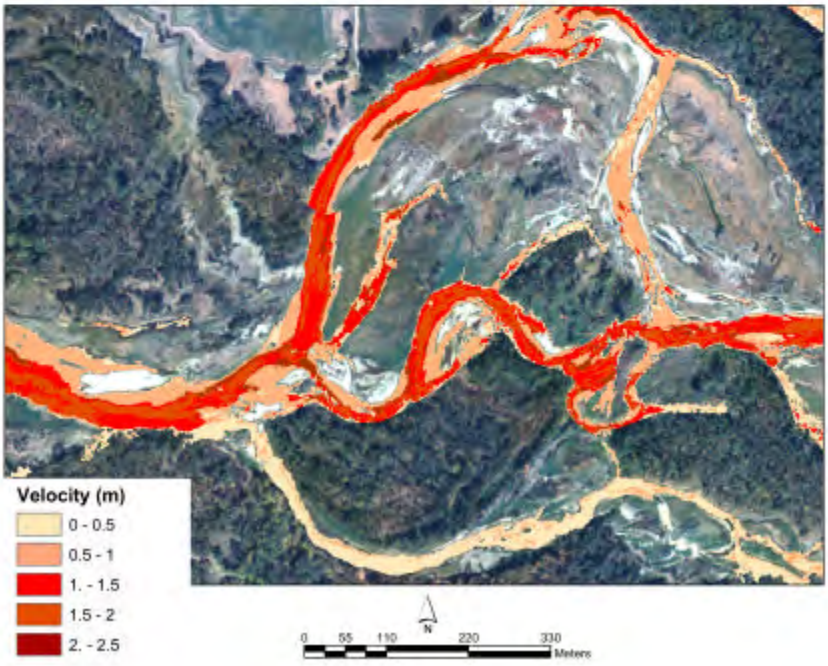

Figure 8. ADP data were distributed in the GIS environment to aggregate classes and assign unique depth and velocity categories. These initial classifications of water depth and flow velocity, illustrated here, form the basis of the following hydraulic and habitat classifications.

varies as a function of the number of satellites available and their position in the sky. In addition, both velocity and depth are recorded as the average velocity over a 5 second interval. Thus, depending on flow and geomorphic conditions, an individual profile could be an average of multiple flow and depth conditions for a given GPS location. Hence, the true ADP position can be as much as 3 to 4 m away from the GPS recorded position resulting in variance between the measured ADP profile and the hyperspectral imagery.

Rectification errors, aircraft turbulence distortions, and GPS errors (Figure 9) all contribute to potential misclassifications in the accuracy assessments. These errors account for 5 to 15% of the error in the 'pure' accuracy assessment. However, the use of the 'fuzzy' assessment helps minimize these affects, by evaluating classification within the context of neighboring classes. While the 'fuzzy' assessment may overestimate the classification accuracy, the 'pure' assessment clearly underestimates the accuracy. Despite the various sources of potential error, hydrologic and geomorphic structure (i.e., depth and velocity) and the associated aquatic habitats (i.e., pools, riffles, rapids and shallows) all appear in appropriate juxtapositions and orientations in river channels and distributed across the floodplain in logical places that we were able to confirm through direct observation in the field.

Creating a Floodplain Digital Elevation Model (DEM)

We produced a detailed floodplain DEM from the hyperspectral imagery and ground based topographic surveys. We then used the discharge stage level on the dates of the remote sensing image acquisitions to establish elevation reference from which to evaluate water depth across all discharges. This allowed delineation of floodplain areas likely to be inundated and reworked during potential flooding events.

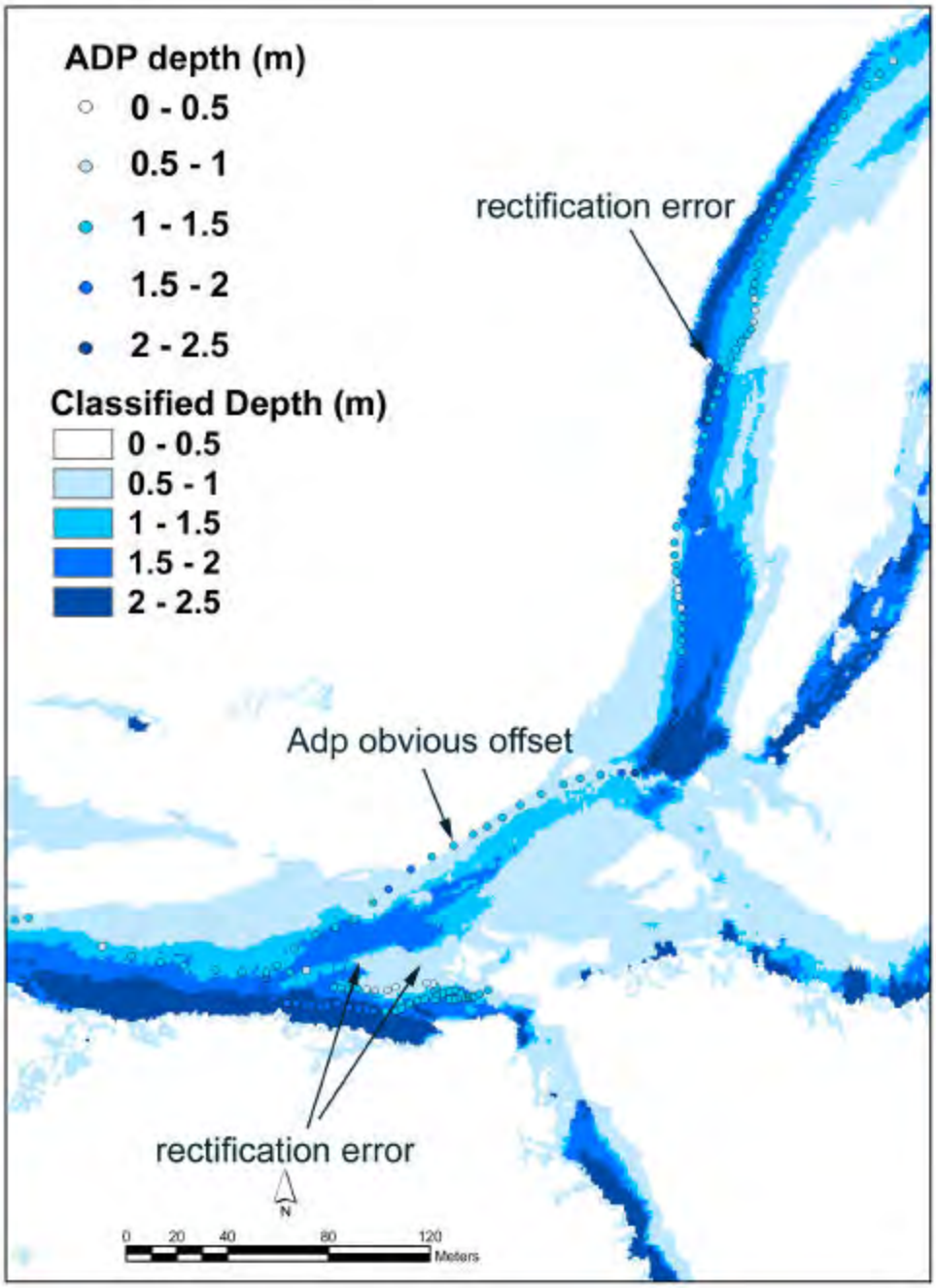

Figure 9. Typical rectification errors and misalignment of ADP tracks caused by inherent GPS error, georectification error and turbulence during hyperspectral data collection.

One-meter contour intervals were derived by re-sampling the 30 m resolution USGS DEM information. These data were superimposed onto the co-registered, hyperspectral imagery to provide first-order estimates of floodplain slopes. However, this level of topographic information was not of sufficient resolution to delineate detailed floodplain topography, especially critical features such as relic backwater channels that may provide new channels following future avulsions. Moreover, it is not feasible to use traditional survey methods to measure the topography adequately over the many square kilometers represented by our floodplain study reaches. To obtain sufficient topographic information for our modeling needs, we combined focused topographical survey information with airborne remote sensing data to assign relative elevations to classified floodplain cover type features (Figure 10).

Topographic surveys were conducted along transects that extended across the floodplain. These transects were chosen to include a broad range of topography (e.g., slope, elevation) across as many cover type features as possible. Other features captured by these surveys included relative elevations and slopes between gravel bars, water surface and bank top elevations throughout the floodplain reach. Unsupervised and supervised classifications of the airborne hyperspectral remote sensing imagery were conducted to classify major land cover features, including vegetation (e.g., grassland, forest), side channels, springbrooks, cobble bars, terraces and others. The survey data was then overlaid on the various classified cover types and assigned a relative elevation to the main channel, as well as a typical slope value, to characterize the transition from one cover type to the next. For example, water surface elevation in the main channel was set to zero in all cross-sections and all other cover types were assigned relative elevations (i.e., +/- change in elevation from the main channel). Hence, relative elevations and slopes, both across and between cover types, were assigned to the identified major land cover

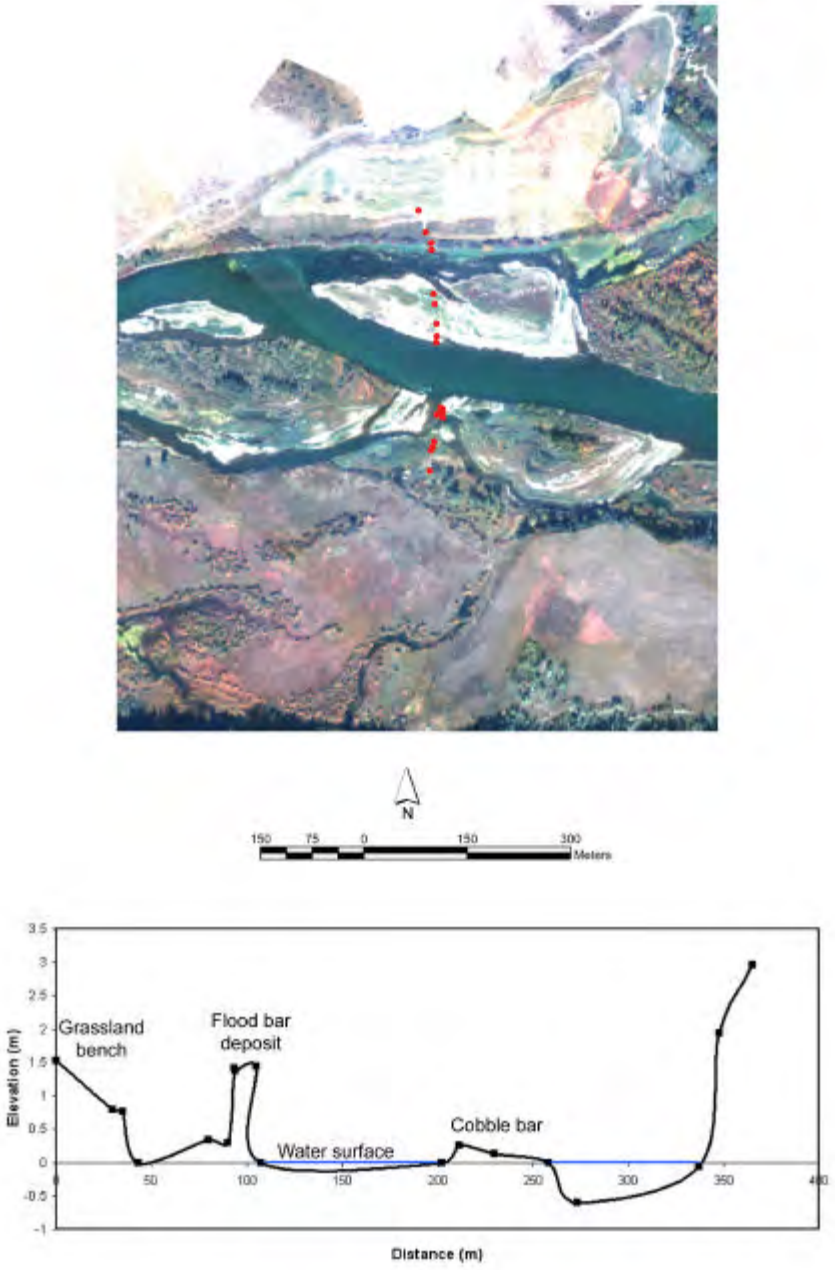

Figure 10. Survey data points are represented by red dots in the hyperspectral image of the Fisher floodplain (top panel). A cross-sectional plot of the survey data is shown in the lower panel.

features classified from the hyperspectral imagery. With this combination of data (i.e., survey data, hyperspectral imagery, and the USGS DEM) we were able to produce a high resolution DEM of each floodplain.

Floodplain inundation was modeled at 10cm stage increments using the higher resolution DEM. We compared modeled flood inundation, with geo-rectified imagery on June 20, 2002 (~11, 000 cfs) and April 12, 2003 (~1500 cfs) to match discharge with inundation extent for each reach. Similarly, we used airborne video taken on June 17, 1997 (~37000 cfs) to generate flood inundation maps for each reach. These three inundation maps (Figure 11) were used to calibrate our stage-discharge relationships for each reach.

Modeling Flow Depth and Velocity at Higher Discharges

We modeled flow velocity at varying discharges by establishing a basic relationship between velocity and river stage for all reaches. This relationship was developed by multiple measures of flow and depth at various discharge levels during the duration of our study (discussed above). Our modeling algorithms also included flow velocities for areas of the floodplain where flow velocity decreases as stage increases due to incorporation of large flow resistance elements. However, we were not able to accurately predict the formation or existence of slow or even calm "eddy drop zones" that occur on the shorelines bordering the downstream end of a riffle or rapid that dumps into a run. Fortunately, these water types do not represent a large portion of the total water surface area being modeled nor are they important for estimating avulsion processes. Although we were not able to directly model eddy drop zones in association with riffles and rapids, which are important potential aquatic habitats, we can accurately model

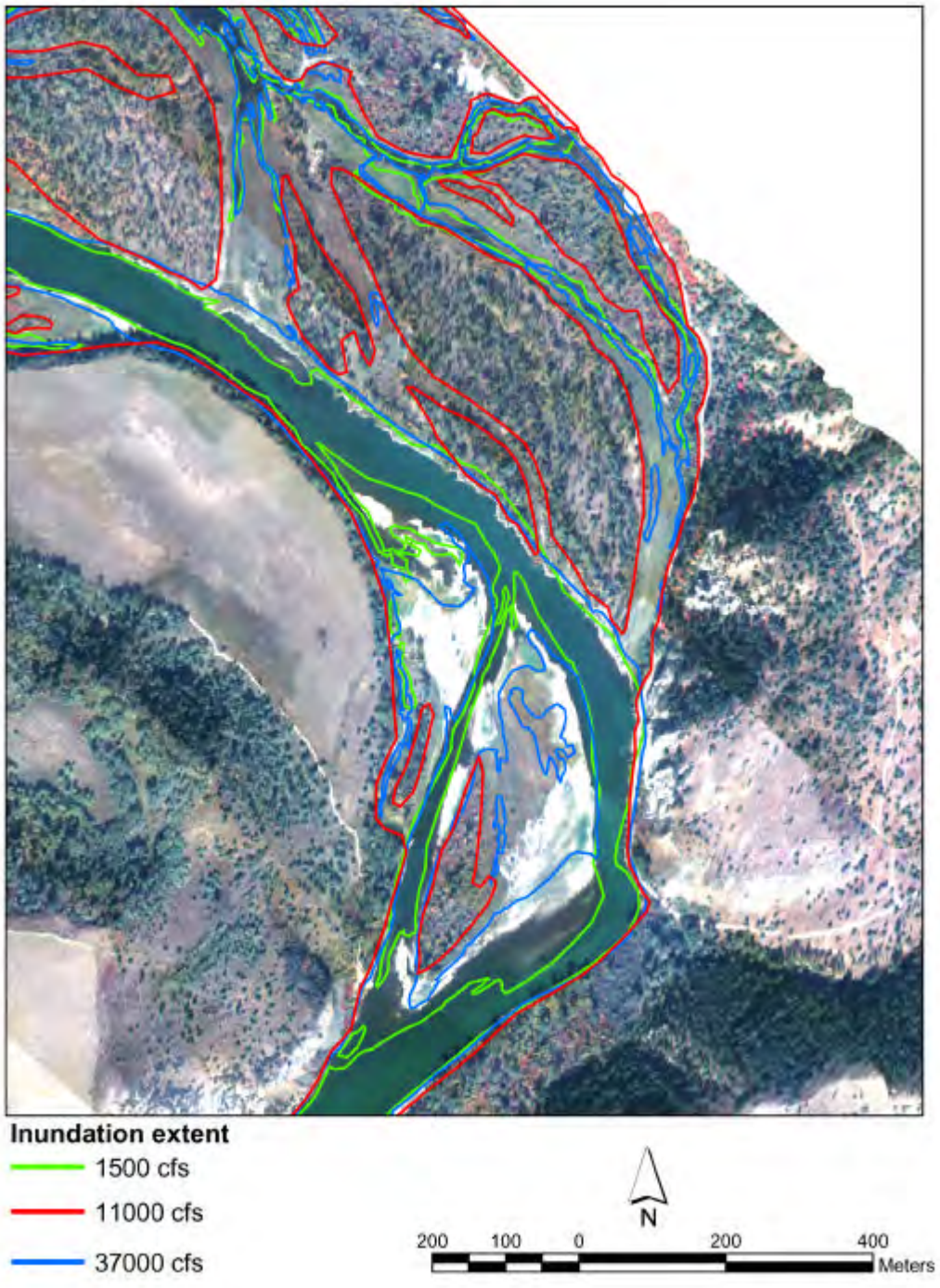

Figure 11. Colored lines show the extent of inundation for three different levels of discharge on this hyperspectral image of a portion of the Fisher floodplain.

changes in the associated water types (e.g. riffles, rapids and runs) and identify ecotones characterized by rapid change in velocity (see discussion of aquatic habitat below).

Estimates of flow velocity for the flooding scenarios were based on the initial velocity classification generated from the September imagery (5,000 cfs). Velocity was then increased according to equations (1) and (2) below, generated from depth-velocity relationships measured in the ADP surveys (Figure 12) and the data collected from a hand-held ADV (Acoustic Doppler Velocimeter) (Figure 13). The hand-held ADV was used exclusively in shallow waters (< 1 m) where the boat-mounted ADP looses signal. Equation 1 was used to simulate velocity for water depths > 0.8 m and equation 2 was used for water depths < 0.8 m, where *x* is the water depth at a given stage.

$$y = 0.4493 \ln(x) + 1.3986 \quad (1)$$

$$y = 1.789(x) - 0.2042 \quad (2)$$

After velocity was modeled for a given stage, we set an upper limit on water velocity for each modeled depth based on a Froude threshold (Figure 14). Using 10 cm stage increments, depths and velocities were modeled for each reach to represent discharge regimes from 1,500 cfs to 37,000 cfs. To check the accuracy of the modeled velocities and depths, the ADP surveys from November (1,500 cfs), August (8,000 cfs), and June (11,000 cfs) were used as reference data. For example, from the stage-discharge relationships in the Conant reach, we estimated the 11,000 cfs discharge corresponded to a stage increase of 0.5 m. Using the depths and velocities that were modeled at the 0.5 m stage increase, error matrices (Table 6) were generated from the appropriate ADP survey (i.e., the 11000 cfs survey) to validate the modeled results of depth and velocity (Figure 15). Our modeled estimates of flow velocity are in the same range

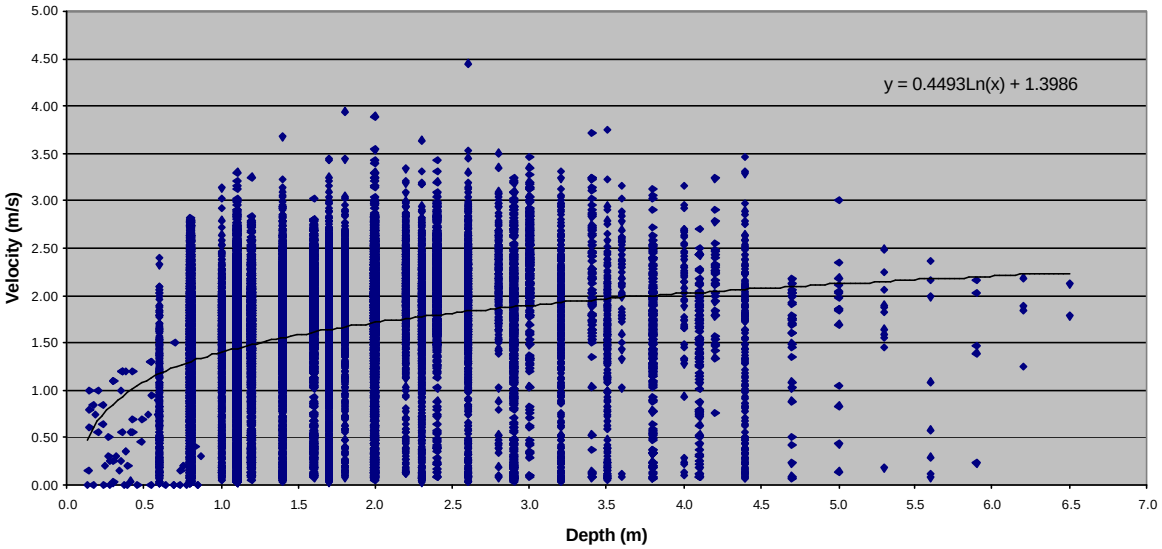

Figure 12. A plot of measured water depth and flow velocity for 25,308, locations from all floodplains in the study over 5 discharge levels. The log regression curve of these data was used to determine variation in flow velocity with change in stage.

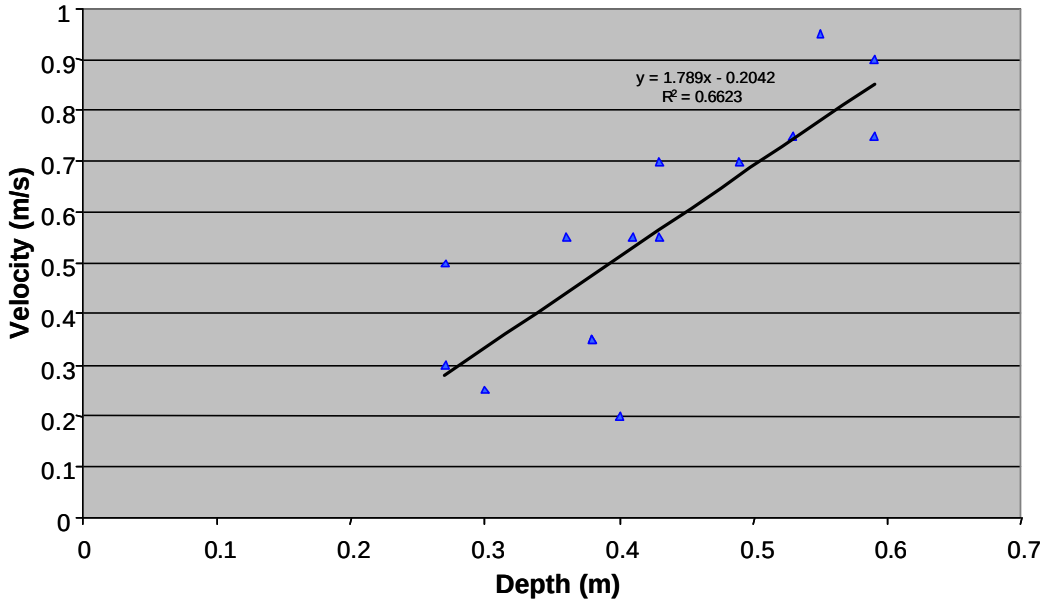

Figure 13. Correlation between measured water depth and flow velocity for water depths < 0.8 m across in a single shallow riffle area.

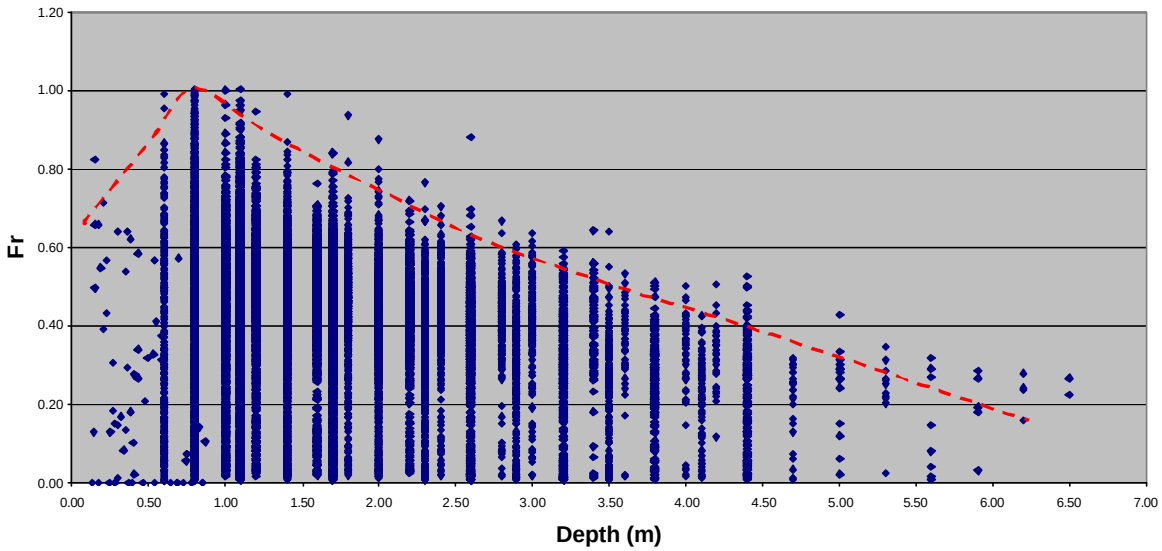

Figure 14. A plot of Froude number vs water depth for all ADP measures. The red line represents the accepted Froude maximum used in the GIS modeling of flow velocities.

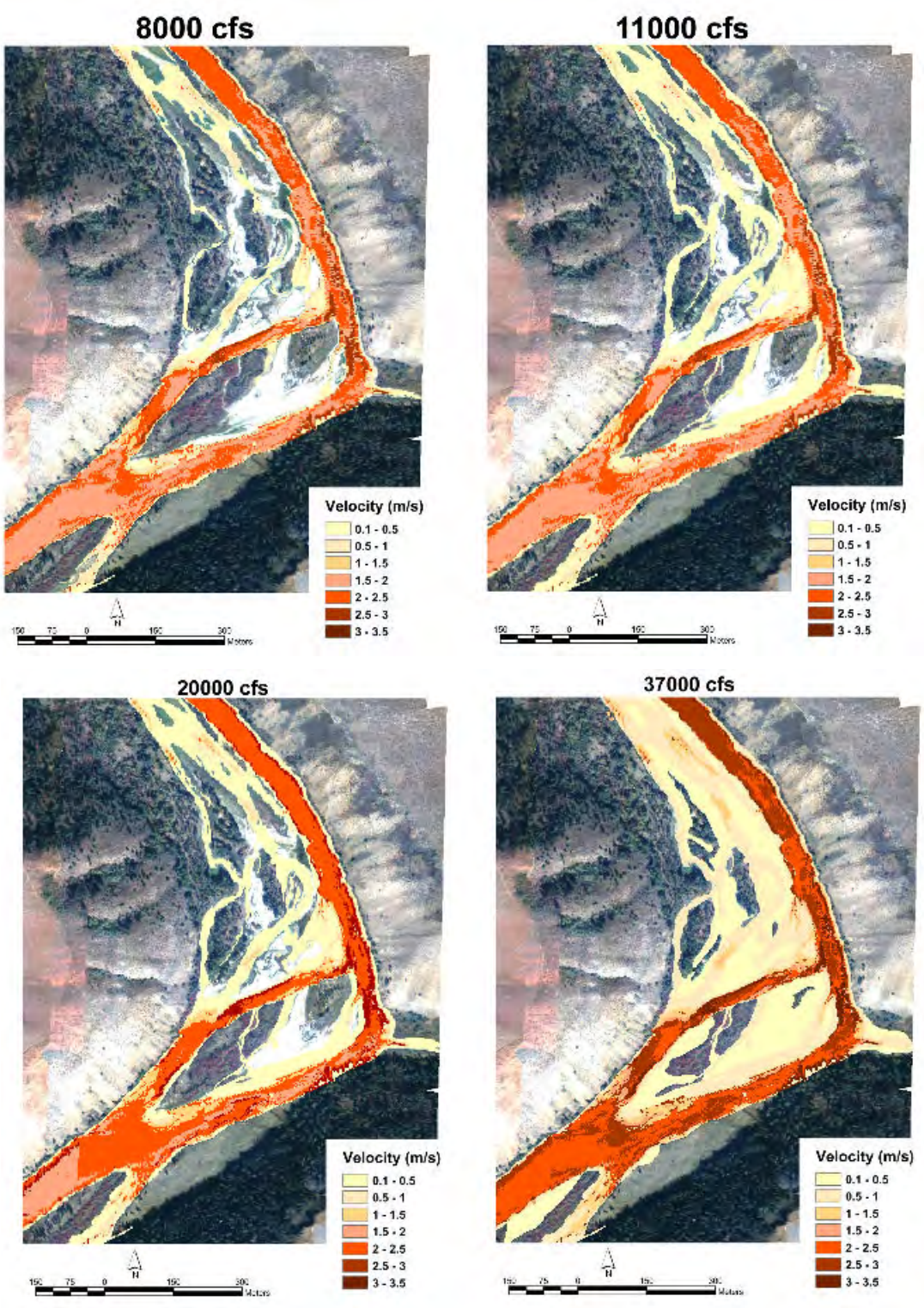

Figure 15. A plot of the spatial distribution of modeled flow velocity for discharges of 8000 11000, 20000, and 37000 cfs in the lower part of the Conant floodplain.

of accuracy we found for the original classification of the hyperspectral imagery at 5,000 cfs (Table 4). However, we are much better at estimating flood velocities versus flow velocity for base flows. This is probably due to the difference between local energy gradients increasing as stage drops making it difficult to accurately model a change in velocity based on a linear equation.

Aquatic Habitats

Aquatic habitats were derived from a combination of depth and velocity classification data, modeling output, and known relative positions of habitats associated with different channel and floodplain characteristics. As 1x1m unique classifications, pixels of one classification may appear within a group of pixels classified to a different depth and velocity. This often gives the appearance of stippling in the classified image. In our habitat classification procedure, we first aggregated depth-velocity pixels (DVP) into common patches, plotted as polygons, by conducting a "majority filter" step in the GIS environment. Each filtered DVP patch was then assigned a unique aquatic habitat type. The area and dimensions for each aquatic habitat across each of 5 discharges (1500, 5000, 11600, 25000, 37000 cfs) was then compiled through the GIS. We then analyzed the various characteristics of the aquatic habitat patches (e.g., patch shape, edge relationship, edge length).

Vegetation classification

The September imagery was used for land cover classification because of the high contrast between vegetation types during autumnal senescence. A combination of supervised and unsupervised classifications was used to produce a land cover map for each reach. First, an

Table 4. An example of error assessment tables for each class of depth and velocity for the Conant Valley flood plain at 11,000 cfs.

Conant Velocity 11000 cfs

Classified (m/s)	*Reference (m/s)* 0 - 0.5	0.5 - 1	1 - 1.5	1.5 - 2	> 2	*Classified Total*	*User's Accuracy Pure (% correct)*	*User's Accuracy Fuzzy (% correct)*
0 - 0.5	9		4			13	69.23	69.23
0.5 - 1		1	3	3	1	8	12.50	50.00
1 - 1.5	2	6	5	6	2	21	23.81	80.95
1.5 - 2		2	33	95	167	297	31.99	99.33
> 2		6	18	59	164	247	66.40	90.28
Reference Total	11	15	63	163	334	586		
						0.46757679		
Producer's Accuracy Pure (% correct)	81.82	6.67	7.94	58.28	49.10			
						548		
						0.93515358		
Producer's Accuracy Fuzzy (% correct)	81.82	46.67	65.08	98.16	99.10			

Overall Classification Pure = 46.76%

Overall Classification Fuzzy = 93.52%

Conant Depth 11000 cfs

Classified (m)	*Reference (m)* 0 - 1	1 - 1.5	1.5 - 2	> 2	*Classified Total*	*User's Accuracy Pure (% correct)*	*User's Accuracy Fuzzy (% correct)*
0 - 1	19	7	11	3	40	47.50	65.00
1 - 1.5	17	10	3		30	33.33	100.00
1.5 - 2	25	63	77	9	174	44.25	85.63
> 2	1	15	131	196	343	57.14	95.34
Reference Total	62	95	222	208	587		
					0.51448041		
Producer's Accuracy Pure (% correct)	30.65	10.53	34.68	94.23			
					532		
					0.90630324		
Producer's Accuracy Fuzzy (% correct)	58.06	84.21	95.05	98.56			

Overall Classification Pure = 51.45%

Overall Classification Fuzzy = 90.63%

unsupervised classification was used to discriminate between vegetative cover and non-vegetative cover (i.e. vegetation vs cobble and water). This was followed by a supervised classification approach for the vegetative cover. To help discriminate among different vegetation types, homogeneous stands of the varying cover types (e.g., cottonwood, willow, reed canary grass, dry grass) were identified and associated with specific hyperspectral signatures. These specific imagery signatures were used as "training areas" to classify the image into the different land cover types. Mean spectral signatures (Figure 16) were calculated for each cover type and subsequently used in a supervised classification. Using the spectral signatures, the Mixed Tune Matched Filtering (MTMF) algorithm in ENVI (RSI 2000) was then applied to the vegetative component of the imagery to discriminate the varying vegetation types. For each reach, a final land cover map was produced consisting of 8 dominant cover types (i.e., water, cobble, deciduous – predominately cottonwood, willow, mixed grasses, dry grasses, reed canary grass, and shadows). In the Twin reach, willows were not easily differentiated from cottonwood; therefore, cottonwood and willow were aggregated into a single coverage identified as a "deciduous" category. A pasture category was also added in the Conant reach.

This method of classifying vegetation is a significant departure from approaches involving digitizing and photo-interpretation. We were able to take this approach of conducting an integrated supervised and unsupervised classification because of the application of the hyperspectral imagery allowing vegetation specific differentiation. We were also then able to conduct various analyses on the vegetation coverage that would not have been feasible using traditional photo-interpretation methods.

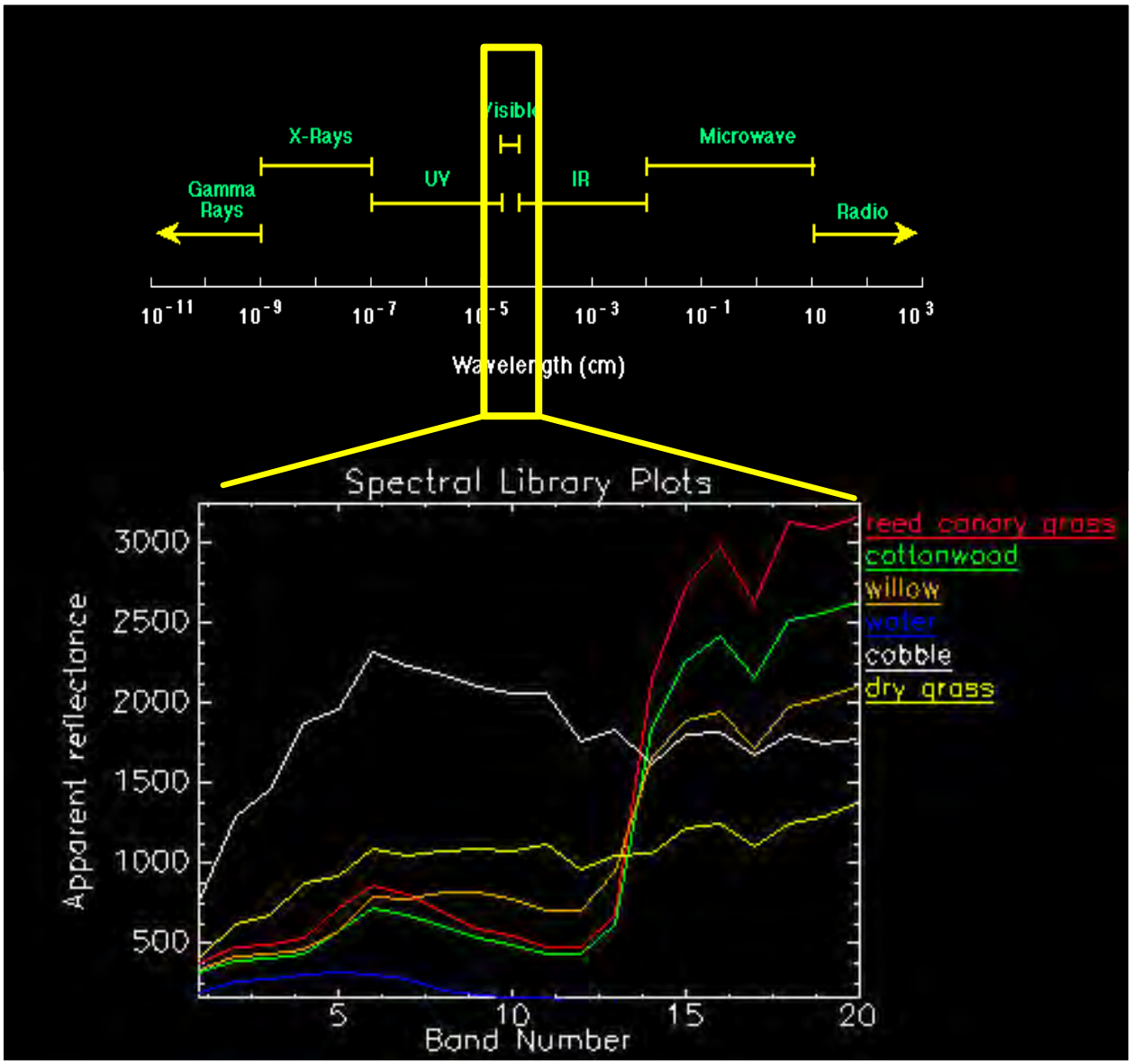

Figure 16. Mean spectral signatures of the hyperspectral reflectance data calculated for each cover type and subsequently used in a supervised classification.

RESULTS AND DISCUSSION

Hydrographic Regimes

Historically, the hydrologic regime of the Upper Snake River basin was characterized by spring snowmelt as demonstrated by pre-dam hydrographs (Figure 17). These natural discharge regimes supported extensive surface water and ground water exchange, a dynamic cottonwood gallery forest, a vibrant native fishery dominated by Yellowstone cutthroat trout, and a high diversity of riparian plants and animals, particularly on the expansive unconfined alluvial floodplains.

Groundwater-surface water exchange functions as a hydrologic and thermal buffer, distributing the energy of peak flows and moving cool, spring snowmelt water out onto the floodplains. Lateral inundation also plays an important role in the annual recharge of shallow, surficial aquifers. Based on fundamental hydrologic principles, groundwater recharge into floodplain aquifers plays an important role in maintaining base flows, and provides areas of cooler thermal refugia as summer progresses and air temperatures increase. Floodplain groundwater return flows also maintain warmer winter temperatures, preventing or reducing the risk of anchor ice Bansak (1998) and Baxter and Hauer (2000).

Annual inundation and recharge of floodplain segments maintain the connectivity and flow to backwaters and springbrooks. These represent habitats that are critical for successful completion of the life-history cycles of numerous fish species and other biota (e.g., Ward et al. 1999). The water is rich in nutrients owing to the biogeochemical cycling of organic material that flows through the subsurface matrix of the abandoned channels (Stanford et al. 2001). This nutrient rich water supports a robust shallow water food web that provides critical food-web

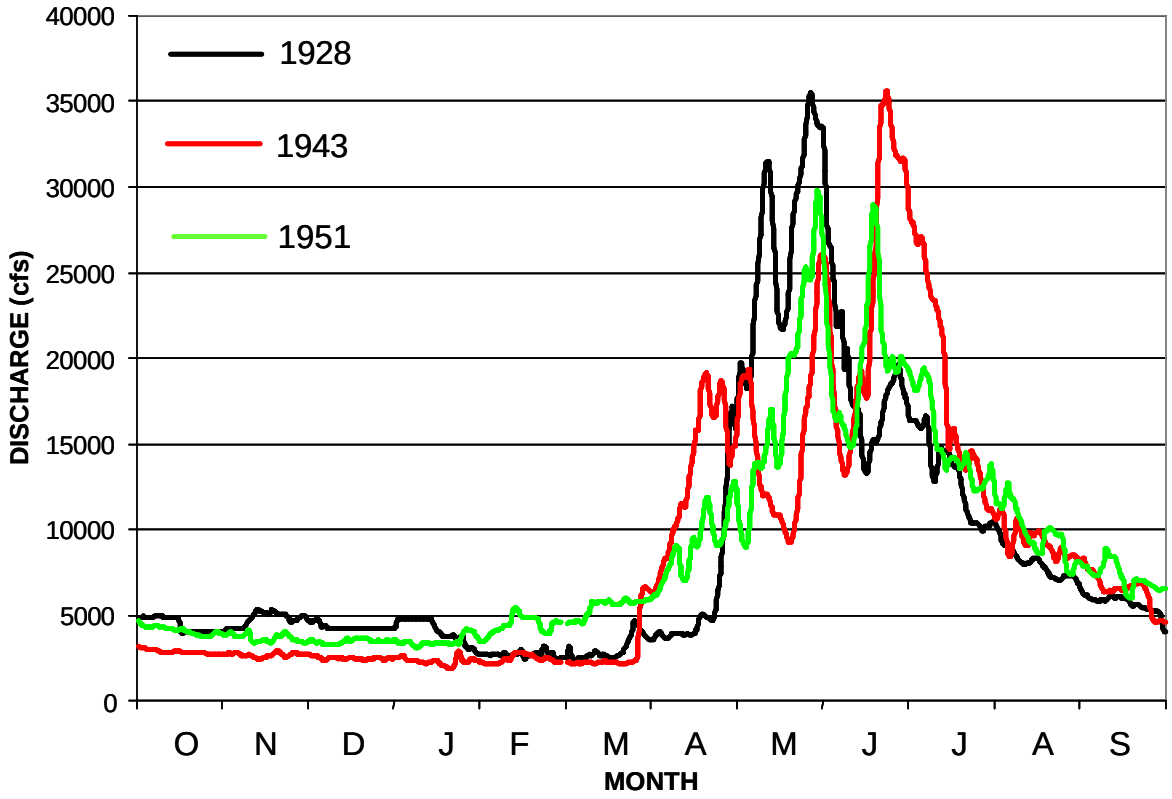

Figure 17. Historical hydrologic regimes of the Upper Snake River basin characterized by spring snowmelt as demonstrated by these pre-dam hydrographs.

support. Historic maps and photographs, coupled with analysis of hydrographic regimes, indicate that these types of habitats are likely affected most by anthropogenic alteration of flow and geomorphic modifications on the floodplains.

The following hydrologic analysis focuses on the Heise hydrologic record with comparison references to the records from Irwin and Lorenzo. Over the nearly 90 year record from Heise, there is considerable interannual variation in the total discharge for each water year (Figure 18). Although there is no record of the natural hydrograph in the Snake River since Jackson Lake dam that was constructed in the 1900's and USGS gauging of the river discharge did not begin until 1911, a comparison of daily mean discharge at Moran Wyoming during the period 1920-1939 compared to 1980-1999 illustrates a highly modified hydrographic regime during the early part of the 20th century compared to more recent discharge regimes that feature a near normal hydrographic pattern (Figure 19).

These discharge patterns show typical spring/summer snowmelt dominated hydrographs. Discharge is low during fall and winter. The rising limb of the spring snowmelt prior to construction of Palisades Dam (although as noted, partly regulated by Jackson Lake) typically began in late March and early April. Peak in discharge typically occurred in late May or in June. Discharge patterns in the Snake River at Heise since construction of Palisades Dam have changed dramatically, particularly among high discharge years (Figure 17). In each of the three years illustrated increased discharge typical of the onset of spring snowmelt was initiated in late February and early March rather than the natural discharge regime beginning in late March and April. When compared to high discharge years prior to Palisades Dam, the early discharge represents a 30 to 45 day earlier initiation of a rising spring hydrograph. Hydrographic patterns among low discharge years were similar before and after dam construction.

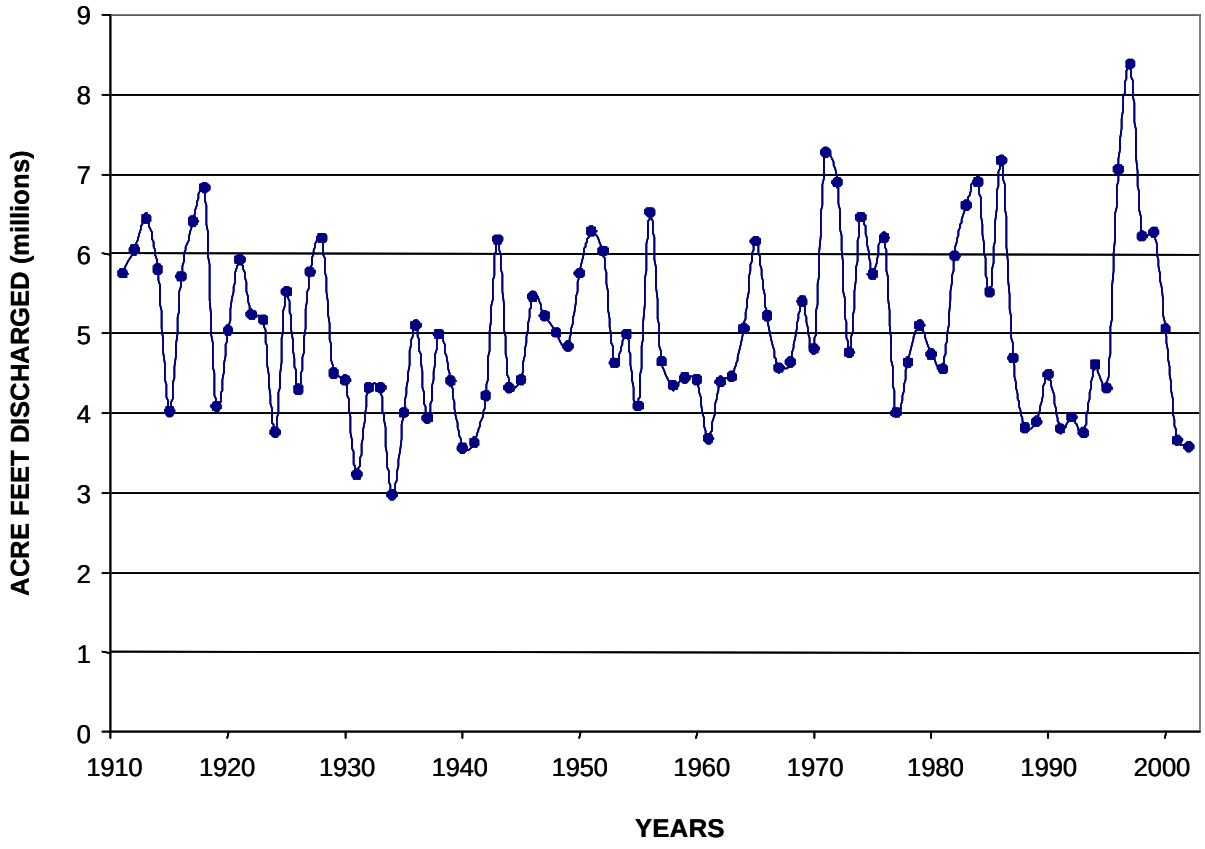

Figure 18. Interannual variation in the total discharge expressed as millions of acre feet for each water year from 1911 – 2002.

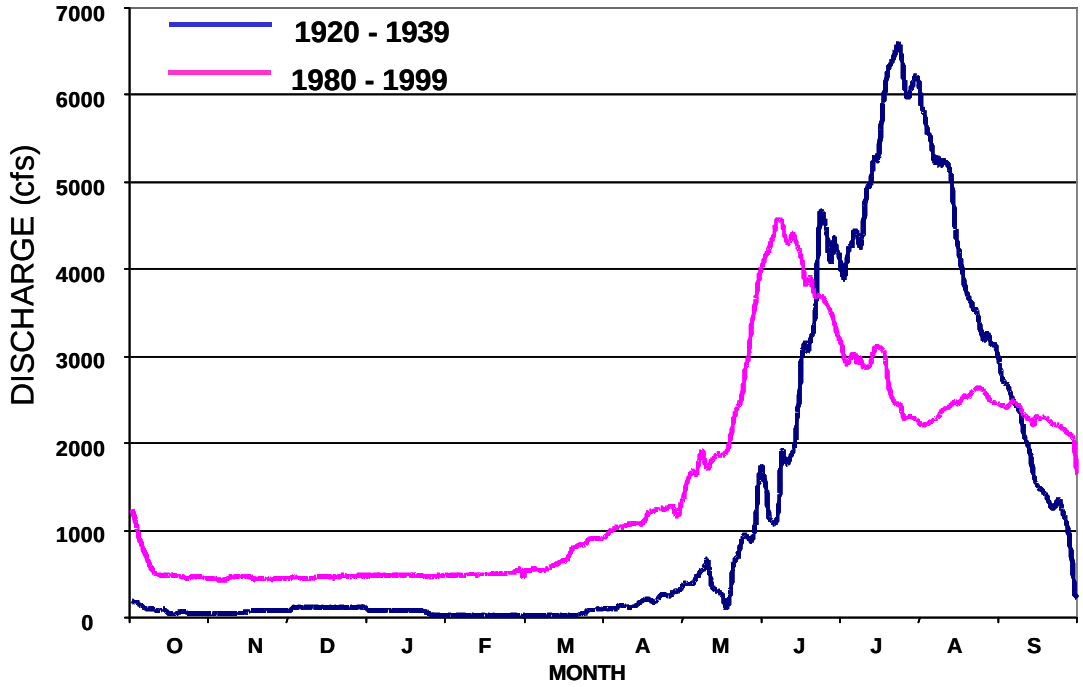

Figure 19. Average mean daily discharge (cfs) of the Snake River at Moran (below Jackson Lake dam) during 1920 – 1939 compared to 1980 – 1999. Note the temporal change in river discharge between these time periods, reflecting the change in dam operation.

The change in hydrographic patterns between high water years before and after dam construction is the result of operator anticipation of high discharge coming from the upper basin. The intent of spilling water in mid-winter is to maximize potential water storage in Palisades Reservoir and minimize risk of flooding. This general pattern is seen clearly in the 3 example water years, 1965, 1974 and 1986 in the Snake River at Heise (Figure 20). Note the much greater variation in discharge during February – April after dam construction compared with the same time intervals prior to dam construction.

The natural hydrographic regime played an essential role in the biodiversity and productivity of the river-floodplain system as various species (e.g. cottonwood, willow, cutthroat trout) evolved specific life cycle strategies to natural flow regimes. Organisms tend to be well adapted to pulse-disturbance; however, regulated flow, as observed in Figure 20, that repeatedly produces press- and ramp-disturbance (Lake 2000) and interferes with life cycles of critical species result in stress upon aquatic species as well as the riparian gallery forest. This has been well documented in other regulated rivers throughout the northern Rocky Mountains (Hauer and Stanford 1991, Stanford and Hauer 1992). Life cycle interference may take the form of direct lethal impact (e.g., winter freezing, summer desiccation) or long-term impact (e.g., loss of the Shifting Habitat Mosaic).

The narrowleaf cottonwood (Populus angustifolia) and its gallery forests are the dominant plant species and cover type of the study floodplain corridor. The effects of Palisades Dam on the colonization, survival, and distribution of the cottonwood gallery have been previously investigated (Merigliano 1996). Likewise, other studies have closely linked the heterogeneity and "system health" of western riparian gallery forests with the diversity and abundance of neo-tropical birds, amphibians, and terrestrial and aquatic insects.

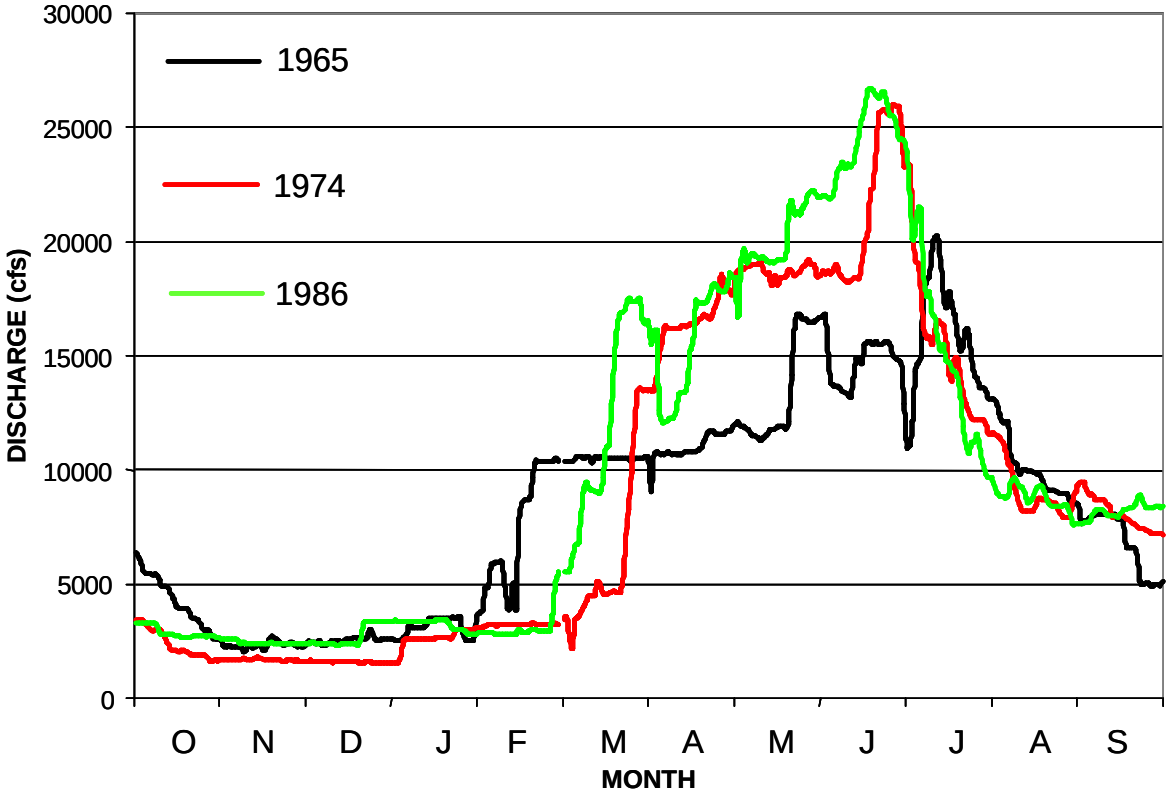

Figure 20. Hydrologic regimes during three example high volume water years of the Upper Snake River basin after dam construction. Note the high discharges during February an March and comparatively low maximum discharges during June and July.

Merigliano estimated linkages of flow regimes to cottonwood forest patches suggesting that flows from 40,000 to 60,000 cfs created and maintained the pre-dam cottonwood gallery forests. However, this estimate was based on channel cross-section profiles rather than a determination of landscape scale flood modeling as presented here. Nonetheless, an examination of annual peak discharge and the recurrence intervals of flood flows clearly shows that Palisades Dam has had a significant effect on the relationship between flood frequency and maximum discharge attained during annual snowmelt (Figure 21). (Note: recurrence interval (T) was determined using the Cunnane plotting position, where:

$$T = \frac{[(N+1) - 2a]}{(m - a)} \qquad (3)$$

N = number of years of record, m = rank of the event where the largest event has a rank of 1, and $\alpha = 0.4$ (Cunnane 1974).

During the 46 years of record prior to Palisades Dam operation, the Snake River at Heise achieved or exceeded 30,000 cfs 12 times. In contrast, during the 46 years of record since dam operation, 30,000 cfs has been exceeded only once (1997). Although reservoir storage permits capture of water in high water years for distribution in low water years, an examination of the relationship between annual maximum discharge and the total discharge for each water year showed that prior to the dam there were no years where there was more than 6.9 million acre feet in total discharge, but 6 years where this discharge was exceeded since operation of the dam. This increase in total annual discharge for those years was due to release of stored water carried

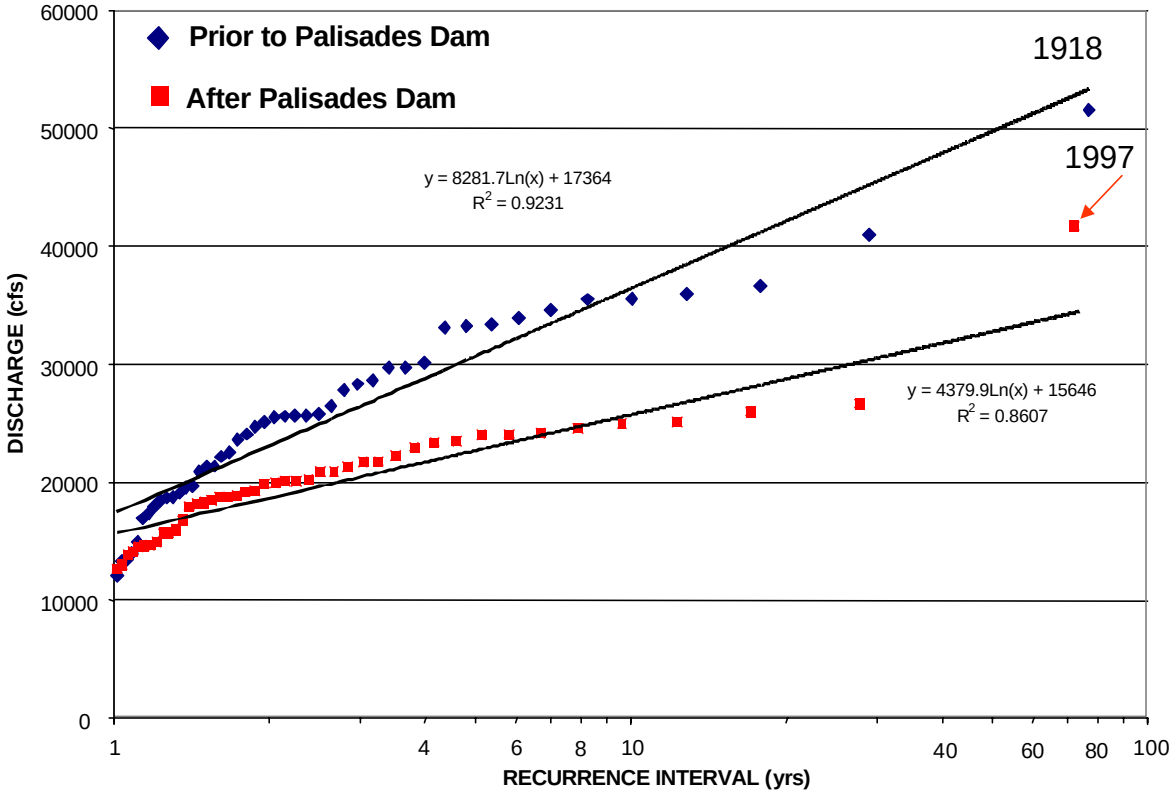

Figure 21. The average recurrence intervals of annual peak discharge were computed from the Cunnane plotting position with $\alpha = 0.4$. Number of years prior to Palisades Dam = 46. Number of years after Palisades Dam = 44. The discharge of 1997 (marked by the red arrow) was not included in the "after Palisades regression curve).

over from the previous year and released in the spring in anticipation of high discharge based on winter snow pack. We discuss the impact of these discharges and their implication for maintaining the SHM in later sections.

Temperature and Groundwater-Surface Water Interactions

Groundwater-surface water (GW-SW) interactions are a central hallmark characteristic of alluvial, gravel-bed river floodplains. We focused our examination of GW-SW exchange between the river and the floodplain on the Fisher floodplain. We installed 86 piezometers into the substratum of the river channel, side channels and backwaters of the floodplain following the protocols of Baxter et al. (2003). These piezometers were clustered into 8 groups (A – H). We distributed the clusters across the length of the floodplain to determine the complexity of GW-SW interactions and observe the patterns of vertical hydraulic gradients (VHG) associated with the geomorphic legacy of past flooding, avulsions, and the presence of subsurface zones of preferential flow characteristic of a Shifting Habitat Mosaic (Figure 22).

We observed a general trend of downwelling (-VHG) at the upstream end of the Fisher floodplain, which was replaced by strong trends of upwelling (+VHG) through the central and lower end of the floodplain (Figure 23 and see Appendix A). Groundwater return flows appeared in both backwater channels and directly in the main river channel. It has been noted elsewhere that zones of strong GW-SW interactions greatly influence spawning site selection by salmonids (Baxter and Hauer 2000). While the Snake River Yellowstone cutthroat trout are known to be primarily tributary spawners, cutthroat may also use floodplain springbrooks as spawning sites.

Figure 22. Groups of locations of 86 piezometer installations and measures of vertical hydraulic gradient (VHG) in the Fisher floodplain.

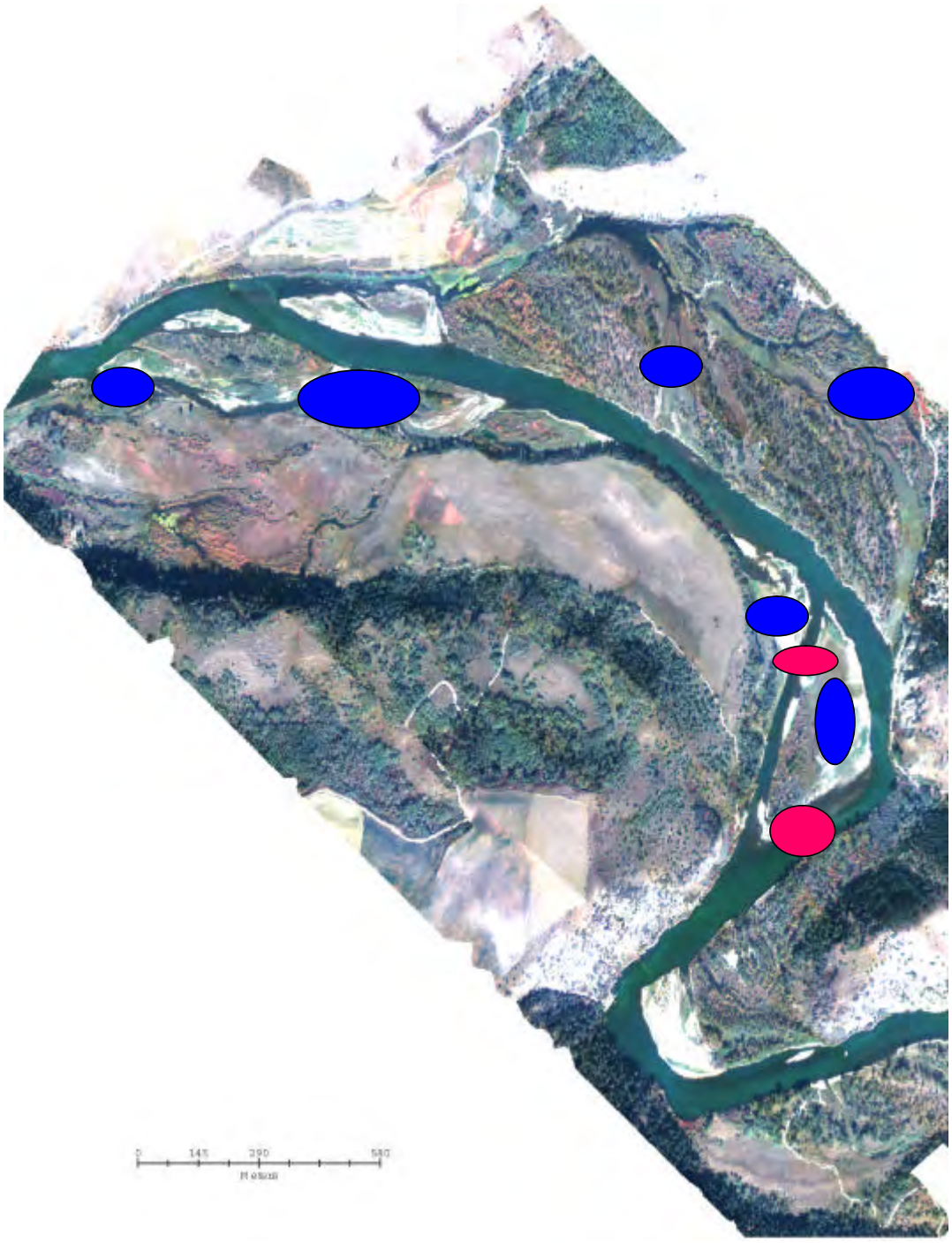

Figure 23. Zones of -VHG (downwelling) in red and zones of general +VHG (upwelling) marked in blue determined from the 86 piezometer installations and measures of vertical hydraulic gradient (VHG) in the Fisher floodplain.

Groundwater-surface water interactions, as measured here across the Fisher floodplain, are known to be particularly important in biogeochemical cycling of major nutrients in gravel-bed river systems. Elsewhere, it has been clearly demonstrated that groundwater as hyporheic return flow to the surface has comparatively high concentrations of nitrogen and phosphorus, which results in focused areas of high primary production (Bansak 1998), increased growth of riparian vegetation (Harner and Stanford 2003) and increased growth rate and density of benthic invertebrates (Pepin and Hauer 2002). The long-term sustainability of GW-SW interactions is a fundamental feature of sustainable river-floodplain ecosystems.

Thermal regimes, variation in temperature associated with GW-SW and their distribution across the floodplain was examined by placing 10 continuously recording temperature loggers at strategic sites in various side channel and backwater areas of the Fisher floodplain. From these temperature data, we see high variation in thermal regimes and patterns between different types of habitats associated with the variation in hydrogeomorphic structure on the floodplain. Thermograph A (Figure 24) illustrates a typical temperature pattern of waters receiving little GW-SW influence. In contrast, Thermograph B shows data from one of the springbrooks on the floodplain in which temperatures are highly moderated in both summer and winter by the upwelling of groundwater from the floodplain hyporheic zone (Figure 24).

Temperature is an important environmental factor affecting growth and production of virtually all aquatic organisms. The complexity of temperature, as it is distributed across the floodplains, plays an important role in structuring species and habitat use patterns. For example, groundwater –surface water interactions directly in the main channel may have a significant affect on the spawning site selection of the non-native rainbow trout. Understanding where

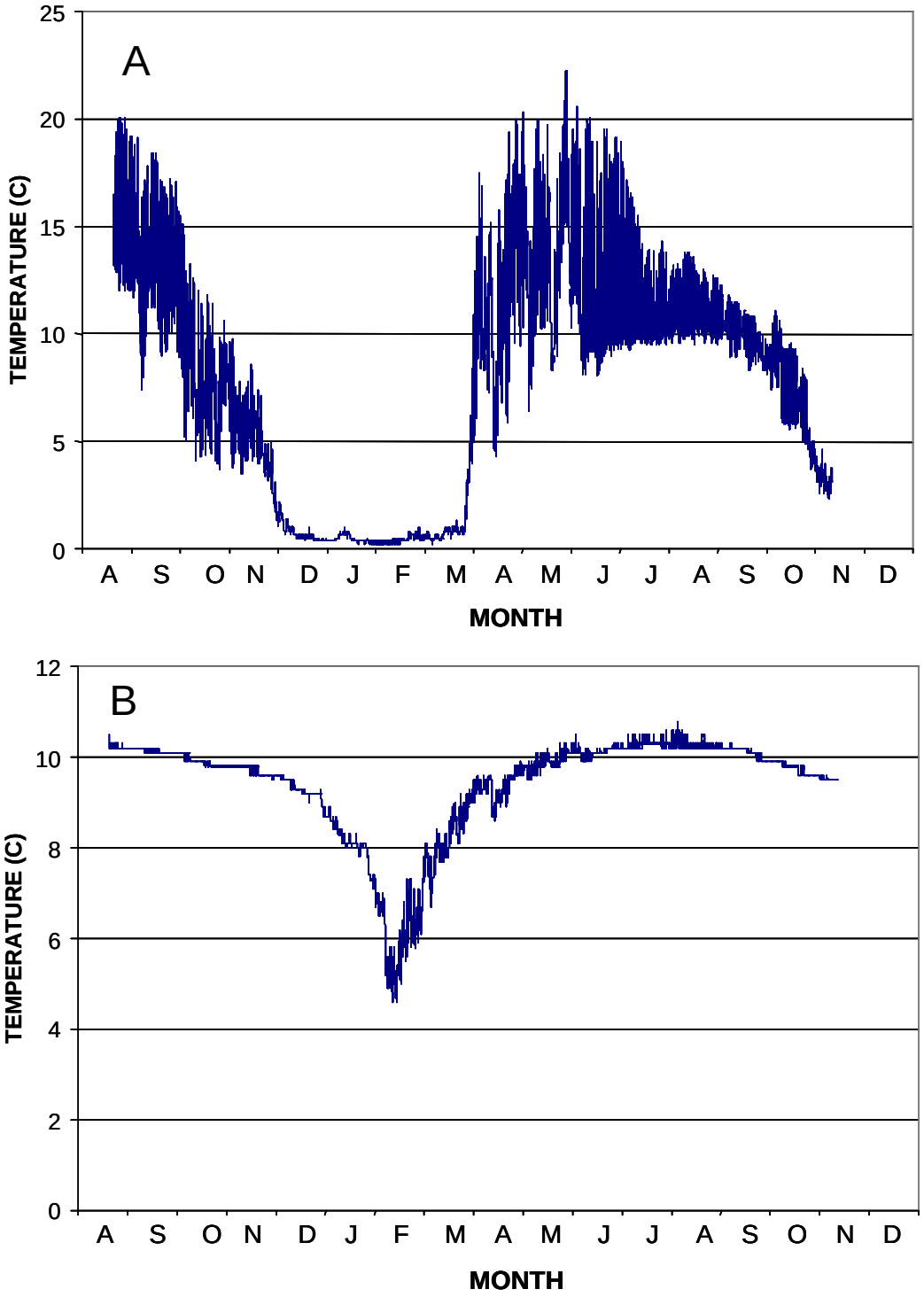

Figure 24. Two hour interval temperature regimes over a 16 month period (Aug 2001 – Nov 2002 from two thermographs sited in off-channel aquatic habitats on the Fisher floodplain. Panel A shows a typical temperature regime for a site with little GW-SW interaction, whereas Panel B shows data collected from a site with significant GW influence.

GW-SW interactions occur as well as gravel mobility and spawning selectivity will likely play an important role in the long-term management strategies for targeting an enhancement of the native species.

Historical Aerial Photographs and Discharge Records

The Shifting Habitat Mosaic of river floodplains is spatially and temporally dynamic in response to flow hydraulics associated with floods. Floods provide sufficient stream power to do the geomorphic work (i.e., cut-and-fill alluviation, channel avulsion) of maintaining a shifting habitat. However, not every flood does significant geomorphic work to identify a change at the scale of most historical aerial photographs. One of our objectives was to determine what discharge volumes and regimes are necessary to produce sufficient power to sustain the geomorphic template of the SHM. We examined the historical record of aerial photographs and identified past channel avulsions and large scale depositional features (e.g., formation of islands, gravel bars) (Figure 25) that occurred between each photographic record. We then examined the discharge data from the USGS-Heise gauging station and identified the major discharge events that occurred during the time interval between aerial photos (Figure 26). We observed that what appeared to be the result of geomorphic work only occurred when discharge in the river achieved at least 20,000 cfs. In most intervals showing geomorphic change, a discharge >30,000 cfs had occurred and occasionally nearly 40,000 cfs or more.

From this level of analysis, we can estimate that the minimum geomorphic threshold might be around 20,000 cfs to 30,000 cfs. One might argue that a discharge of 40,000 cfs is necessary on a regular basis to "set-up" the system for additional observed work to be done at the lower discharge levels. Unfortunately, most of the photographic record is relatively recent

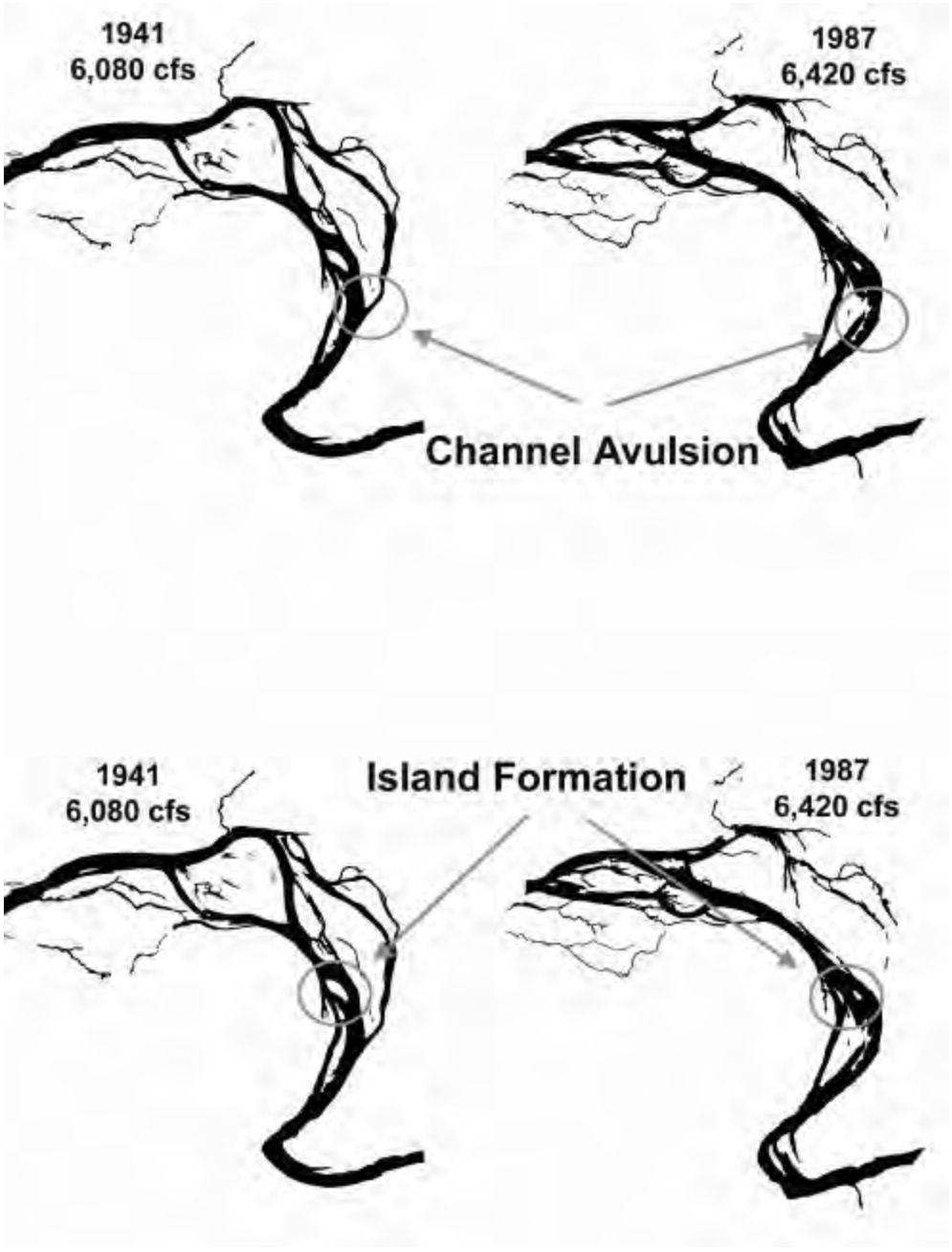

Figure 25. Historical record using aerial photographs and identified past channel avulsions and large scale depositional features (e.g., formation of islands, gravel bars).

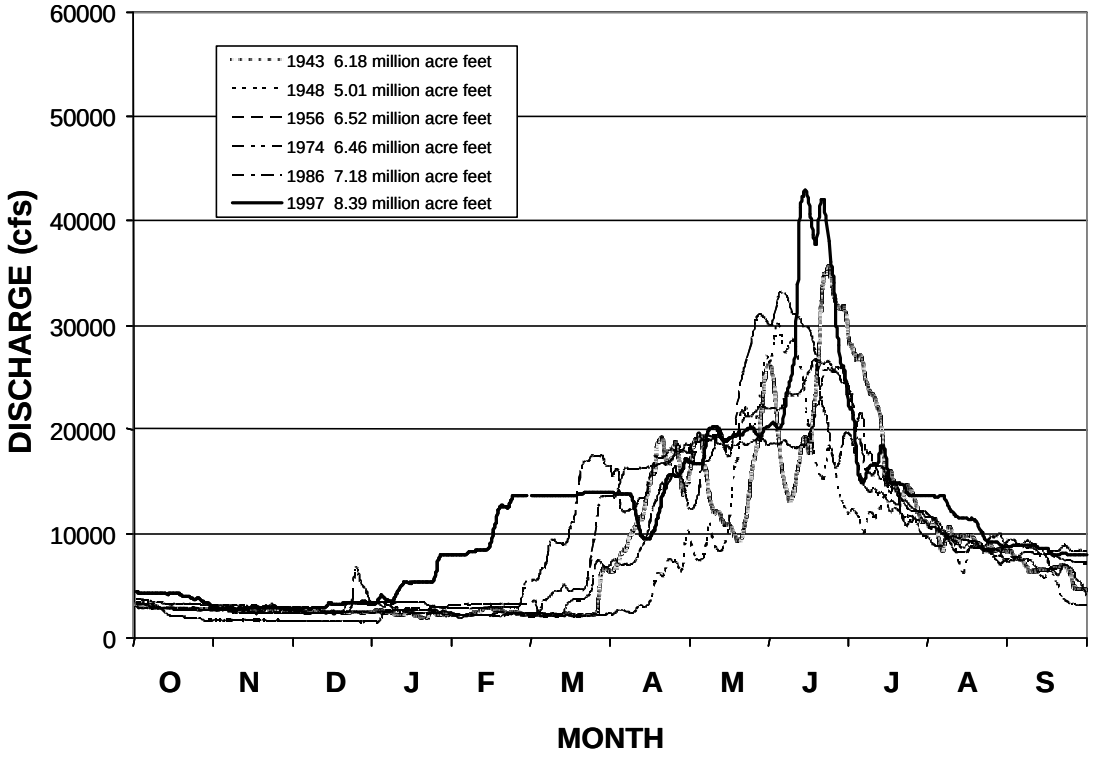

Figure 26. A plot of daily discharge for each water year identified through interpretation of the aerial photograph time-series as a probable water years responsible for the observed channel avulsions and island formation. All years reach at least 20,000 cfs, and some reach 30,000 with the maximum discharge being 40,000 cfs. The actual minimum thresholds for geomorphic work must occur somewhere with in the range indicated by the arrow.

coming after dam construction. We also examined the discharge record prior to the earliest aerial photographs to compare discharges that were shaping the floodplains under a natural system to get a sense of what levels of flooding produced the landscape that we observe in the earliest aerial photographs.

Analysis of the five largest discharge years prior to the earliest aerial photograph shows that the 30,000 cfs return interval was about every 3-4 years with the maximum reaching over 50,000 cfs (Figure 27). While very limited in scope, we conclude that this analysis of historical aerial photographs and the discharge record indicates that floods between 20,000 cfs to 50,000 cfs are necessary to maintain the SHM. This range is too broad to serve as a guide for regulating the flow of water from Palisades dam. While this examination of a photographic record provides important insight, it was inadequate in estimating either the flows or the level of geomorphic activity necessary to sustain the Shifting Habitat Mosaic that could be achieved within the constraints of contractual obligations under which Palisades dam must operate.

Hyperspectral Imagery and Determination of Flow Depth and Velocity

We deployed the AISA Hyperspectral Spectrophotometer from an airborne platform and collected imagery at discharge levels of 11,600, 5000 and 1,500 cfs for each of the six study floodplains. Following the methods and protocols described above, we used a combination of the hyperspectral data, ADP data, topographical survey data, USGS DEM data, USGS discharge data to classify depth and velocity at 1x1m pixel resolution across each floodplain at a discharge of 5000 cfs (Figure 28). We use our flow model to estimate flow depth and velocity for discharges of 1500, 11600, 25000 and 37000 cfs and provide tables of these data in Appendix A

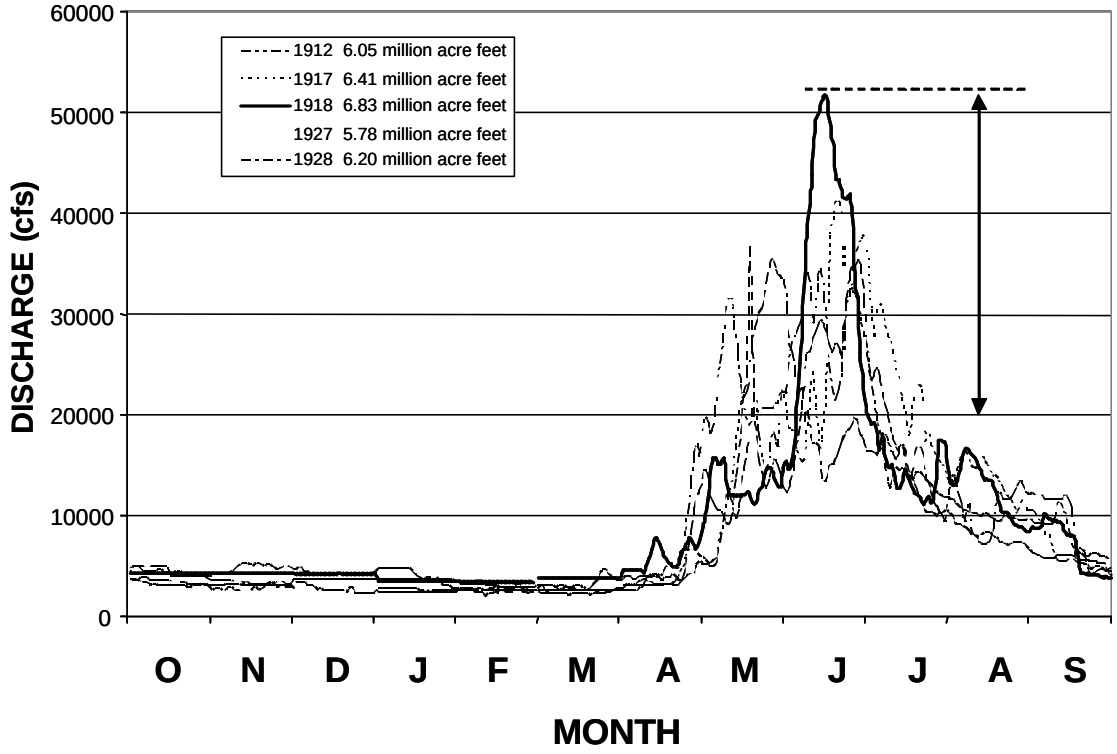

Figure 27. A plot of daily discharge for the five largest discharge years in the historical record prior to the earliest aerial photograph (1943). All of these years reach 20,000 cfs Most going above 30,000 cfs and with the highest discharge, 53,000 cfs, occurring in 1918. The actual minimum thresholds for geomorphic work prior to flow regulation must occur somewhere with in this range indicated by the arrow.

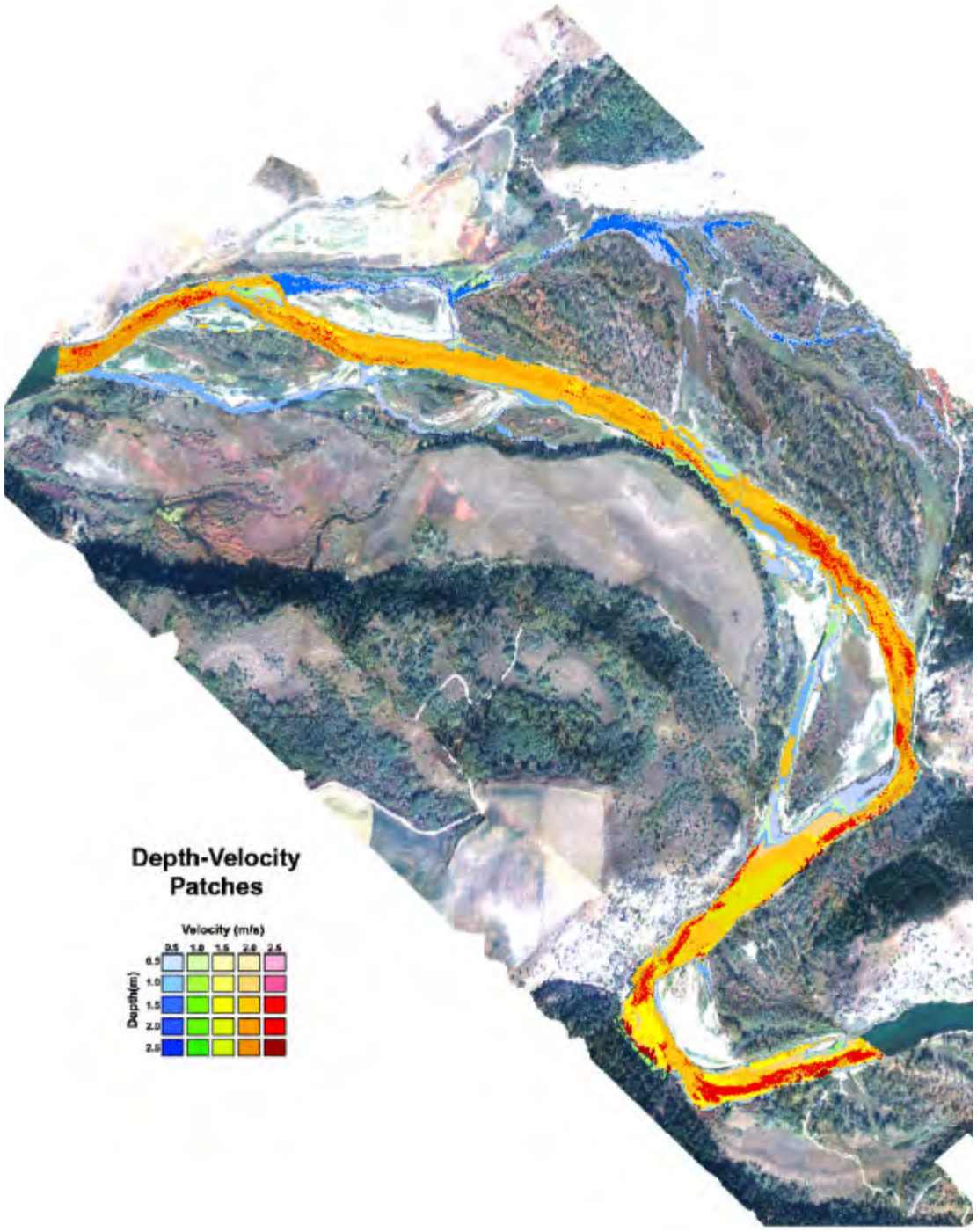

Figure 28. Graphical model of depth and velocity at 1x1 m resolution distributed across the Fisher floodplain. This is representative of various depth and hydraulic characteristics as they occur across a spectrum of discharges (see Appendix B).

and colored maps of the same data in Appendix B. We used our model to quantify and graphically express the frequency with which the various depth and hydraulic characteristics occur across the spectrum of discharges. We can thus also derive other data vital to evaluating river habitats and the ability of the river to do geomorphic work.

Stream power and Potential Geomorphic Work

As discussed above, the ability of the river to do geomorphic work is an essential component of maintaining the Shifting Habitat Mosaic that, in turn, is fundamental to a the river ecological integrity and sustainability. Using the hyperspectral data, we have developed an approach to modeling of stream power to determine more precisely minimum threshold levels of discharge necessary to do the geomorphic work necessary the SHM.

Stream power (P, W m^{-2}) is a fundamental measure of the potential of a river to perform work, such as bank erosion and sediment transport, resulting in specific outcomes (e.g., channel avulsion, formation of gravel bars). Bagnold (1966) defined unit stream power (P) as

$$P = \rho g h S V \qquad (4)$$

calculated along some length of river once spatially explicit estimates of the energy slope (S), water depth (h), and flow velocity (V) are determined and where ρ and g are the density of water and the gravitational constant, respectively. Equation (4) states that as water depth, flow velocity and/or slope increase, stream power increases proportionately. And, the more energy that is available to perform the geomorphic work of cut-and-fill alluviation and channel avulsion, the more regeneration there is of new habitat features. It is generally true for most of the river and channel bottom that stream power increases as discharge increases. However, this may not be

true everywhere on the floodplain nor across all discharges. In some areas as discharge increases, flow resistance (e.g., large wood jam, newly formed gravel bar) can alter the local energy gradient, reduce velocity, and locally reduce the available stream power. For alluvial channels this would result in sediment deposition and the formation of gravel bars.

Our modeling follows Equation (4) explicitly, hence at this time, we cannot accurately predict areas that have lower stream power at high discharges. However, we know these areas are small and represent some of the error we record in the contingency tables stated earlier. The mean fuzzy classification is 81 % valid classification of velocity for all discharges between 5,000 cfs and 11,000 cfs. We estimate that 15 % of remaining 19% error in the classified pixels are a result of the 1) rectification and GPS errors discussed above, radiometric differences within and between flight lines, turbulence induced error, and errors related with the accuracy of the Digital Elevation Model. Some portion of the remaining 5 % of error was associated with flow resistance. We would need to collect ADP data at a higher discharge to quantitatively assess the model accuracy above 11,600 cfs. Unfortunately, this was not possible during the low water volume years that dominated during this study.

We used a 30 m resolution USGS DEM (Digital Elevation Model) to estimate the slope of the water surface. This is only a rough estimate of (S) that captures the general slope inflections along the river. Some of the steeper slopes associated with rapids at the ends of bars and pool-riffle sequences are not completely resolved at the resolution of a 30 m DEM. To resolve some of the inherent variation and loss of detail associated with the coarse spatial resolution of the USGS 30m DEM, we focused additional effort on the Fisher floodplain where we conducted detailed surveys of water slope with a Leica survey total-station. Surveying the water surface slope for all of the floodplains was not feasible. In spite of the coarse scale of the

30 m DEM, the resulting power calculations for the other floodplains provided a reasonably accurate estimate of the spatial distribution of stream power along the floodplain study corridor. The slope value for all power calculations over all discharges was kept constant. Hence, the power estimates mainly reflect changes in water depth and flow velocity.

In our approach to modeling power, we set a large, coarse scale spatial pattern partially driven by the 30 m USGS DEM. However, within zones of similar slope we have great variability in stream power predictions because of the more accurate and spatially explicit direct measures and modeled estimates of water depth and flow velocity. We also increased the resolution of our estimates of lateral flooding by comparing modeled flood inundation with actual extent of flood wetted floodplain at three different discharge levels from 8,000, 11,000 and 37,000 cfs (note: the 37K cfs data were derived from an aerial video taken by Reclamation in 1997). Using these data, flow resistance becomes indirectly incorporated into our modeling estimates through the calibration of discharge and stage for each floodplain (Figure 29). This also corrected some of the error associated with the estimate of flooding and the actual accuracy level for each floodplain DEM.

After determining stream power for each within-channel pixel of the hyperspectral image based on the classification of DVPs and DEM slope, we reclassified each pixel based on the degree of departure from the mean power and then calculated each pixel as a function of the standard deviation. From this we selected the zones of high stream power (Figure 30) as those with the highest standard deviation departures above the mean. Displaying stream power in this manner spatially illustrates where along the river corridor stream power is high relative to the mean and incorporates fine detail associated with various channel morphology and water surface depth-velocity patches. Hence, this approach provided a valuable tool for predicting where

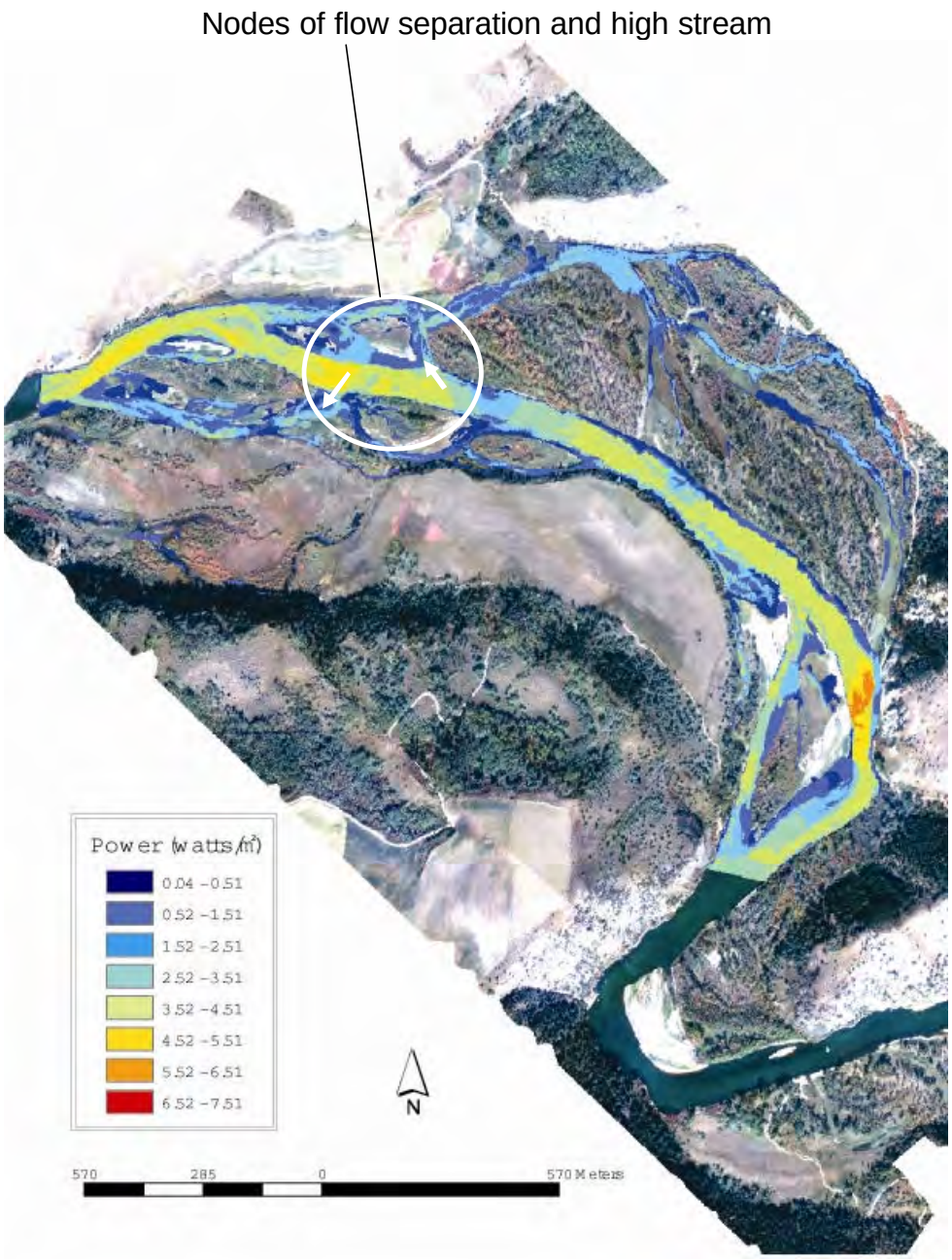

Figure 29. A plot of the spatial distribution of stream power (watts.m2) for the Fisher floodplain at a mean discharge level (19,000 cfs) required to create and maintain secondary channels throughout the Parafluvial zone. The white circle indicates areas where secondary channels are actively flowing and the main channel has relatively high stream power associated with those nodes of flow separation (white arrows).

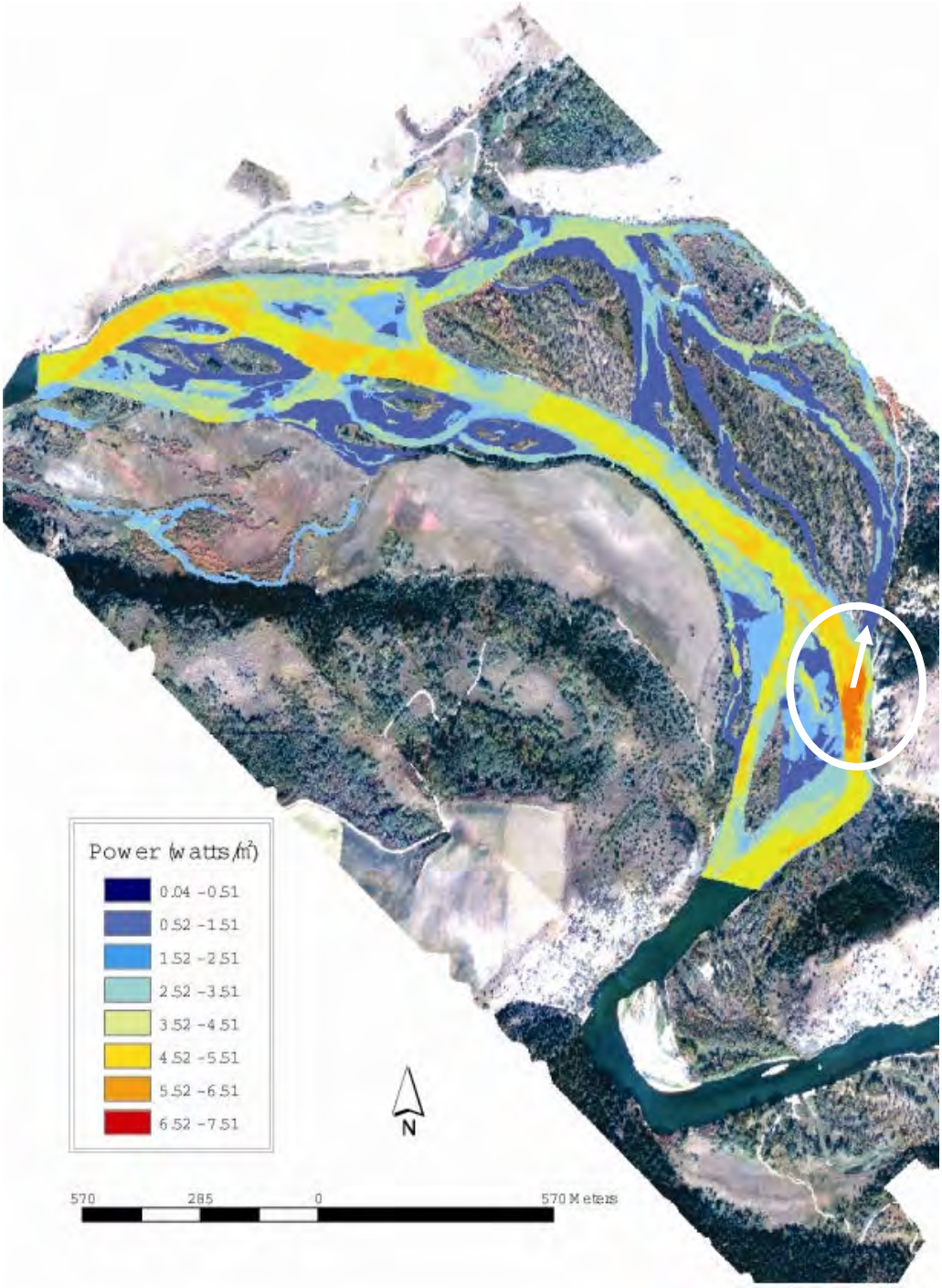

Figure 30. A plot of the spatial distribution of stream power (watts/m^2) for the Fisher flood plain at a discharge level (34,800 cfs) required for a potential orthofluvial avulsion event to occur in this particular flood plain. The white circle indicates a node of flow separation where an orthofluvial flood channel connects to the main channel and is correlated with a zone of high stream power. In this example the high stream power is directed straight towards an activated orthofluvial flood channel.

channel avulsions are likely to occur, as well as where processes of cut and fill alluviation are apt to be most active. These types of plots were made for 10 cm incremental increases in stage for each floodplain. Because we calibrated each individual floodplain stage and discharge relationship, we were able to not only determine the spatial distribution of potential geomorphic work, but also the corresponding discharge that might be associated with that geomorphic work. Integral to our thesis of stream power and geomorphic work is that when nodes of flow separation correlate with zones of high stream power, avulsion potential exists. Therefore, we can quantify important geomorphic thresholds by determining what discharge level is necessary to initiate a channel avulsion event.

We used the combined hyperspectral-GIS modeling approach to identify two geomorphic threshold levels defined by potential channel avulsion activity, first in the Parafluvial region and second in the Orthofluvial region of the floodplain. Parafluvial avulsion events result in the formation and maintenance of secondary channels within the annual scour zone of the river. Parafluvial cut and fill alluviation and avulsion are the first and minimum geomorphic threshold events needed as part of the long term sustaining processes of a viable SHM. Orthofluvial avulsion events result from complete abandonment of the main channel, or a splitting of the channel into a new main or secondary channel, that flows through Orthofluvial region. These events leave the abandoned Parafluvial region to become new off-channel and spring-brook habitats of the future Orthofluvial region of the floodplain and set new surfaces to be colonized by riparian vegetation.

We have developed two criteria to determine the discharge that corresponds to a minimum geomorphic threshold for potential Parafluvial avulsion and potential Orthofluvial avulsion. The criteria is similar for both types,

1) the formation of nodes of flow separation due to connection of Parafluvial secondary channels or Orthofluvial flood channels with the main channel (Figure 30).

2) the correlation of zones of high stream power associated with those nodes of flow separation (Figure 31).

The potential Parafluvial geomorphic threshold is the discharge when secondary channels, within the Parafluvial channel, begin to form and connect with the main channel and are also co-located with zones of relative high stream power (Figure 30). Likewise, a potential Orthofluvial geomorphic threshold occurs when Orthofluvial flood-channels connect to the main channel and are co-located with nodes of flow separation and high stream power (Figure 31).

We produced graphic representations of stream power as the standard deviation (see Appendix B) at 10 cm flood-stage intervals from 5,000 cfs up to 37,000 cfs. We recorded the discharge levels for each signature pattern of power that met our criteria for each floodplain at both Parafluvial and Orthofluvial levels of discharge. The criteria for assigning an upper threshold of highest potential was the discharge where further increase in stage did not produce significant changes in the first two criteria. From our analysis, we concluded that on average for all floodplains a minimum of 15,000 cfs is required for Parafulvial avulsion potential to initiate and that at 20,000 cfs the highest potential was reached (Table 5). Our Orthofluvial threshold analysis concluded that on average among all floodplains a minimum of 28,000 cfs is required for avulsion events to potentially initiate. At 34,000 cfs the highest potential for Orthofluvial

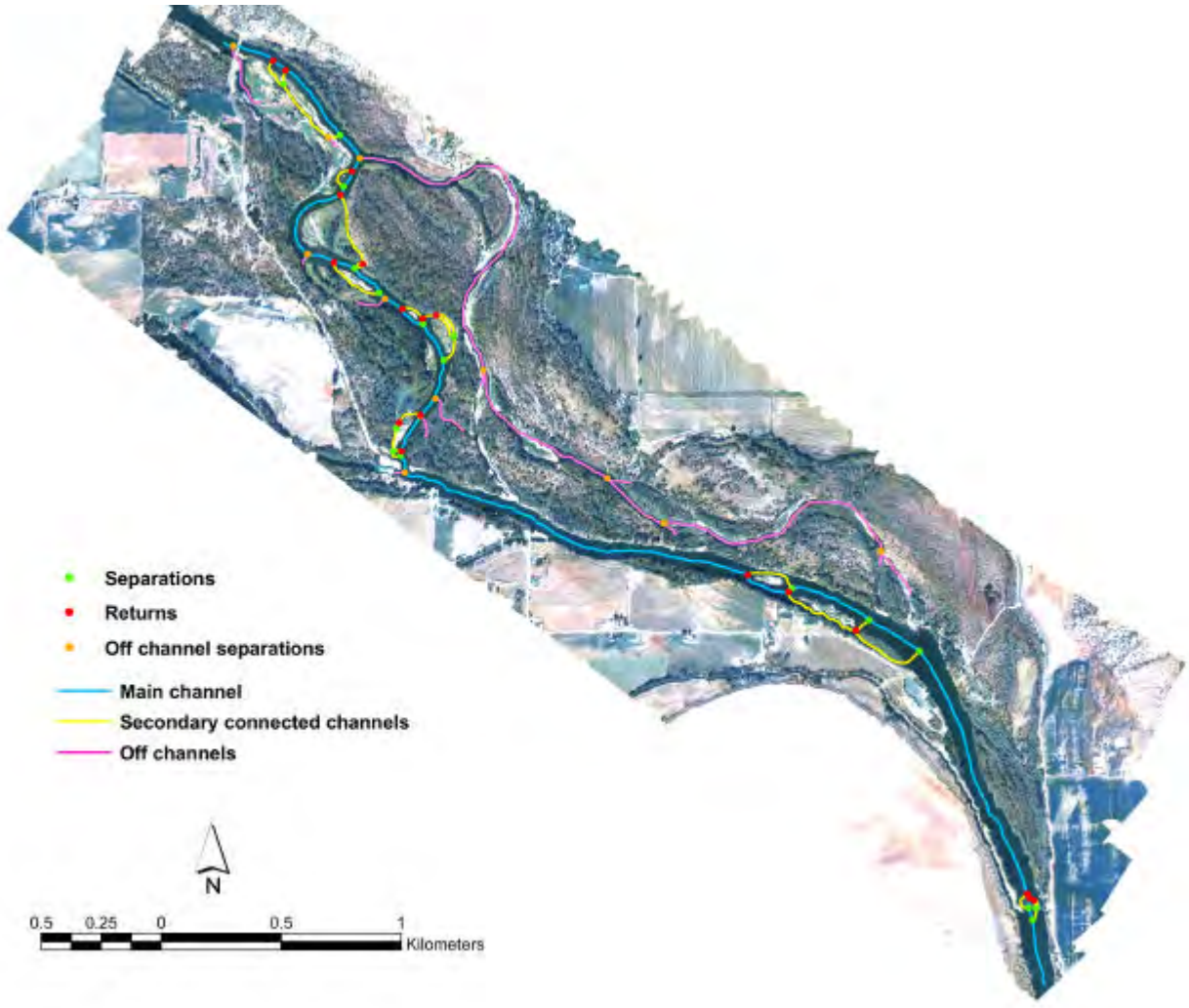

Figure 30. Hyperspectral image showing nodes of flow separation and returns, off channel separations and different associated channel types (main channel, secondary channels and off-channels). Geomorphic complexity can be determined automatically within a GIS and measured by identifying these variables within the hyperspectral imagery.

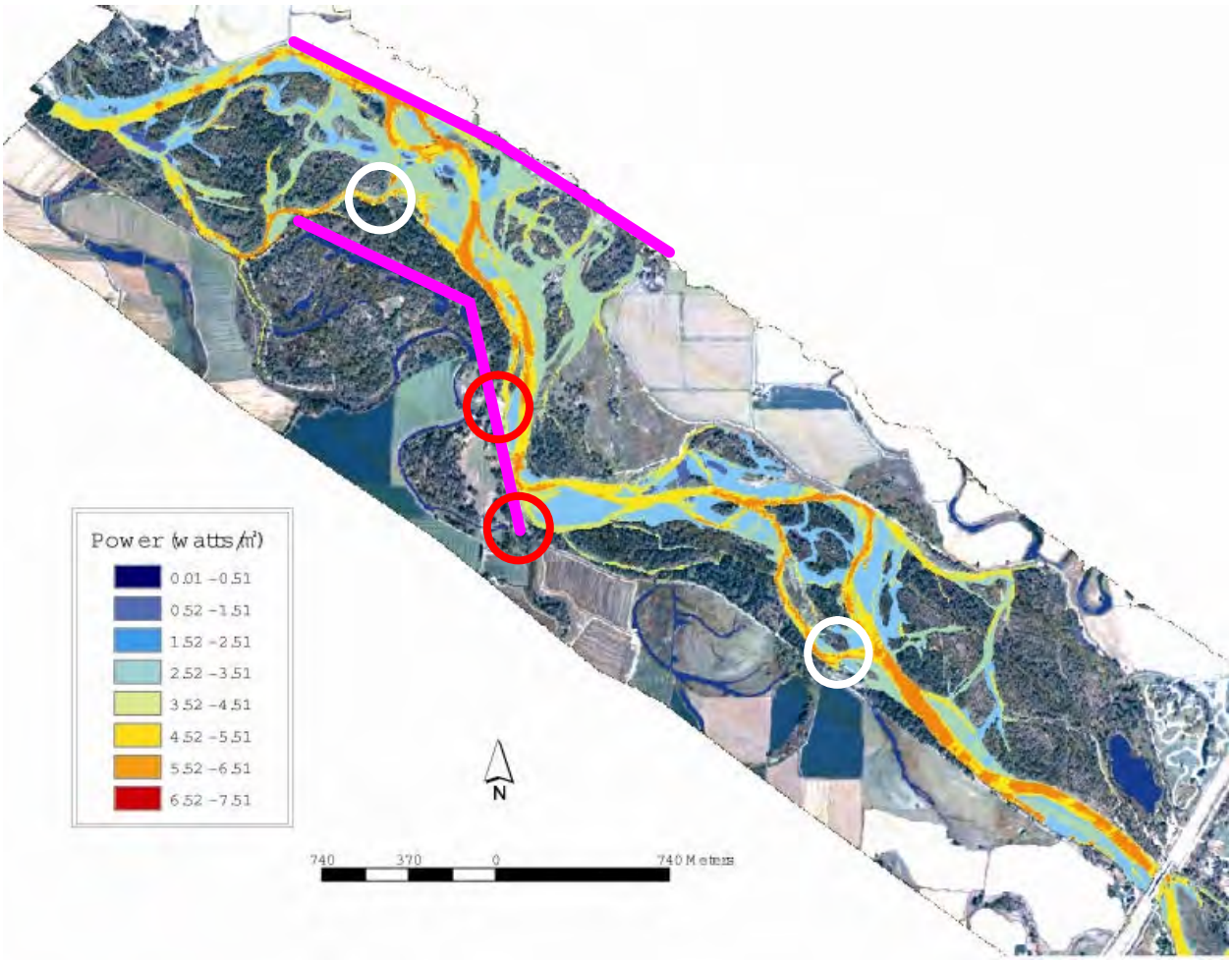

Figure 31. A plot of the spatial distribution of stream power (watts/m^2) for the Lower-Twin flood plain just above the confluence with the Henrys Fork River at a discharge level (27,000 cfs) required for a potential Orthofluvial avulsion event to occur in this particular floodplain. The white circles indicate nodes of flow separation where an Orthofluvial flood channel connects to the main channel and is correlated with zones of high stream power. The red circles indicate nodes of *potential* channel avulsion, however construction of a rock revetment (pink lines) is preventing the activation of the existing Orthofluvial flood channels and the possibility of an Orthofluvial avulsion to occur.

Table 5. A comparison of the range of discharges ($X10^3$ rounded to the nearest 500 cfs) necessary to promote Parafulvial and Orthofluvial geomorphic work. The numbers in parenthesis are the mean values.

Flood Plain	Parafluvial	Orthofluvial
Swan	5 to 19 (12)	20 to 37 (28.5)
Conant	11 to 19 (15)	20 to 26 (23)
Fisher	9 to 24 (16.5)	26 to 34 (30)
Heise	5 to 21 (13)	21 to 37 (29)
Upper-Twin	13 to 18 (15.5)	22 to 34 (28)
Lower-Twin	13 to 18 (15.5)	22 to 34 (28)
total means	9 to 20 (15)	22 to 34 (28)

avulsion was reached (Table 5). Increasing discharge above both maximum potential would simply increase the rate or intensity at which geomorphic work could be preformed.

The results show that there is variation between floodplains (Table 6) and that each floodplain has a slightly different balance between the available stream power to transport sediment (i.e., capacity), the supply of sediment and limitations of lateral floodplain expansion. The more confined a floodplain, the smaller the lateral extent and the higher stream power for a given discharge. A confined reach results when lateral expansion is limited and the capacity of the stream is greater than the supply of sediment. As soon as supply becomes greater than capacity, gravel bars begin to form that ultimately have the potential to force channel avulsions. Both the Swan and Upper and Lower Twin floodplains have broad flood plains due to limited valley confinement; whereas Conant, Fisher and Heise have greater degrees of valley confinement.

Higher supply of sediment, relative to stream capacity, results in greater number of avulsion nodes and the broader range over which Parafluvial and Orthofluvial avulsion events can occur. Geomorphic complexity is also related to the number of separation and convergence nodes per river kilometer. Thus, geomorphic complexity and threshold discharge levels are related. Moreover, geomorphic complexity is then easily identifiable from airborne remote sensing data (Figures 30 and 31). The more separation nodes, the higher the frequency of secondary channels, off-channels and backchannel habitat that exist in the floodplain. Thus, the frequency of separation nodes and reconnections is a measure of channel complexity. On the Snake River study area Upper and Lower Twin floodplains were the most complex and Fisher the least (Table 6). Increasing the amount of power available to do work on the floodplain, by

Table 6. A comparison of the metrics used to assess geomorphic complexity for each flood plain studied. Twin is the widest and most complex flood plain and Fisher is the most confined and lowest geomorphic complexity.

Flood Plain	Main Channel (km)	Seconday Channel (km)	Off channel (km)	Separations	Off Channel Separations	Average Separtions per river km
Swan	7.9	12.3	5.0	48	20.0	6.1
Conant	8.0	5.8	1.1	43	13.0	5.4
Fisher	4.1	3.1	1.6	8	11.0	1.9
Heise	6.5	3.6	5.3	18	12.0	2.8
Twin	17.5	27.2	7.1	152	50.0	8.7

allowing higher discharges and increasing the duration of discharge above threshold levels will result in the creation of more diversity of floodplain habitat. However, this only applies for floodplains that are not limited in lateral expansion by levees and rip-rap. The Upper and Lower Twin floodplains and Heise floodplain have the greatest amount of floodplain encroachment due to levees. The nodal-stream power analysis shows clearly that Upper and Lower Twin and Heise have limitations on potential avulsion events due to the construction of rock levees that are preventing the river from avulsing into old Orthofluvial flood channels beginning at a discharge of 27,000 cfs (see Table 6).

Analysis of Aquatic Habitats

We combined the hyperspectral imagery, the corresponding analysis of depth and velocity, stream power, the nodal analysis of channel complexity and our general understanding of aquatic habitats and developed an analysis and GIS mapping of aquatic habitats across each of the floodplains and for each of the five discharge regimes; 1500, 5000, 11600, 25000, and 37000 cfs. Illustrated here is the aquatic habitat mapping of Fisher floodplain at 11,600 cfs (Figure 32). The aquatic habitat maps for all floodplains and each discharge are illustrated in Appendix B.

We classified aquatic environs on the Snake River floodplains into 14 distinct aquatic habitats. There were 6 habitat types associated with turbulent runs; low turbulent runs (ltr), medium turbulent runs (mtr), and high turbulent runs. Low turbulent runs are characterized by relatively low slopes and extended river length where swirling and lightly turbulent waters reach the water surface. Medium turbulent runs are similar to ltr habitats, but have relatively faster velocities and greater interaction with the substratum being expressed at the surface as the presence of standing waves. High turbulent runs are very fast waters, often >2 m/sec, with

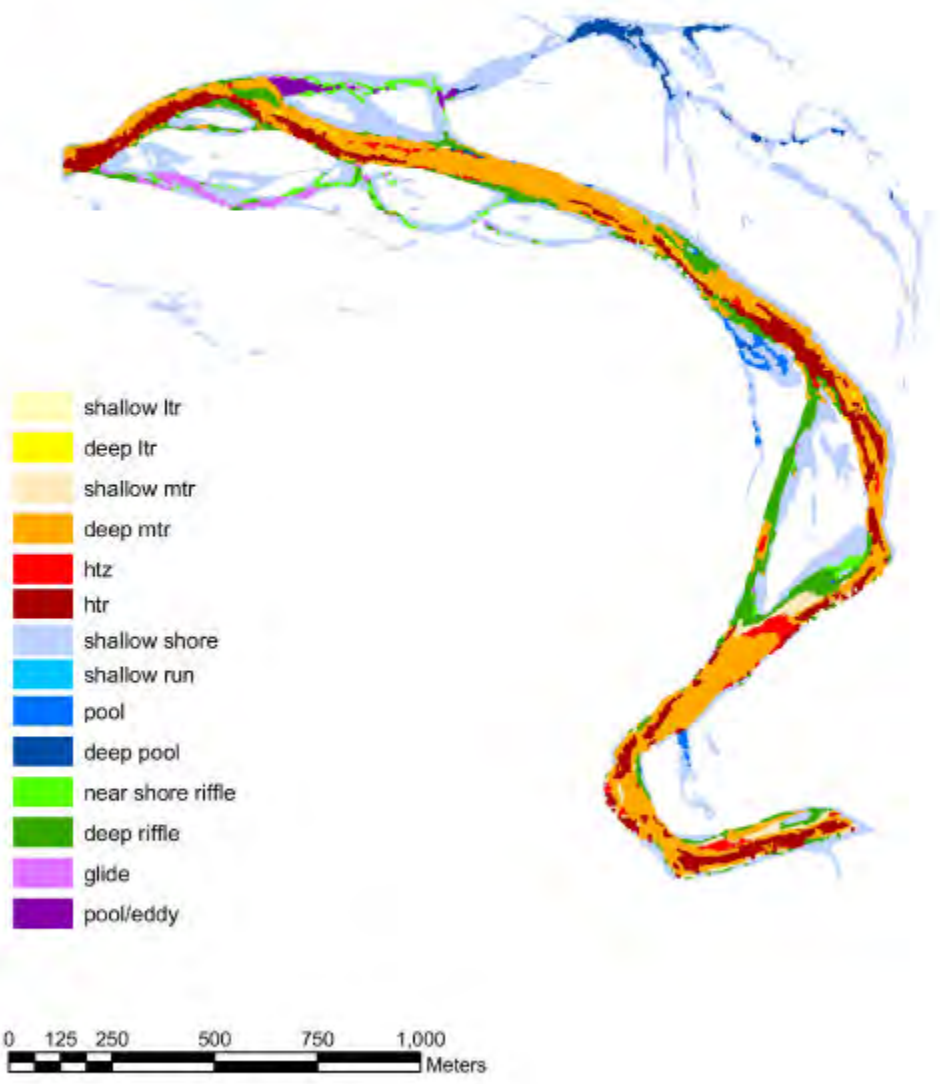

Figure 32. Aquatic habitats of the Fisher floodplain during a discharge of 11,600 cfs separated into 14 distinct ecologically meaningful habitat types. Habitats vary with change in discharge.

surface boils and a dominance of standing waves present on the water surface. In Swan and Conant floodplains, turbulent runs were the most prevalent habitats across most discharges (Figure 33 a-e). Medium and high turbulent runs became increasingly prevalent as discharge increased on all floodplains. The combined analysis of Upper and Lower Twin (Figure 33e) increased in turbulent runs the least among all floodplain complexes.

The nearshore shallow habitats that generally form the hydraulic zone between fast moving waters near the center of the river channel (i.e., thalweg) and the riparian shoreline were highly prevalent across all floodplains and all discharges. Interestingly, the general trend toward increasing shallow shore habitat with increasing discharge was never continuous on a floodplain nor was it consistent between floodplains. This is consistent with the general observation that as discharge increases shallow slow moving aquatic habitats increase and decrease in size as Parafluvial and Orthofluvial regions of the floodplain are inundated. Since we found that each floodplain had its own specific inundation pattern as a function of its landscape scale geomorphology, this important habitat feature increased and decreased in non-linear patterns.

Pools and deep pools, consisting of calm standing waters connected to the main channel, were highly variable in frequency among and between floodplains. For example this habitat became most abundant in the Twin floodplains as discharge was at high flood stages; in contrast, pools were comparatively absent from the Swan floodplain regardless of discharge. We found pools and deep pools where ever the main channel backed waters into off channel reaches composed of floodplain geomorphology derived from an old, abandoned channel. We found this type of habitat least prevalent in the Swan floodplain where most of the complexity is derived from side channels that remain connected to the main channel.

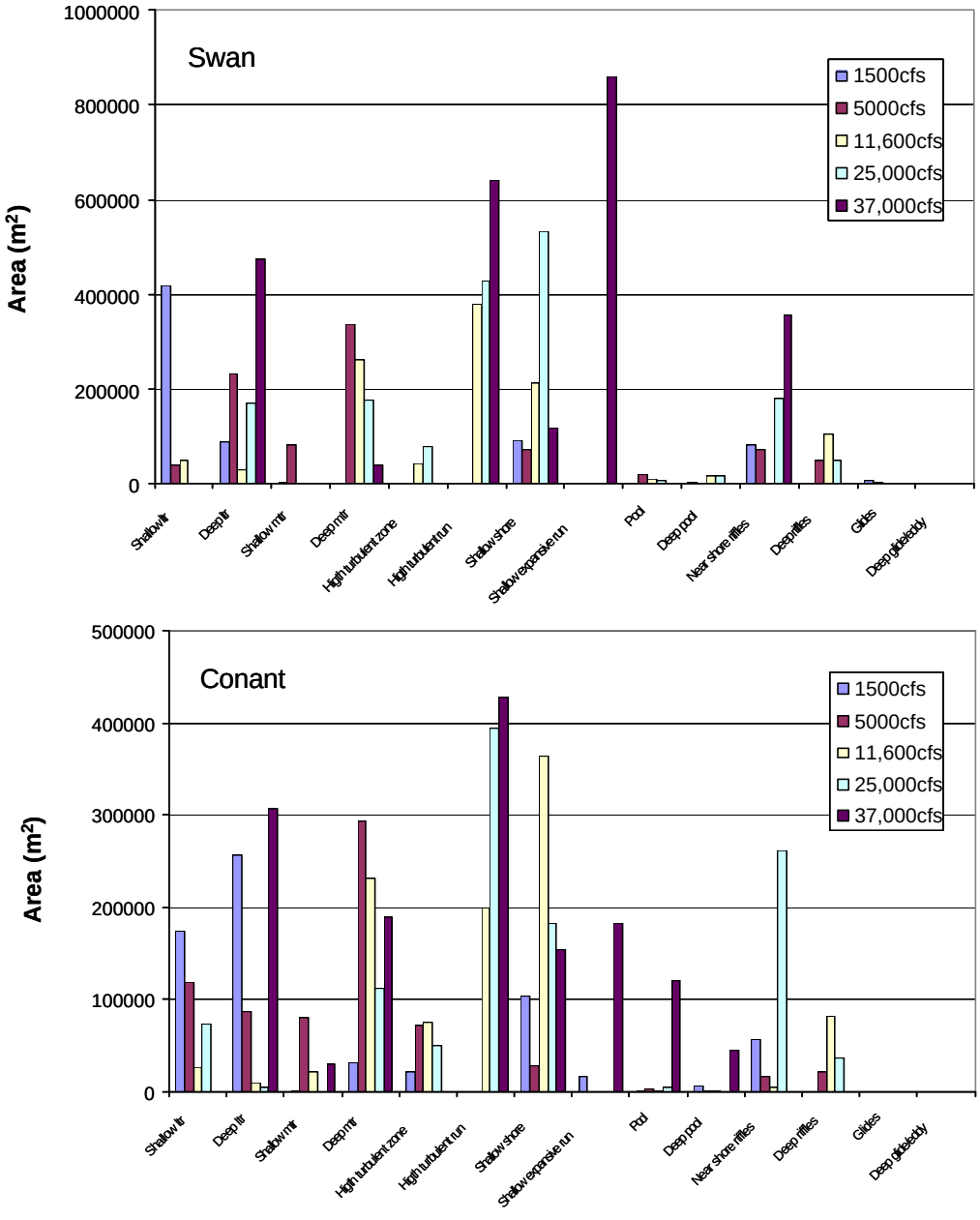

Figure 33a-b. Histogram of aquatic habitat frequency expressed as total area on the Swan and Conant floodplains of the Snake River. Absolute areas occupied by each habitat varies in response to change in discharge from 1,500 to 37,000 cfs.

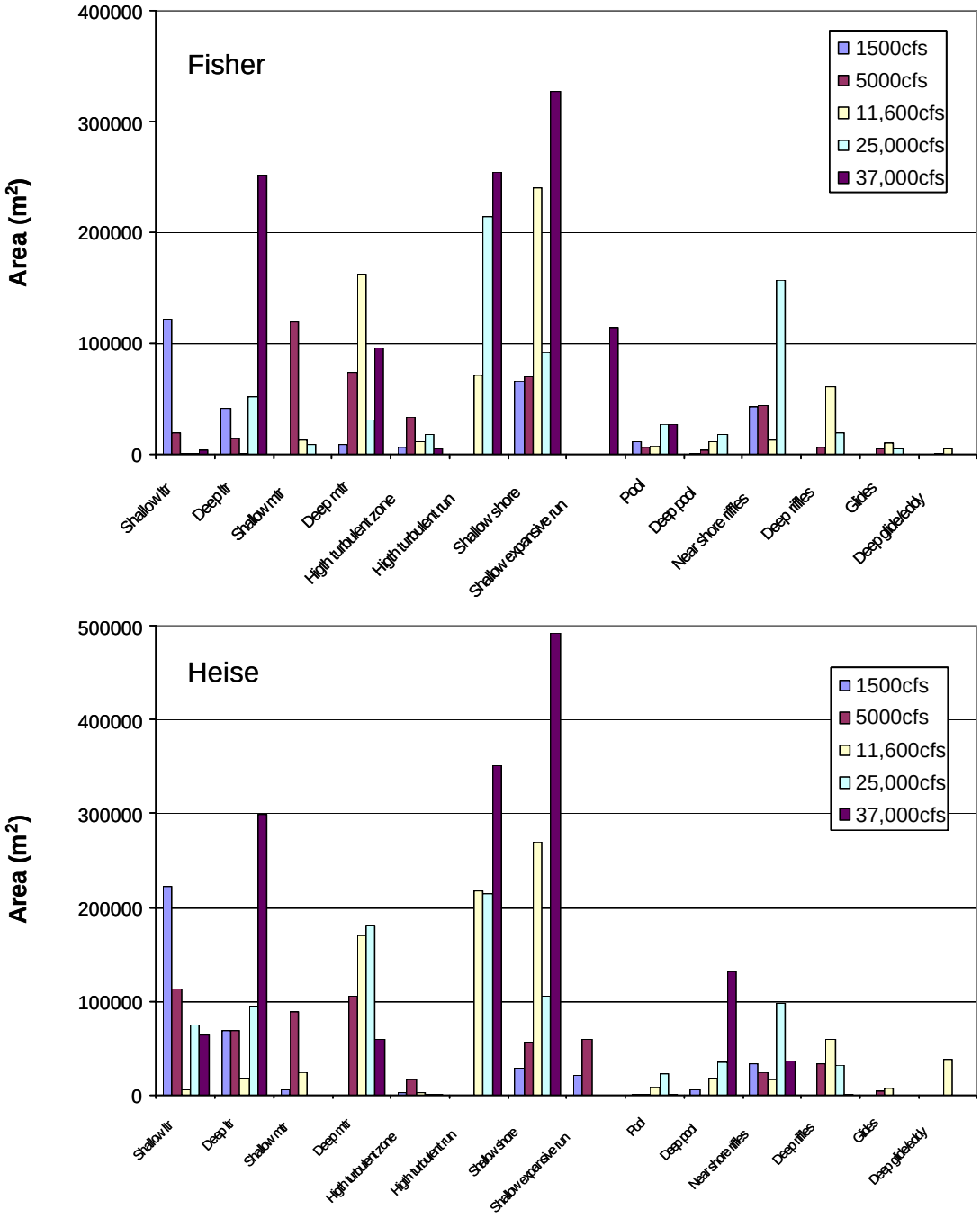

Figure 33c-d. Histogram of aquatic habitat frequency expressed as total area on the Fisher and Heise floodplains of the Snake River. Absolute areas occupied by each habitat varies in response to change in discharge from 1,500 to 37,000 cfs.

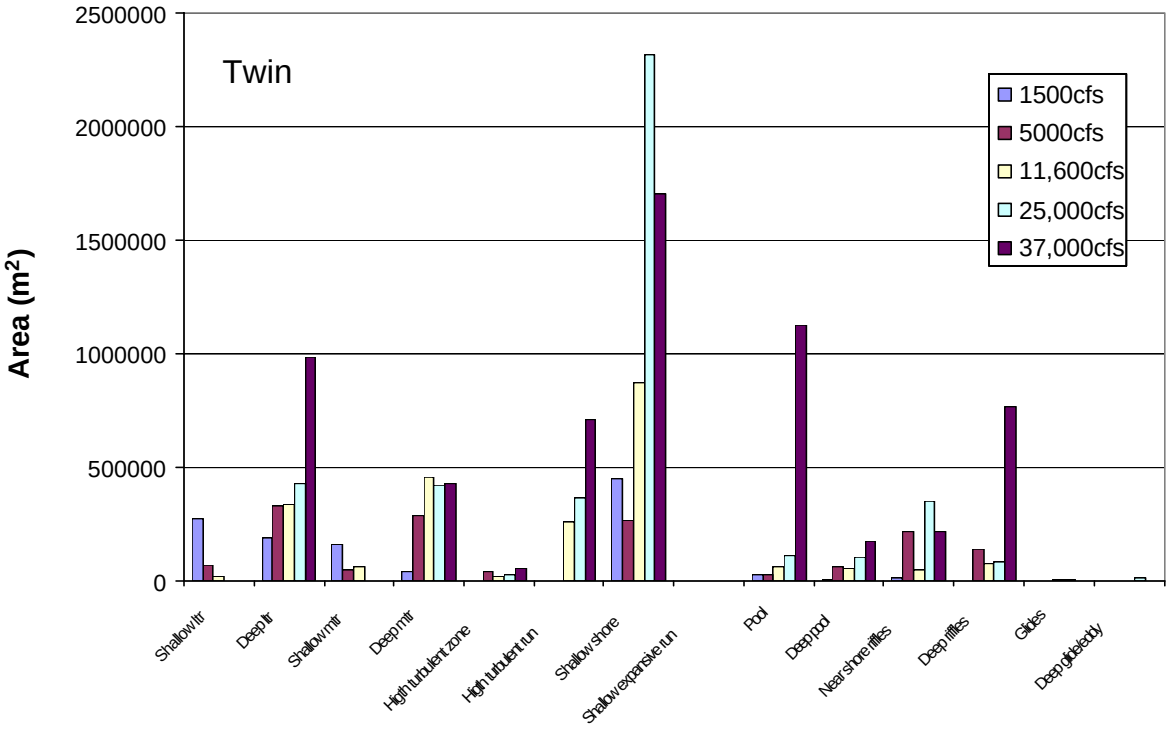

Ltr = low turbulent run
Mtr = medium turbulent run
Htr = high turbulent run
Variation between low, medium and high turbulent runs are discussed in text

Figure 33e. Histogram of aquatic habitat frequency expressed as total area on the Upper and Lower Twin (combined) floodplains of the Snake River. Absolute areas occupied by each habitat varies in response to change in discharge from 1,500 to 37,000 cfs.

Riffles and deep riffles are characterized by fast flowing, but relatively shallow water, that produces a distinctly broken surface flow appearing as choppy and sometimes indistinct waves. Riffles and deep riffles are extremely important habitat. These habitats tend to be among the most productive per m^2 for benthic macroinvertebrates, which are the primary food items of salmonid fishes living in river environments. We found near shore and deep riffles to generally increase in frequency as discharge increased. But, as one might expect, these habitats are highly variable spatially with change in discharge. In short, they move around on the floodplain as the river increases in discharge and what may have been a riffle habitat at a low discharge becomes part of a high turbulent run at high discharge.

We found habitats that could be classified as glides and eddies (i.e., slow moving with little disturbance of the surface) as composing a comparatively small portion of the aquatic habitats across all floodplains and discharges. This may be partly because as inundation occurs slow moving waters were more often classified as low turbulent runs.

Among the most important of habitat characteristics is the rapid transition of adjacent but dissimilar habitats forming sharp edges of high transition, particularly flow velocity; for example, where deep medium to high turbulent runs contact very slow moving backwater glide habitats (Figure 34). The quantity of sharp edge habitat can be remarkably abundant, several times the total length of the floodplain, and change dramatically with changing discharge. This is clearly seen in the example of the Fisher floodplain where over a river length of about 2 km the quantity of edge habitat between fast moving waters and slow is in excess of 14 km when the discharge was at 5000 cfs and increased to more than 22 km over the 2 km reach as discharge increased to 11,600 cfs.

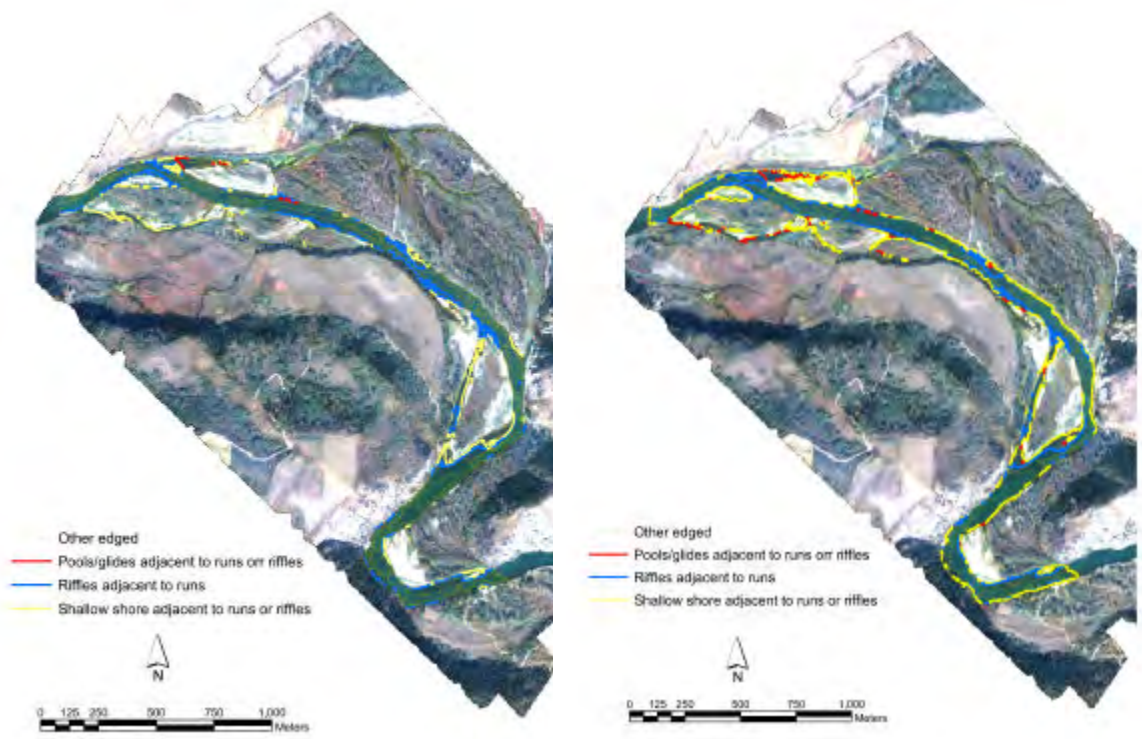

Figure 34. Hyperspectral image of the Fisher floodplain illustrating the transition and frequency of edges between aquatic habitats with markedly different hydraulic and depth characteristics. The left panel is representative of habitat edges at 5000 cfs, the right panel is representative of habitat edges at 11,600 cfs.

This is the first time that we are aware, where aquatic habitats have been evaluated in this detail derived from remote sensing of river depth and velocity. Therefore it is not possible to compare how aquatic habitats of the Snake River have changed from before dam operations to today. However, based on fundamental principles of river hydrology and understanding of river floodplain ecology, we expect that the aquatic habitats have been becoming increasingly simplified. This is consistent with the concept of the Shifting Habitat Mosaic and the processes that sustain it and the resultant complexity of habitats that are available to support a diversity of organisms.

As ecologically based systems management decisions may be instituted, continued analysis of aquatic habitats and the complexity of corresponding edge habitats will be a highly useful tool in evaluating the long-term success of management actions. We would expect for example, that as stream power is reapplied to the river floodplains resulting in increased substrate mobility and cut-and-fill alluviation, there would be a corresponding increase in the complexity of aquatic habitats and an increase in the frequency of high transition edges. Thus, this variable can become an excellent metric of management success in the context of monitoring efforts established to evaluate management success.

Riparian Vegetation

We used the hyperspectral imagery to classify floodplain vegetation. We used imagery taken in the autumn to maximize spectral differentiation of the various species. Imagery was collected when discharge was at 5000 cfs; thus, all references to vegetation, water surface, cobble or other classified cover types are given as percentages and are based on the entire floodplain.

We were able to differentiate vegetation within the gallery forest between cottonwood and willow and classify herbaceous vegetation into mixed grasses, dry grass and the non-native reed canary grass (Figure 35). The cover type labeled as "open gallery" appeared as shadows in the imagery. Shadowed pixels represent areas where there was very little to no reflectance of light back to the hyperspectral imager during data collection. This occurred almost exclusively where the gallery forest either opened in the interior of the canopy or along a canopy edge. We were able to interpret these shadows as heterogeneity and breaks in the canopy surface, which allowed surface light to penetrate the gallery forest, but did not reflect light back out. We observed the highest degree of shadow mixed within the gallery forest canopy in the most complex floodplains (Swan and Upper and Lower Twin; see Appendix B and Figure 36).

Our analysis of channel complexity (Figures 30 and 31) suggest that the legacy of hydrologic characteristics and interactions between river power and floodplain sediment supply also leads to the highest gallery forest complexity. This has strong implications for the long-term sustainability of both flora and fauna dependant on the sustainability of channel complexity and the viability and restoration of processes that sustain the Shifting Habitat Mosaic. This is highly significant in the consideration of flora diversity and complexity of riparian habitats. For example, the Ute ladies' tresses (*Spiranthes diluvialis*) occur in fine sediment filled, Orthofluvial channels abandoned following avulsion. These rare orchids do not appear in either very old (>150 yrs) nor in recently abandoned channels (<25 yrs). Thus, the long term sustainability of Ute ladies' tresses and other plants like it may very well be dependant on the sustainability of the Shifting Habitat Mosaic and the floodplain complexity associated with re-engaging river power , the river channel and the riparian regions of the floodplain. We address this issue in greater detail in the following section.

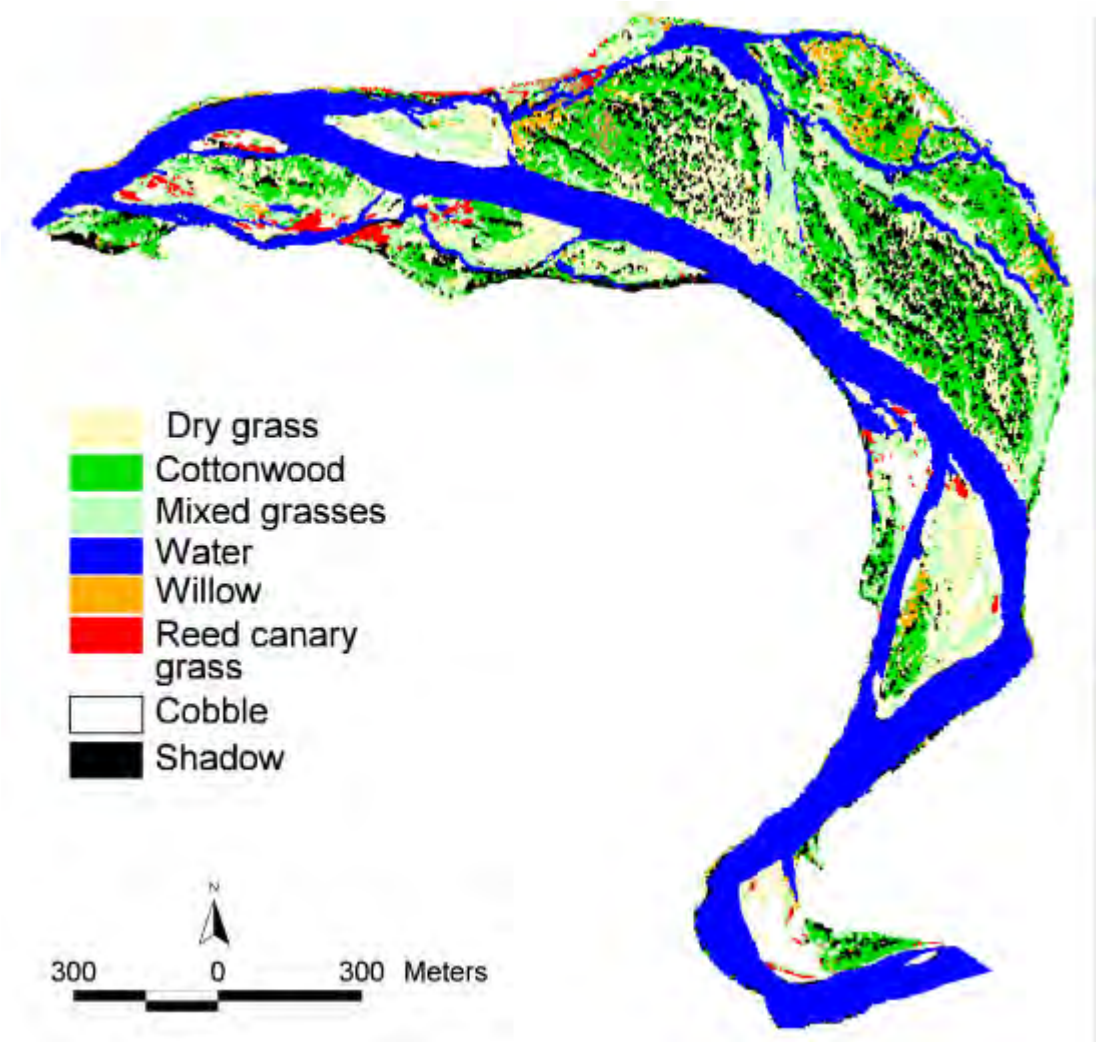

Figure 35. Classified hyperspectral image of the Fisher floodplain illustrating the differentiation of various vegetation coverages. Image acquisition illustrated here was at 5,000 cfs.

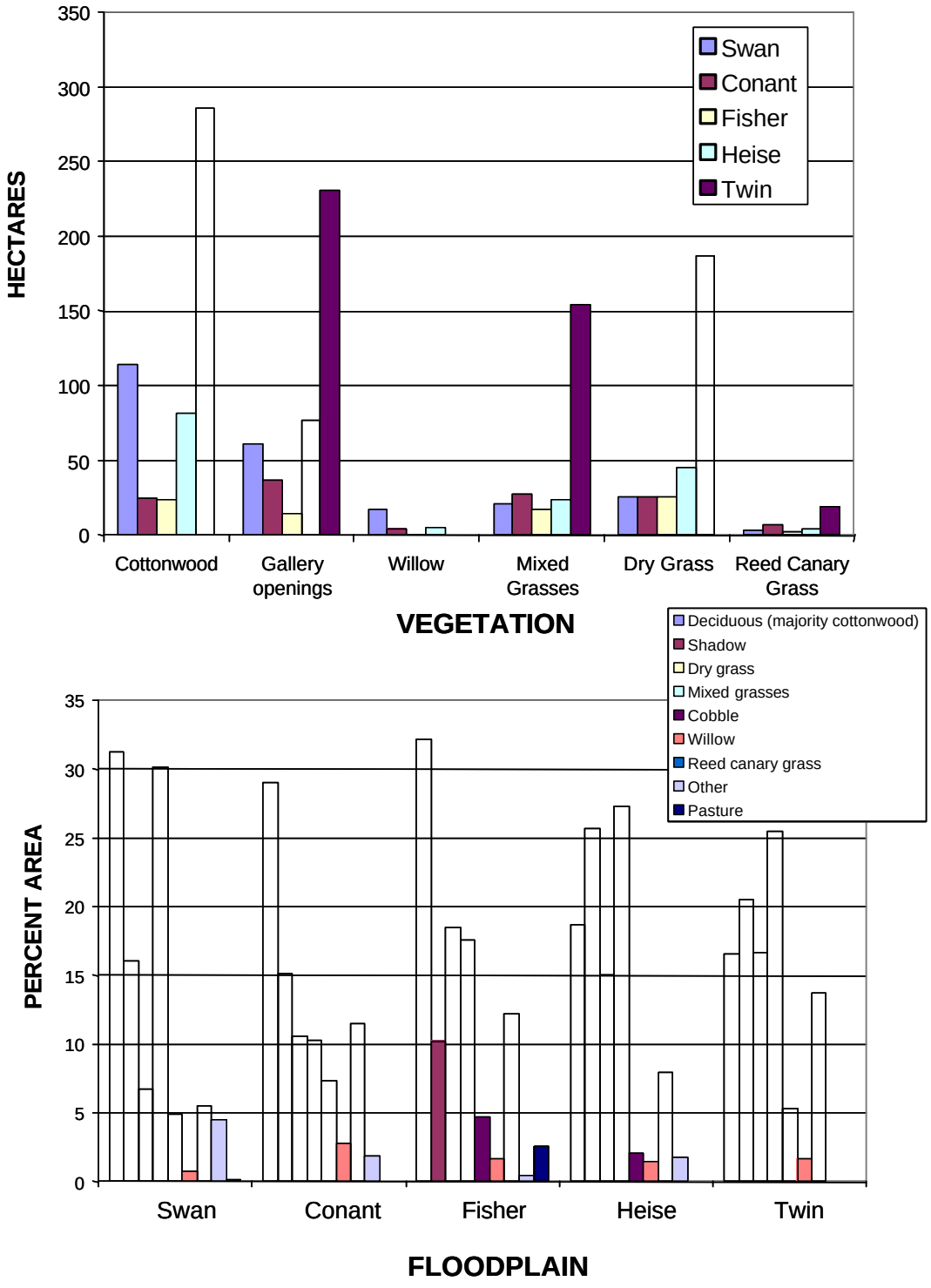

Figure 36. Upper panel illustrates the area (hectare = 100x100m) of different vegetation types on each floodplain. The lower panel illustrates the percent area of the various vegetations across floodplains.

ECOLOGICALLY BASED SYSTEMS MANAGEMENT:

FINAL ANALYSIS AND RECOMMENDATIONS FOR SYSTEM RESTORATION

Evaluation of Flow Regimes, Aquatic Habitats, and Floodplain Vegetation

In the INTRODUCTION section of this report, we introduced 5 critical intervals of the annual discharge regime necessary for Ecologically Based Systems Management to address to restore the range of ecological function to the Snake River study area (see Figure 3). Each interval addresses specific ecological bottlenecks that directly or indirectly affect the Shifting Habitat Mosaic or the life histories of the organisms using these environments and habitats.

During the winter (Interval 1), the primary concern is winter aquatic habitat for native fish and by inference other native species that are pre-adapted to natural winter flow regimes of the Snake River. Prior to dam construction, dam operation and control of winter flows, the long-term average of discharge in mid-winter was approximately 2500 cfs (Figure 37). The minimum flows during winter for each day from December through March fluctuated between 1500 and 2000 cfs. Our analysis of aquatic habitats at these low flows revealed a comparatively high frequency of shallow low turbulent runs, shallow shore, and shallow near shore riffles (Figure 33 a-e). The frequency of these slower waters decrease, both in real terms and as a function of overall percentage of total aquatic habitat, as flows approach 5000 cfs (Figure 33).

Maintaining low flow habitat during cold water temperatures is particularly important as fishes seek to minimize activity as metabolic rates decrease and their ability to sustain position in rapidly moving waters diminishes. It is also important to maintain similar flow regimes throughout the winter period, rather than manipulate flows in response to anticipated high or low water volume (Figure 37), which addresses the issues highlighted in Interval 2 (see Figure 3).

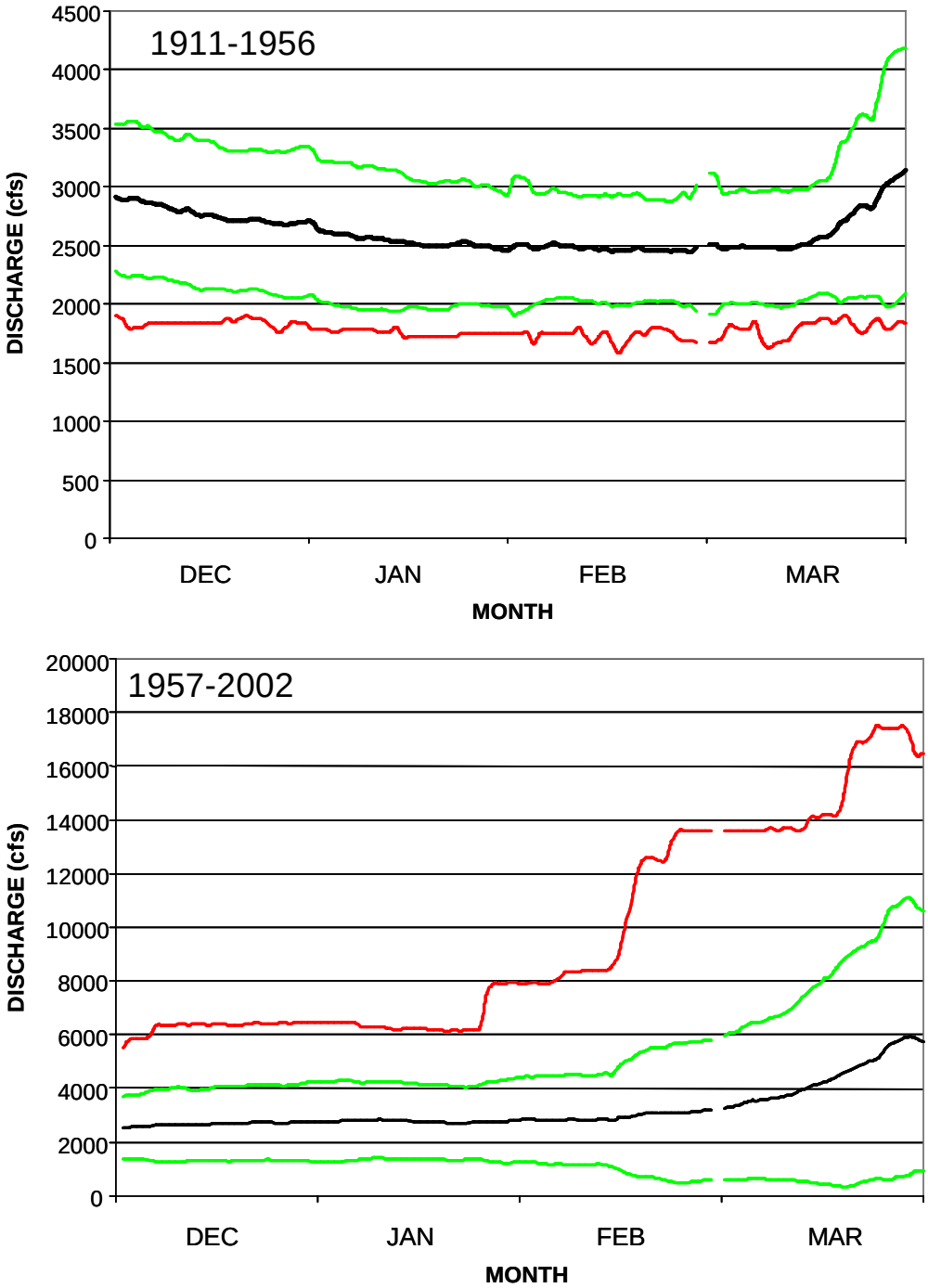

Figure 37. Upper panel represents the pre-dam winter hydrograph; the lower panel is the winter hydrograph since dam operations began in 1957. Black lines are the mean discharges, green lines are the standard deviation. In the upper panel the red line is the minimum daily discharge for the period of record pre-dam; the red line in the lower panel is the maximum daily discharge post-dam.

Early reservoir draw-down has resulted in significant change in the flow regimes of the Snake River in many years with flows in mid-winter often reaching 5000 to 6000 cfs. The maximum winter discharge illustrated in Figure 37 shows discharges increasing as early as late January and exceeding 10,000 cfs by mid-February. This is, with all likelihood, very deleterious to the fishery and other organisms associated with the aquatic habitats of the Snake River in the study area. Response to reservoir water volumes and anticipated should be addressed during the natural spring freshet period, which typically began in the pre-dam period after April 1.

In sections above, we discussed the minimum geomorphic threshold discharge levels necessary to initiate mobilization of the gravel/cobble bed-sediments of the floodplains in the study area. This and the duration of those flows are the focus of Interval 3 (Figure 3). Geomorphic work not only depends on the peak flows and the exceedance of threshold discharges, but also depends on the duration of these discharges, and thus, the length of time over which work is done. Costa and O'Connor (1979) demonstrated that for some stream systems in the Cascade Mountains, extreme discharges of short duration did not do significant amounts of geomorphic work compared to lower level discharges that were maintained over much longer durations. They concluded that this was mainly a characteristic of well vegetated floodplains exposed to flashy discharge regimes (e.g., climatically event driven spates of high peak discharge but very short duration).

In order to address the duration factor, we examined the relationship between discharge and total cumulative power applied to the floodplain. We determined the relationship of discharge to cumulative power for approximately 1000 cfs increments from 1500 to 37,000 cfs for the Fisher floodplain (Figure 38). We then used a best-fit, third-degree polynomial regression

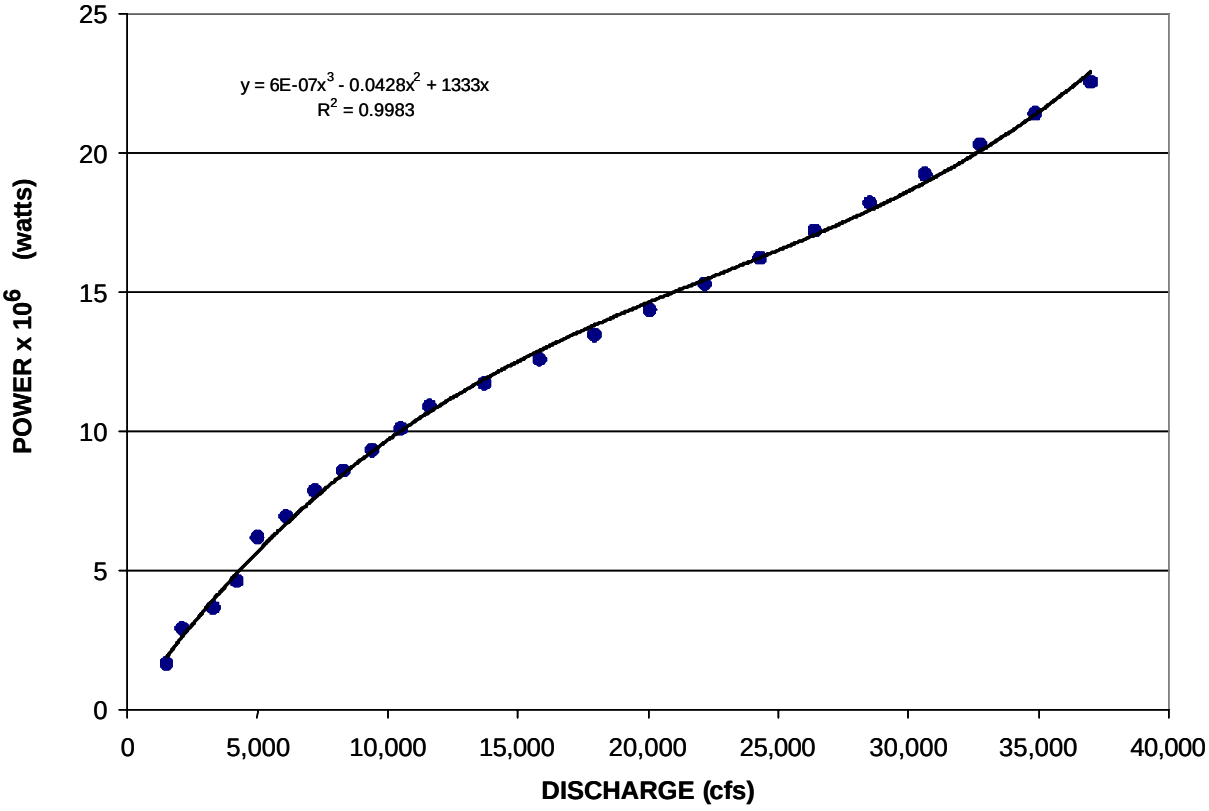

Figure 38. The relationship between discharge and total available stream power acting on the Fisher floodplain. Data are derived from the hyperspectral imagery, modeling of depth and velocity and the determination of river power across discharge regime from 1000 to 37,000 cfs.

equation to correlate stream power across discharges:

$$Y = 6 \times 10^{-7}x^3 - 0.0428x^2 + 1333 \qquad r^2 = 0.99 \qquad (5)$$

Based on our earlier analysis of the discharges necessary for Parafluvial avulsion, we estimated daily power for the Fisher floodplain comparing the annual distribution of power for various historical discharge events as discharge exceeded 19,000 cfs. We selected 19,000 cfs as this is the average threshold discharge to initiate Parafluvial avulsions. We selected the 10 water years with the highest total annual discharge prior to dam construction and applied the power analysis for each of the 10 years (Figure 39). We compared these data to 10 water years with the highest total annual discharge after dam construction and applied the power analysis for each of the years (Figure 39). Although total volume of water in the before dam and after dam years were similar, there was a significant reduction in power available to do geomorphic work in the after-dam years (Figure 39). Clearly, this is mainly due to the reduction of both peak flow and duration of flows exceeding 19,000 cfs as flood control strategies that have been integral to the management practices and general operation of Palisades dam.

The following power analysis examines how duration of the annual flood volume of water can be used to maximize the available stream power to do the geomorphic work. We compared the total annual cumulative power when 19,000 cfs is achieved or exceeded among each of the 20 highest discharge volume water years prior to dam operation (Figure 40; black data points) with the 10 largest flood years for the dam operation after 1957 (Figure 40; blue data points) [Note: these are the cumulative power data as appear in Figure 39, but with 20 years covered before the dam].

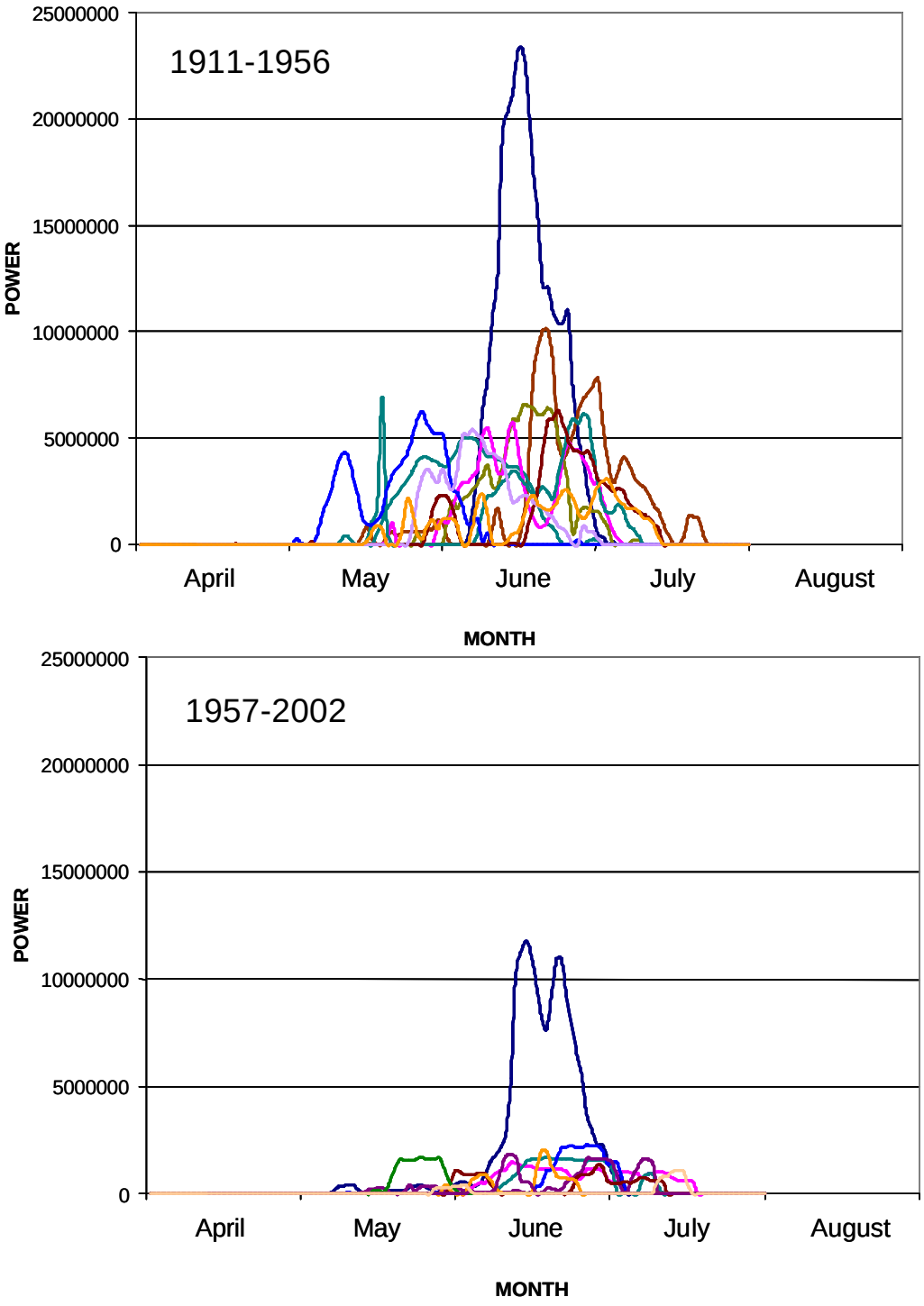

Figure 39. Upper panel illustrates the total daily power (total watts/floodplain) on the Fisher floodplain for the 10 highest water years prior to dam operations; the lower panel illustrates the comparative data for the 10 highest water years post-dam.

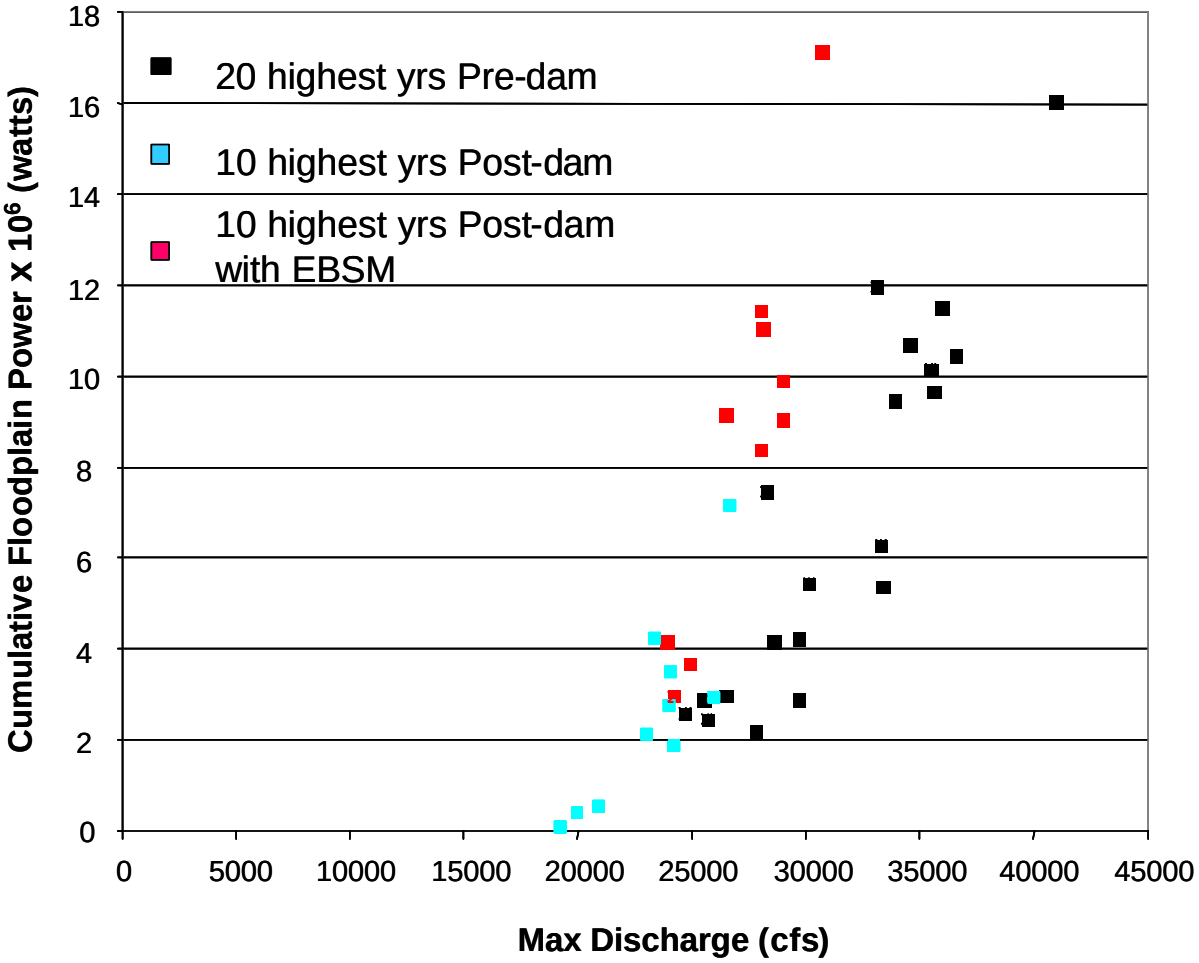

Figure 40. Cumulative annual power (watts/floodplain) on the Fisher floodplain for the 20 years of the highest water volume discharge prior to dam construction (black data points), for 10 years of the highest water volume discharge after dam construction (light blue data points, and for 10 years of the highest water volume discharge after dam construction with Ecologically Based System Management discharge scenarios applied to the annual hydrographic regime

Recall from our earlier analyses above that peak discharge among post-dam years (except for 1997) have remained under 30,000 cfs with annual cumulative power between 2 and 4 x 10^6 watts. Also as discussed above among post-dam water years, peak discharge in very wet years achieved the highest maximum discharges only approaching the 28,000 cfs threshold that is required for Orthofluvial avulsion events. Also note that the 28,000 cfs is a *threshold* for the potential to initiate Orthofluvial avulsions across all the study floodplains. A 34,000 cfs discharge level is required to achieve the *highest* potential for Orthofluvial avulsion, which has never been achieved but once since dam construction (1997). In contrast, there were 7 pre-dam years (1911-1956) that achieved or nearly achieved the 34,000 cfs, where the highest potential for Orthofluvial geomorphic work is obtained. On the Fisher floodplain these high and sustained discharges generate annual cumulative power between 9 and 12 x 10^6 watts (Figure 40). This likely represents an approximate level of *THRESHOLD CUMULATIVE POWER*, adjusted for floodplain area, necessary to achieve the Orthofluvial avulsions for all the floodplains in the study area.

To more fully address the issue of peak flow and duration of flow, we further evaluated the flow regimes of the 10 high discharge volume years post-dam assessed above in Figure 40 [blue data points]. To accomplish this we adjusted the spring discharges occurring before April 1 (i.e., as addressed above in Figure 3 - Interval 2) to be discharged during the natural spring freshet. The results of these analyses are that power to do geomorphic work could be significantly increased above threshold levels and the cumulative power necessary to sustain Parafluvial avulsions were easily achieved and that Orthofluvial avulsion could be realized without having to release or sustain discharges above 30,000 cfs (Figure 40; red data points). To reiterate; in this illustration of the data (Figure 40), the post-dam high water volume years and the power they derived are expressed as blue data points. The same water years with EBSM

adjusted discharge regimes (which we discuss and illustrate in detail below), using the same volume of water, generate power to do geomorphic work illustrated by the red data points. By making these adjustments to the discharge regime in Palisades operations, the Snake River achieves discharges in wet and moderately wet years that group between 9 and 12 x 10^6 watts, similar to the power generated in wet years prior to dam operations (Figure 40; black data points). We believe that this is a central issue in the EBSM flow regimes and critical to the restoration and sustainability of the Snake River Shifting Habitat Mosaic and the organisms that are dependant on its dynamics.

Intervals 4 and 5 of Figure 3 are focused on the rate of the descending limb of the hydrograph after peak discharge and the sustaining of water volume throughout the summer. These issues are important ecologically and are central to the contractual obligations of Reclamation and the operating license of Palisades dam. Peak discharges typically occur throughout the Rocky Mountain big rivers (e.g., Snake, Yellowstone, Flathead, Bitterroot) in May and June as snow melts in the higher elevations of the mountains. The high discharges discussed above are not only important for the transport of sediments, but are important for the deposition of new surfaces that can be colonized by cottonwood seedlings. Natural discharges that occurred in the Snake River prior to dam construction and that occur elsewhere among unregulated river in the region, typically have descending hydrographs that do not exceed rates of approximately 5% per day. This rate of discharge decline allows the cottonwood seedlings that have germinated on newly formed sediment surfaces during the high flows to grow tap roots that are capable of maintaining capillary contact with the descending water table on the floodplain. In our EBSM discharge scenarios, not only are river power thresholds achieved, but there is sufficient water volume to maintain the appropriate rate of decline.

A major concern of the agricultural community and irrigators using Snake River water is that high discharge in June (in order to do geomorphic work), followed by a 5% decline in the hydrograph (to sustain cottonwood regeneration) will result in depleted water reserves for irrigation late in the summer. However, with the EBSM scenarios that we present below, late summer water volumes are maintained at or above that which was realized the year from which these scenarios were developed.

Working Scenarios of EBSM River Discharge Regimes

The following approach is based on the analysis of river power, aquatic habitat availability across discharges, and the life history dynamics of the native flora and fauna (as we understand them) of the Snake River in the study area. As we pointed out earlier in this report, there are competing interests vying for the water resources of the Snake River below Palisades dam. While some studies have suggested that regular river discharges as high as 40 - 60,000 cfs may be necessary to reestablish the regeneration of the cottonwood forest, the agriculture community desires to retain as much water for irrigation in summer as possible and the US Army Corps of Engineers is concerned about flood control. Furthermore, over the past several years winter discharges have been highly variable from year to year and within years, again as a function of competing interests, in winter usually between fisheries concerns and irrigators risk. In very wet years, high discharges have been the rule of operation during winter and spring to capture an anticipated runoff and to eliminate risk of flooding. These various competing interests have been generally based on single species *foci* or single management interests and have in general lead to a river system that has been compromised in its ecosystem scale ecological integrity.

We present here a series of post-dam water years illustrating the discharge regime as it occurred and an example of an Ecologically Based Systems Management scenario discharge regime that meets the various criteria for an ecosystem level restoration of Snake River ecological integrity. For illustration here, we selected a wet year, a moderately wet year and dry year to demonstrate the concepts and viability of this approach to river restoration. Each scenario uses the volume of water discharged that year and reshapes the hydrograph the meet ecological criteria within each of the temporal Intervals given in Figure 3. The determination and fine adjustment of these criteria would not have been possible without the application of the technological tools and analyses that we explain in the RESULTS section above.

The first EBSM scenario we have selected is a high water volume year, 1996. That year increased discharge from the dam was initiated in anticipation of high spring snowmelt in mid-February (Figure 41; black line). Maximum discharge in the river occurred in mid-June and the falling hydrograph met the operating criteria and contractual obligations for irrigation water of the Palisades project. Following the criteria of EBSM, we adjusted the existing water volume by maintaining low flow throughout the winter (Figure 41; red line). We increased discharge only after April 1, at a rate not to exceed 10% per day. Given the water volume available, we elected to increase the discharge to achieve the 19,000 cfs Parafluvial geomorphic work threshold rather than the lower discharges that were actually realized that year (i.e., 15,000 to 18,000 cfs). As water volume in the reservoir increased in mid-June, we increased discharge to more than 28,000 cfs and sustained that discharge as long as possible and still meet the descending hydrographic criteria for cottonwood seedling regeneration and irrigation needs. Along the descending limb of the hydrograph, we followed the criteria of not decreasing daily mean discharge at a rate greater

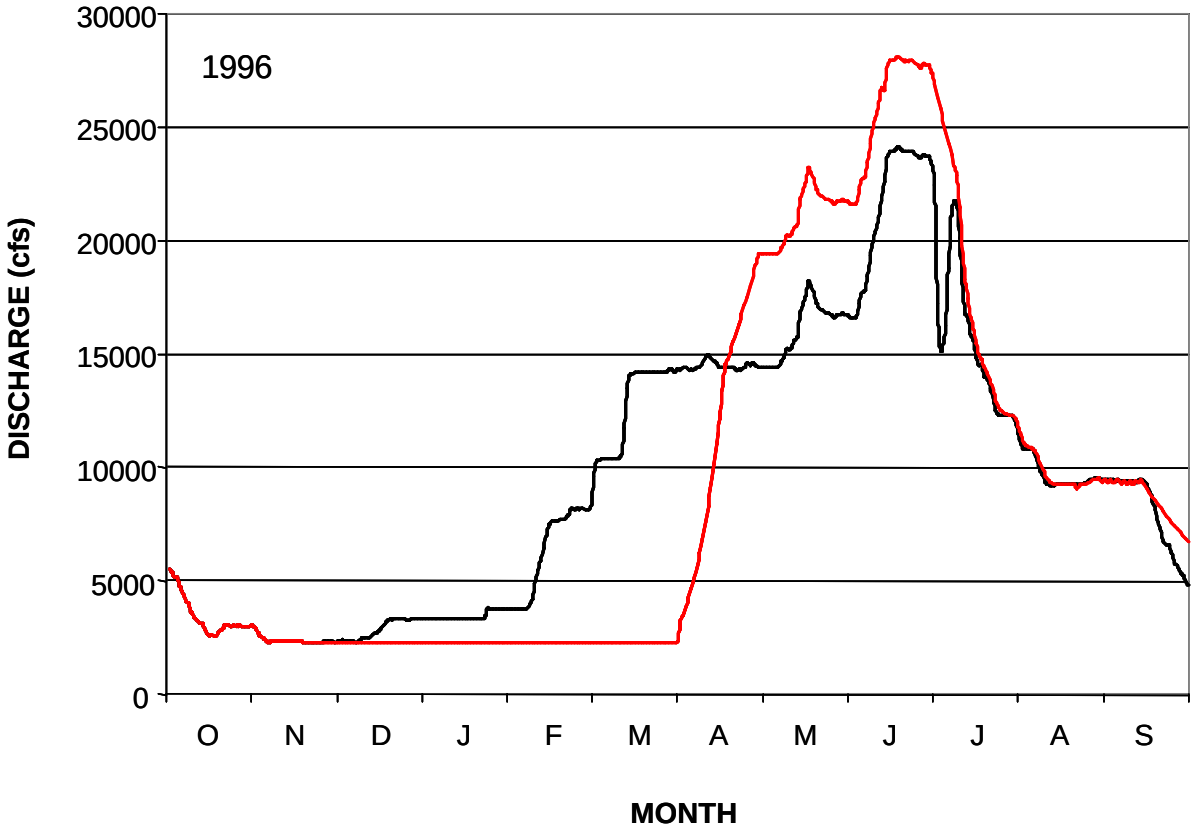

Figure 41. Illustration of the 1996 realized mean daily discharge (USGS Heise) in the wet, high water volume discharge year 1996 (black line). The red line represents an example of applying Ecologically Based Systems Management to reshape the hydrographic regime an meet the ecological criteria of re-engaging the river and floodplain system to restore the processes associated with the Shifting Habitat Mosaic. The corresponding power analysis revealed a >2X increase in geomorphic work being done in the EBSM scenario hydrograph.

than 5% per day. We also maintained the scenario discharge at or just above the realized discharge that year throughout the summer; thus meeting irrigation requirements.

In the second EBSM scenario, the water volume is representative of a moderately wet year, 1999 (Figure 42; black line). We followed the same criteria as expressed above for the 1996 EBSM scenario. In the realized discharge of that year, high discharge was initiated in February and continued into March and April. Maximum discharge in 1999 exceeded 19,000 cfs for only a few days. In the EBSM scenario, we kept water level at the December discharge regime throughout the winter and into April (Figure 42; red line). We allowed the river to increase in discharge at a rate not exceeding 10% until it achieved a level similar to the realized discharge. The realized discharge regime was tracked until mid-June when we increased peak discharge to approach 30,000 cfs. This was maintained for several days and then allowed to decrease at a rate not to exceed 5% per day. We also tracked the rates of decline in the hydrograph to simulate the realized hydrograph. It is clear from this illustration that higher summer discharges were continued throughout most of the summer, thus more than meeting the irrigation and operation requirements of the Palisades project.

In our final example scenario we have chosen to illustrate a dry water year, 2000 (Figure 43). We followed the same criteria as expressed above. However, in keeping with the adaptive management character of the EBSM approach, there is insufficient water volume to achieve high discharges and river power. This should be expected in dry periods and are not dissimilar from the discharge regimes that occurred naturally in dry years in the Snake River study area pre-dam.

Note that in wet and moderately wet water years the EBSM discharge criteria and resulting scenarios remain below the 1997 flood maximum. This is an important consideration in the EBSM approach. Extremely high water years, like 1997, will be realized again in the

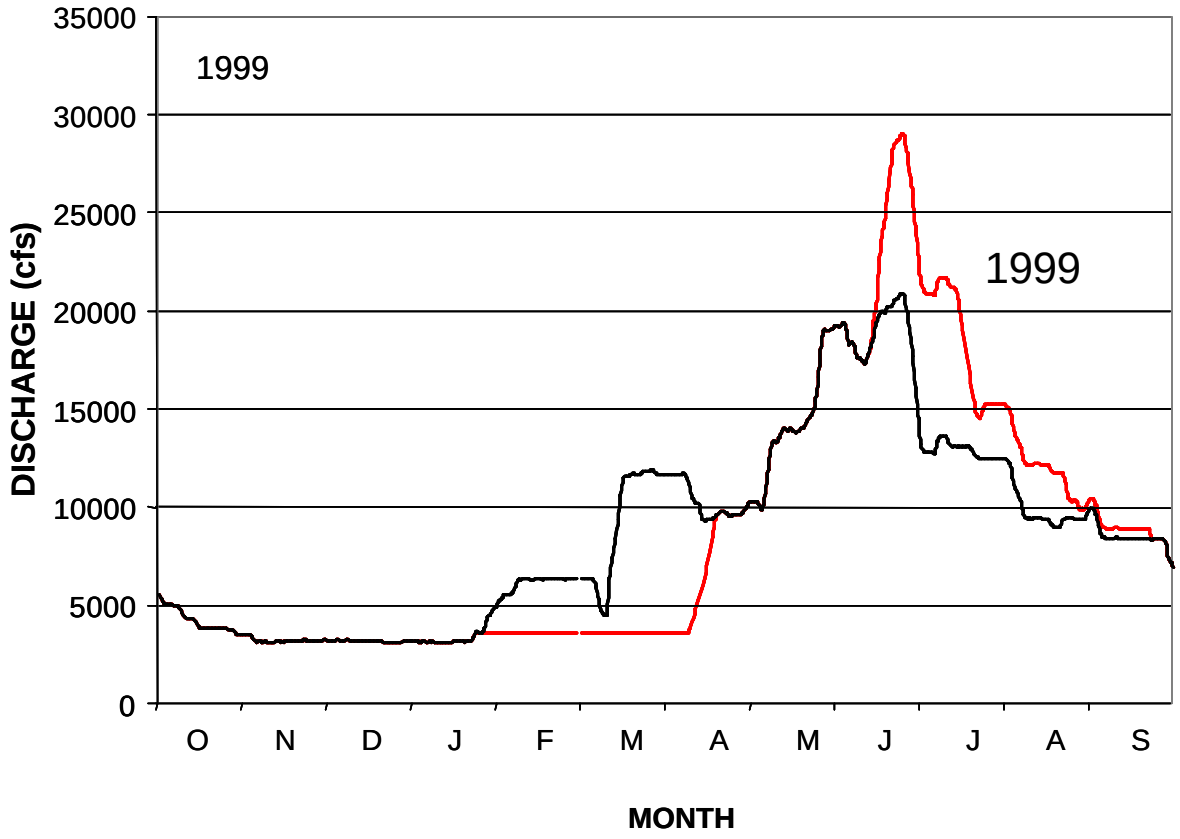

Figure 42. Illustration of the 1999 realized mean daily discharge (USGS Heise) in the moderately wet water volume discharge year (black line). The red line represents an example of applying Ecologically Based Systems Management to reshape the hydrographic regime an meet the ecological criteria of re-engaging the river and floodplain system to restore the processes associated with the Shifting Habitat Mosaic. The corresponding power analysis revealed a >5X increase in geomorphic work being done in the EBSM scenario hydrograph.

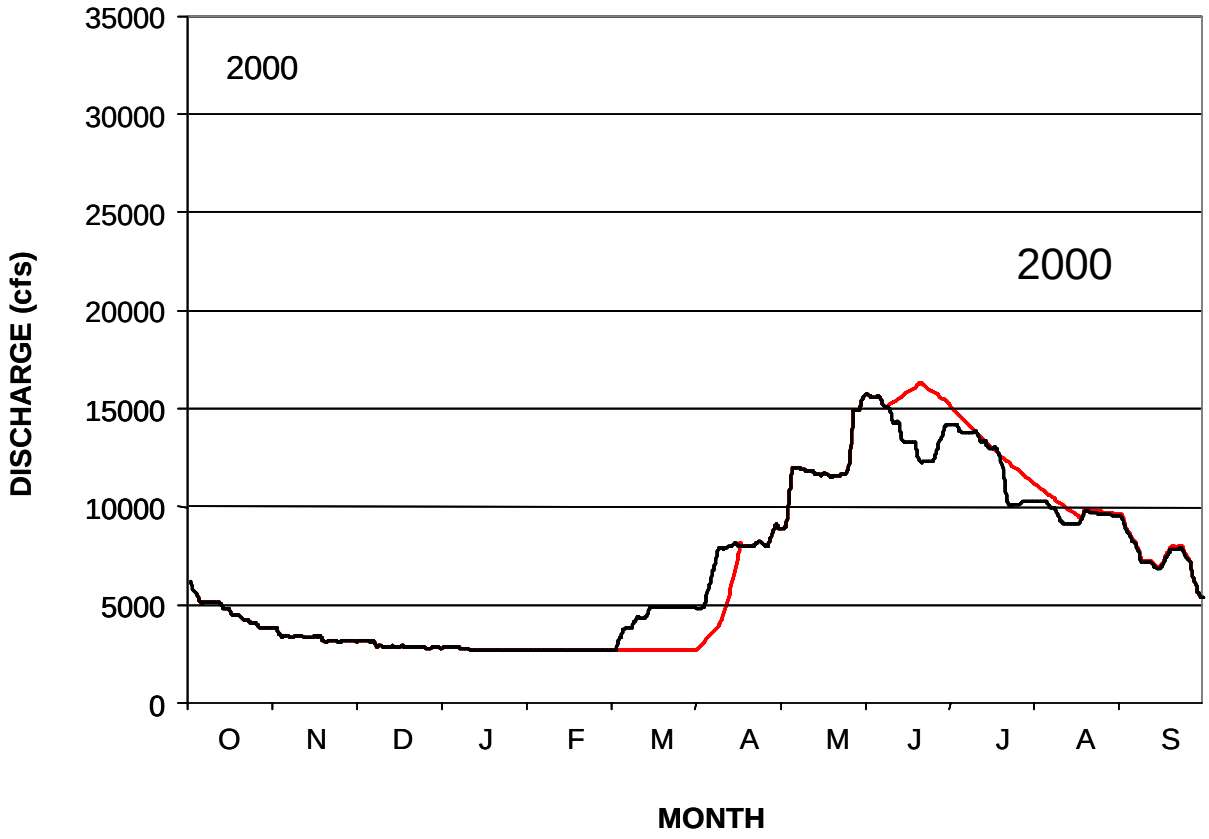

Figure 43. Illustration of the 2000 realized mean daily discharge (USGS Heise) in the dry, low water volume discharge year (black line). The red line represents an example of applying Ecologically Based Systems Management to reshape the hydrographic regime. Without water volume stored or being delivered in dry years, it is appropriate to follow past protocols that our analysis showed are not dissimilar to the natural hydrographic regimes occurring in dry year prior to dam construction.

future. To believe otherwise is to ignore the range of variation in water yield that Rocky Mountain watersheds are capable of generating. The EBSM scenarios do not generate discharges greater than an already established discharge benchmark in the wettest year since dam construction.

The restoration and long-term ecological sustainability of ecosystem structure and function in the Snake River below Palisades dam is dependant on the dynamics of a Shifting Habitat Mosaic. Systems management has the opportunity to reengage the river and its floodplain by implementing the criteria that generated the EBSM scenarios discussed above. However, we must caution not only the Reclamation, but also the US Army Corps of Engineers, state and local government and the citizens of eastern Idaho, that floodplains that are re-engaged by following the EBSM Decision Support System and the criteria outlined herein can still loose ecosystem function and the Shifting Habitat Mosaic by permitting geomorphic modification (i.e., levees, rip-rap, groins, rock bar-points) or construction encroachment (i.e., homes, cabins, roads) onto the floodplain with their accompanying protective structures.

ECOLOGICALLY BASED SYSTEMS MANAGEMENT

SUMMARY OF DISCHARGE CRITERIA

Maximum Annual Discharge

Objectives:

- Geomorphic Work
- Maintain Shifting Habitat Mosaic

Criteria:

- In Ultra-wet years (Total Annual Discharge >7M Acre Ft) [4yrs of last 45yrs] approach 30,000 cfs for as long as possible with >25,000cfs; 12-15 days.
- In Wet years (Total Annual Discharge 5.8 - 6.8M Acre Ft) [11yrs of the last 45yrs] exceed 25,000 cfs; 8 - 12days
- In Moderate years (Total Annual Discharge 4 - 5.8M Acre Ft) [17yrs of last 45yrs] exceed 19,000 – 25,000 cfs and sustain as long as volume allows
- In Dry years - Stay with existing protocols.

Descending Limb and Summer Flow

Objectives:

- Riparian cottonwood recruitment
- Fish Habitat

Criteria:

- In Ultra-wet years (Total Annual Discharge >7M Acre Ft) [4yrs of last 45yrs] reduce discharge from maximum at a rate not to exceed 5%/day for 2-3 weeks;

maintain descending discharge throughout July and August to meet contractual base flows through late August and September.

- In Wet years (Total Annual Discharge 5.8 - 6.8M Acre Ft) [11yrs of the last 45yrs] reduce discharge from maximum at a rate not to exceed 5%/day for 2-3 weeks; maintain descending discharge throughout July and August to meet contractual base flows through late August and September.
- In Moderate years (Total Annual Discharge 4 - 5.8M Acre Ft) [17yrs of last 45yrs] reduce discharge from maximum at a rate not to exceed 5%/day for 2-3 weeks; maintain descending discharge throughout July and August to meet contractual base flows through late August and September.
- In Dry years - Stay with existing protocols.

Winter Flow and Ascending Hydrograph in Spring

Objectives:

- Fish Habitat
- Meet life history requirements of other Aquatic Species

Criteria:

- In Ultra-wet years (Total Annual Discharge >7M Acre Ft) [4yrs of last 45yrs] maintain winter flows to meet fishery requirements to foster native species over non-natives; hold flows constant through the cold winter months at prescribed levels; do not increase discharge before April 1.
- In Wet years (Total Annual Discharge 5.8 - 6.8M Acre Ft) [11yrs of the last 45yrs] maintain winter flows to meet fishery requirements to foster native species over non-

natives; hold flows constant through the cold winter months at prescribed levels; do not increase discharge before April 1.

- In Moderate years (Total Annual Discharge 4 - 5.8M Acre Ft) [17yrs of last 45yrs] maintain winter flows to meet fishery requirements to foster native species over non-natives; hold flows constant through the cold winter months at prescribed levels; do not increase discharge before April 1.
- In Dry years.

  maintain winter flows to meet fishery requirements to foster native species over non-natives; flows may often be designated to be less than 1000 cfs; hold flows constant through the cold winter months at prescribed levels; do not increase discharge before April 1.

REFERENCES

Bagnold, R.A., 1966. An approach to the sediment transport problem from general physics: *U.S. Geol. Survey Prof. Paper:* 422-I.

Bansak, T. S. 1998. The influence of vertical hydraulic exchange on habitat heterogeneity and surficial primary production on a large alluvial flood plain of the Middle Fork Flathead River. The University of Montana, Missoula. 68 pp.

Baxter, C. V. and F. R. Hauer. 2000. Geomorphology, hyporheic exchange, and selection of spawning habitat by bull trout (*Salvelinus confluentus*). Canadian Journal of Fisheries and Aquatic Sciences 57:1470-1481.

Baxter, C. V. and F. R. Hauer and W. W. Woessner. 2003. Measuring groundwater-stream water exchanges: New techniques for installing piezometers, estimating hydraulic conductivity and detecting patterns in groundwater-stream water exchange. Transactions of the American Fisheries Society 132 (3):493-502.

Braatne, J. H., S. B. Rood and P. E. Heilman. 1996. Life history, ecology and conservation of riparian cottonwoods in North America, pp. 57-85. IN: Stettler, R.F., H. D. Bradshaw, P .E. Heilman and T. M. Hinckley (eds.), Biology of *Populus*: Implications for Management and Conservation. National Research Council, Ottawa.

Costa, J.E. and J.E. O'Connor. 1995. Geomorphically Effective Floods, pp. 45-56. IN: Costa, J.E., A.J Miller, K.W. Potter and P.R. Wilcock (eds.), Natural and Anthropogenic Influences in Fluvial Geomorphology. Geophysical Monograph 89: The Wolman Volume

Gopal, S. and C. Woodcock. 1994. Theory and methods for accuracy assessment of thematic maps using fuzzy sets. Photogram. Eng. Remote Sensing 60(2):181-188.

Gregory, S. V., F. J. Swanson, W. A. McKee, and K. W. Cummins. 1991. An ecosystem perspective of riparian zones. BioScience 41:540-552.

Harner, M. J. and J. A. Stanford. 2003. Differences in cottonwood growth between a losing and a gaining reach of an alluvial flood plain. Ecology 84(6):1453–1458.

Hauer, F. R., C. N. Dahm, G. A. Lamberti and J. A. Stanford. 2003. Landscapes and ecological variability of rivers in North America: factors affecting restoration strategies, pp. IN: Wissmar, R. C. and P. A. Bisson (ed.), Strategies for Restoring River Ecosystems: Sources of Variability and Uncertainty in Natural and Managed Systems. American Fisheries Society.

Hauer, F. R. and J. A. Stanford. 1991. Distribution and abundance of Trichoptera in a large regulated river. Verhandlungen der Internationalen Vereinigung fur Theoretische und Angewandte Limnologie 24:1636-1639.

Hauer, F. R., J. A. Stanford, J. J. Giersch and W. H. Lowe. 2000. Distribution and abundance patterns of macroinvertebrates in a mountain stream: an analysis along multiple environmental gradients. Verh. Internat. Verein. Limnol. 27(3):1485-1488.

Hutto, R. L., and J. S. Young. 2002. Regional landbird monitoring: perspectives from the northern Rocky Mountains. Wildlife Society Bulletin 30:738-750.

Karr, J. R. and E. W. Chu. 1999. Restoring Life in Running Waters. Island Press, Washington, D.C. 206 pp.

Kershner, J.L. 1997. Setting riparian/aquatic restoration objectives within a watershed context. Restoration Ecology 5: 15-24.

Lake, P.S. 2000. Distribution, patchiness and diversity in streams. J. North. Am. Benthol. Soc. 19:573-592.

Mahoney, J. M. and S. B. Rood. 1998. Streamflow requirements for cottonwood seedling recruitment--an integrative model. Wetlands. 18:634-645.

Merigliano, M.F. 1996. Flood-plain and vegetation dynamics along a gravel bed, braided river in the northern Rocky Mountains. Ph.D. Dissertation. The University of Montana, Missoula, MT. 180 pp.

Mouw, J.E.B. and Alaback, P.B. 2003. Putting floodplain hyperdiversity in a regional context: an assessment of terrestrial-floodplain connectivity in a montane environment. Journal of Biogeography 30, 87-103.

Muller, S.V., D.A. Walker, F.E. Nelson, N.A. Auerbach, J.G. Bockheim, S. Guyer, and D. Sherpa. 1998. Accuracy assessment of a land-cover map of the Kuparuk River basin, Alaska: Considerations for remote regions. Photogr. Eng. Remote Sensing 64 (6): 619-628.

Pepin, D. M. and F. R. Hauer. 2002. Benthic responses to groundwater-surface water exchange in two alluvial rivers in northwestern Montana. Journal of North American Benthological Society 21(3):370-383.

Rood, S.B., A.R. Kalischuk and J.M. Mahoney. 1998. Initial cottonwood seedling recruitment following the flood of the century of the Oldman River, Alberta, Canada. Wetlands 15:557-570.

Stanford, J. A. 1998. Rivers in the landscape: introduction to the special issue on riparian and groundwater ecology. Freshwater Biology 40(3):402-406.

Stanford, J. A. and F. R. Hauer. 1992. Mitigating the impacts of stream and lake regulation in the Flathead River catchment, Montana, USA: an ecosystem perspective. Aquatic Conservation: Marine and Freshwater Ecosystems 2:35-63.

Stanford, J.A., F.R.Hauer, J.S. Kimball, M.S. Lorang, R. Callaway, and W.W. Woessner. 2001. Biocomplexity-Dynamic Controls on Emergent Properties of River Flood Plains. Funded proposal to the National Science Foundation.

Stanford, J. A. and J. V. Ward. 1988. The hyporheic habitat of river ecosystems. Nature 335:64-66.

Stanford, J. A. and J. V. Ward. 1993. An ecosystem perspective of alluvial rivers: connectivity and the hyporheic corridor. Journal of the North American Benthological Society 12(1):48-60.

Ward J.V., K. Tockner and F. Schiemer 1999. Biodiversity of floodplain river ecosystems: ecotones and connectivity. Regul. Rivers: Res. Mgmt. 15:125-39.

Tou, J. T., and Gonzalez, R. C. 1977. Pattern Recognition Principles. Addison-Wesley, Reading, Massachusetts, USA.

APPENDIX A. Supplemental Tables and Figures

Appendix A Table 1. Area (m^2) of Aquatic Habitats in the Swan Floodplain across discharge regimes fro 1500 to 37,000 cfs.

	1500cfs	5000cfs	11,600cfs	25,000cfs	37,000cfs
Shallow ltr	419049	40611	51417	0	0
Deep ltr	89622	231973	30528	171765	473643
Shallow mtr	4383	82573	0	0	0
Deep mtr	0	336915	262701	177732	38817
Higth turbulent zone	405	0	43083	80928	0
Higth turbulent run	0	0	378891	428301	642285
Shallow shore	90702	72910	213228	532953	119952
Shallow expansive run	0	0	225	0	860724
Pool	432	20780	9828	8685	0
Deep pool	3546	290	18405	16182	0
Near shore riffles	82125	71509	1782	180648	358227
Deep riffles	0	50728	104409	49833	1080
Glides	8595	4325	180	0	0
Deep glide/eddy	0	2205	1134	0	0

Appendix A Table 2. Area (m^2) of Aquatic Habitats in the Conant Floodplain across discharge regimes fro 1500 to 37,000 cfs.

	1500cfs	5000cfs	11,600cfs	25,000cfs	37,000cfs
Shallow ltr	174816	119736	26631	74007	0
Deep ltr	256986	87284	10674	5265	306873
Shallow mtr	1296	81293	21285	666	29799
Deep mtr	31545	294034	232344	112401	190008
Higth turbulent zone	22095	72775	75933	51012	0
Higth turbulent run	0	0	199197	394164	428265
Shallow shore	103149	29081	364545	182988	155160
Shallow expansive run	17055	0	0	0	183267
Pool	891	2608	891	5562	121545
Deep pool	6948	2325	882	288	45576
Near shore riffles	56484	17131	4392	261783	0
Deep riffles	0	21571	81603	37116	0
Glides	0	0	0	0	0
Deep glide/eddy	0	0	0	0	0

Appendix A Table 3. Area (m^2) of Aquatic Habitats in the Fisher Floodplain across discharge regimes fro 1500 to 37,000 cfs.

	1500cfs	5000cfs	11,600c	25,000cfs	37,000cfs
Shallow ltr	122094	19002	1548	657	3177
Deep ltr	41193	13911	1656	51291	252729
Shallow mtr	216	119539	12087	9000	0
Deep mtr	8721	73349	162405	30942	95931
Higth turbulent zone	6228	33771	11763	18045	5022
Higth turbulent run	0	0	71424	214956	254799
Shallow shore	66519	69503	240372	92475	327438
Shallow expansive rur	0	0	0	0	114696
Pool	11934	6468	7056	27207	27387
Deep pool	756	4037	11583	17451	0
Near shore riffles	42165	44520	13077	157212	72
Deep riffles	234	6291	61362	19530	0
Glides	0	4576	9648	5409	0
Deep glide/eddy	0	844	5418	0	0

Appendix A Table 4. Area (m^2) of Aquatic Habitats in the Heise Floodplain across discharge regimes fro 1500 to 37,000 cfs.

	1500cfs	5000cfs	11,600cfs	25,000cfs	37,000cfs
Shallow ltr	221751	113575	6273	75123	64062
Deep ltr	68895	68854	18666	94311	298818
Shallow mtr	5877	88703	23967	171	0
Deep mtr	0	105660	169974	181188	59400
Higth turbulent zone	2844	16501	2745	315	945
Higth turbulent run	0	0	217503	214380	351666
Shallow shore	29304	56842	269451	105831	493011
Shallow expansive rur	20934	59719	0	0	0
Pool	1674	927	9009	21870	837
Deep pool	5922	179	18621	35136	131022
Near shore riffles	32787	24229	16731	97335	36441
Deep riffles	0	33872	58896	32337	279
Glides	0	4576	7155	0	0
Deep glide/eddy	0	0	37809	0	0

Appendix A Table 5. Area (m^2) of Aquatic Habitats in the Twin Floodplain across discharge regimes fro 1500 to 37,000 cfs.

	1500cfs	5000cfs	11,600cfs	25,000cfs	37,000cfs
Shallow ltr	272475	72431	23319	0	0
Deep ltr	187785	332199	335502	428661	985671
Shallow mtr	164232	49673	63216	0	0
Deep mtr	39501	287826	460188	424998	428679
Higth turbulent zone	0	44299	20124	29700	58167
Higth turbulent run	0	0	259119	366030	710325
Shallow shore	452133	268462	871821	2317761	1708749
Shallow expansive run	63	0	0	0	0
Pool	29286	26432	63441	109854	1125009
Deep pool	3672	61303	53064	103977	174861
Near shore riffles	16893	221631	49383	349614	221238
Deep riffles	0	137685	78291	83880	768294
Glides	0	113	10503	10566	0
Deep glide/eddy	0	0	2187	11835	0

Appendix A Table 6. Percent Cover of vegetation cover types across each Floodplain.

Cover Types	Percent Cover				
	Swan	**Conant**	**Fisher**	**Heise**	**Twin**
Water	31.26	29.06	32.22	18.71	16.53
Deciduous (majority cottonwood)	16.09	15.17	10.24	25.70	20.55
Shadow	6.69	10.53	18.53	15.10	16.68
Dry grass	30.16	10.26	17.54	27.32	25.49
Mixed grasses	4.86	7.38	4.70	2.03	5.29
Cobble	0.76	2.78	1.66	1.43	1.69
Willow	5.55	11.54	12.16	7.95	13.77
Reed canary grass	4.48	1.91	0.43	1.77	0.00
Other	0.14	0.00	2.52	0.00	0.00
Pasture	0.00	11.37	0.00	0.00	0.00

Appendix A Table 7. Area (m2) and (Hectares) and Percent Cover of cover types of vegetation and water on the Swan floodplain.

Cover type	Area	Area (ha)	% of fp	
water	1185062	118.5062	0.312571	0.312571
shadow	610193	61.0193	0.160944	0.160944
dry grass	253593	25.3593	0.066887	0.066887
cottonwood	1143533	114.3533	0.301617	0.301617
cobble	184264	18.4264	0.048601	0.048601
reed canary grass	28970	2.897	0.007641	0.007641
mixed grasses	210556	21.0556	0.055536	0.055536
willow	169901	16.9901	0.044813	0.044813
other	5265	0.5265	0.001389	0.001389
pasture	0	0	0	0
	3791337		0.687429	1

Appendix A Table 8. Area (m2) and (Hectares) and Percent Cover of cover types of vegetation and water on the Conant floodplain.

Cover type	Area	Area (ha)	% of fp	
water	701924	70.1924	0.290583	0.290583
shadow	366488	36.6488	0.151719	0.151719
dry grass	254365	25.4365	0.105302	0.105302
cottonwood	247762	24.7762	0.102569	0.102569
cobble	178320	17.832	0.073821	0.073821
reed canary grass	67127	6.7127	0.027789	0.027789
mixed grasses	278838	27.8838	0.115434	0.115434
willow	46022	4.6022	0.019052	0.019052
other	0	0	0	0
pasture	274725	27.4725	0.113731	0.113731

Appendix A Table 9. Area (m2) and (Hectares) and Percent Cover of cover types of vegetation and water on the Fisher floodplain.

Cover type	Area (ha)	%of fp	
water	44.2593	0.322248	0.322248
shadow	14.0634	0.102394	0.102394
dry grass	25.4457	0.185268	0.185268
cottonwood	24.0867	0.175373	0.175373
cobble	6.453	0.046984	0.046984
reed canary grass	2.2797	0.016598	0.016598
mixed grasses	16.6977	0.121575	0.121575
willow	0.5931	0.004318	0.004318
other	3.4668	0.025241	0.025241
pasture	0	0	0

Appendix A Table 10. Area (m2) and (Hectares) and Percent Cover of cover types of vegetation and water on the Fisher floodplain.

Cover type	Area (ha)	%of fp	
water	56.097	0.187062	0.187062
shadow	77.0571	0.256956	0.256956
dry grass	45.2709	0.150961	0.150961
cottonwood	81.9369	0.273228	0.273228
cobble	6.0759	0.020261	0.020261
reed canary grass	4.2957	0.014325	0.014325
mixed grasses	23.8428	0.079507	0.079507
willow	5.3082	0.017701	0.017701
other	0	0	0
pasture	0	0	0

Appendix A Table 11. Area (m2) and (Hectares) and Percent Cover of cover types of vegetation and water on the Upper and Lower Twin floodplain. Willow was not separable from cottonwood in the Twin floodplain and has been recorded with the cottonwood.

Cover type	**Area (ha)**	**%of fp**	
water	185.41133	0.165336	0.165336
shadow	230.41298	0.205466	0.205466
dry grass	187.0803	0.166825	0.166825
cottonwood	285.8445	0.254895	0.254895
cobble	59.3289	0.052905	0.052905
reed canary grass	18.9297	0.01688	0.01688
mixed grass	154.4112	0.137693	0.137693
willow	0	0	0
other	0	0	0
pasture	0	0	0

1500cfs

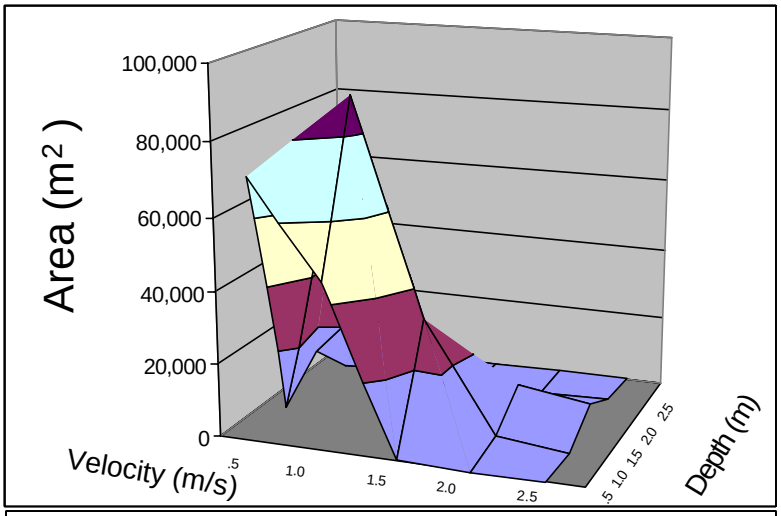

3260cfs

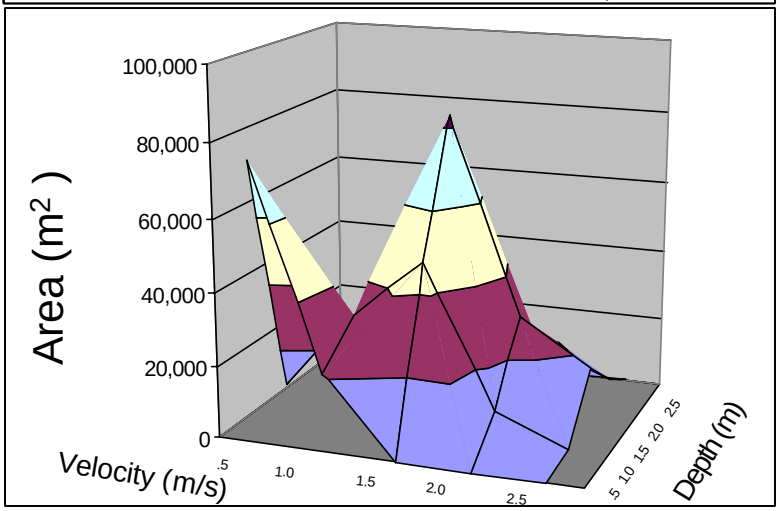

5000cfs

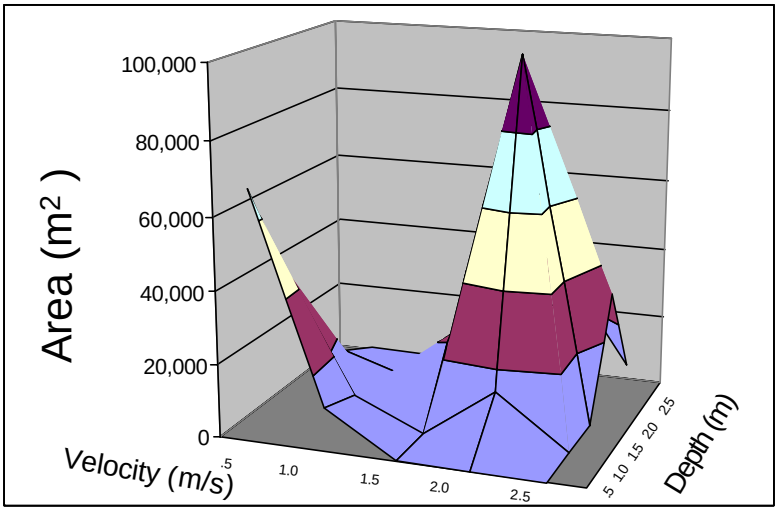

APPENDIX A Figure 1. Area (m^2) by depth and velocity on the Fisher floodplain across three discharges from 1500 to 5000 cfs.

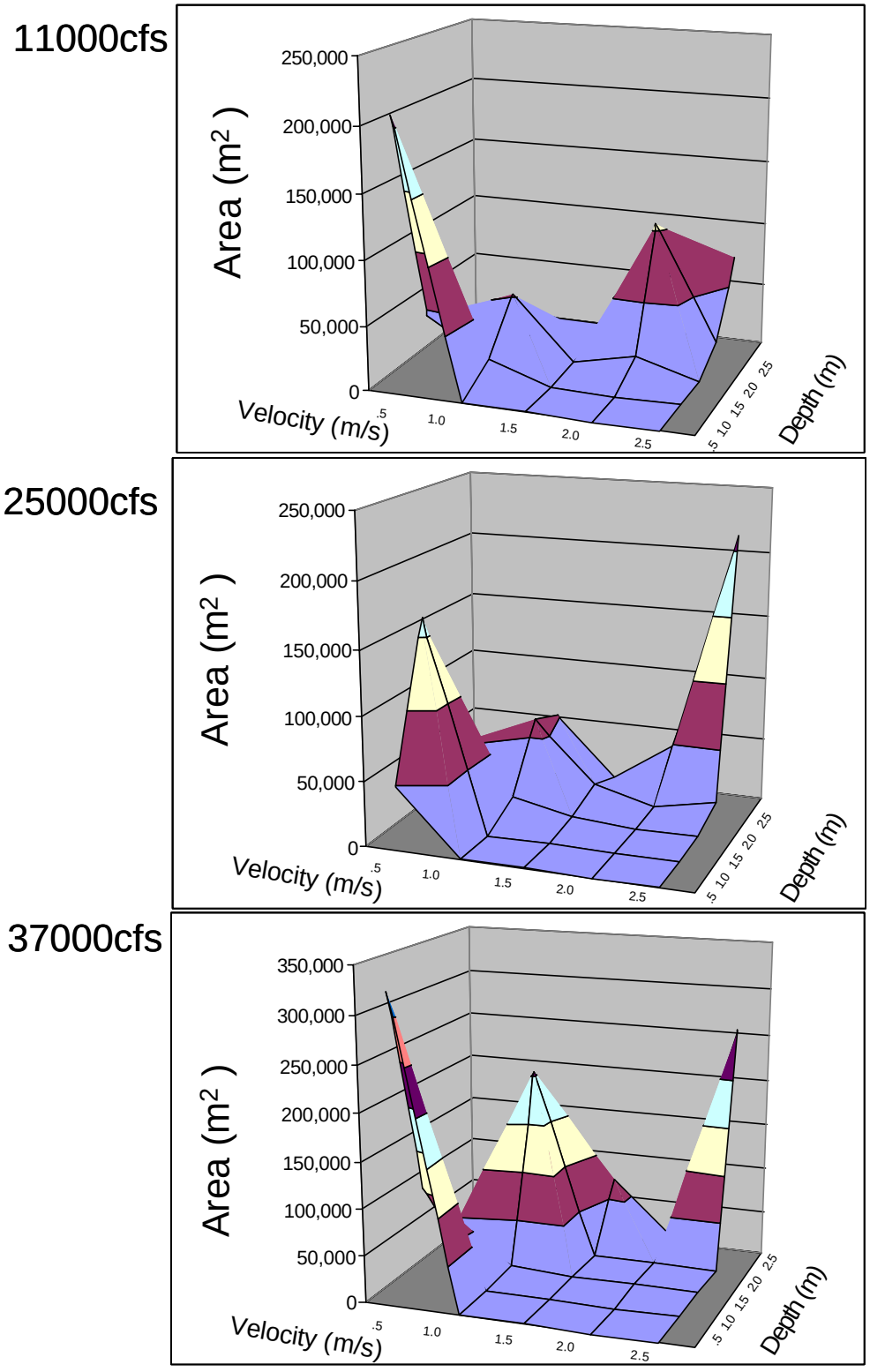

APPENDIX A Figure 2. Area (m^2) by depth and velocity on the Fisher floodplain across three discharges from 11000 to 37000 cfs.

APPENDIX A Figure 3. Georectified hyperspectral image of the Fisher floodplain with piezometer locations A-H .

APPENDIX A Figure 4. Georectified aerial photo with piezometer locations on the Fisher Floodplain. Site correspondence is with Area C.

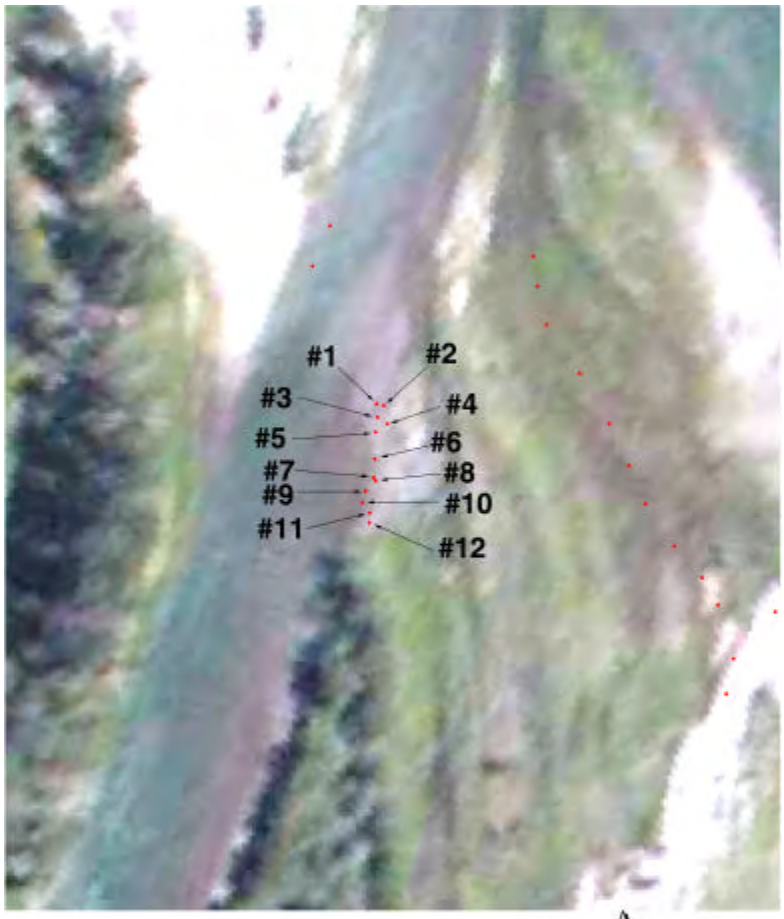

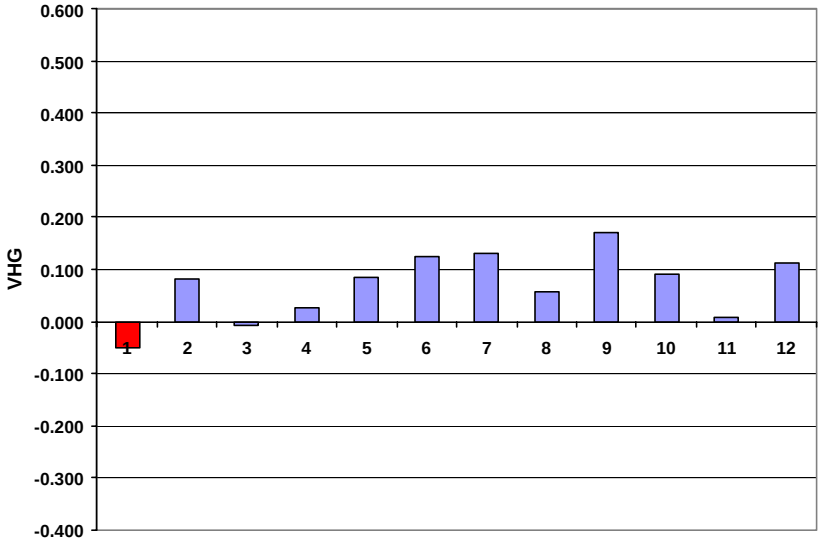

APPENDIX A Figure 5. Georectified aerial photo with piezometer locations on the Fisher Floodplain. Piezometers13-24 correspond with Area B.

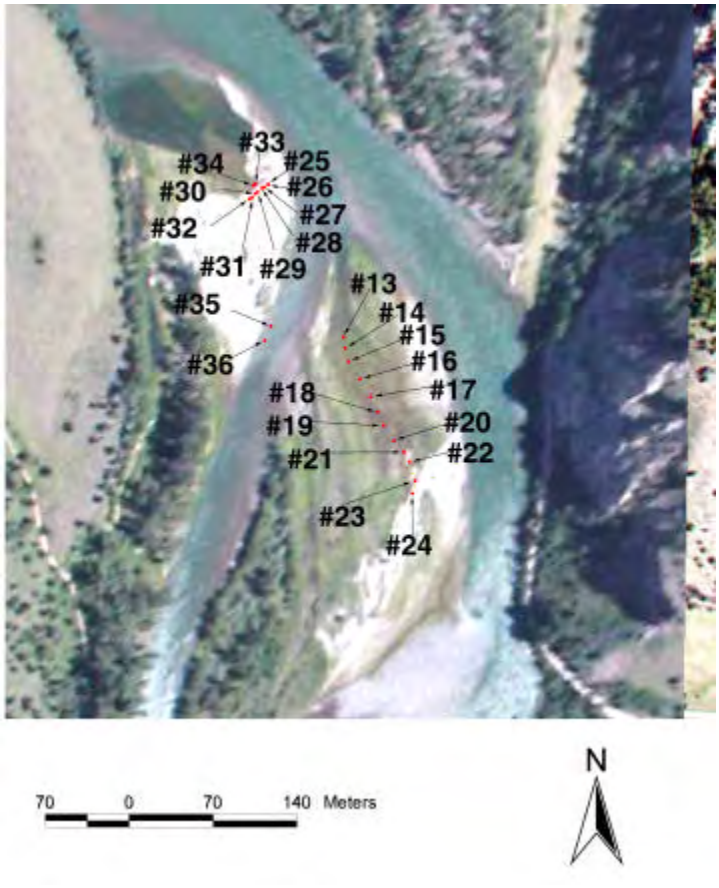

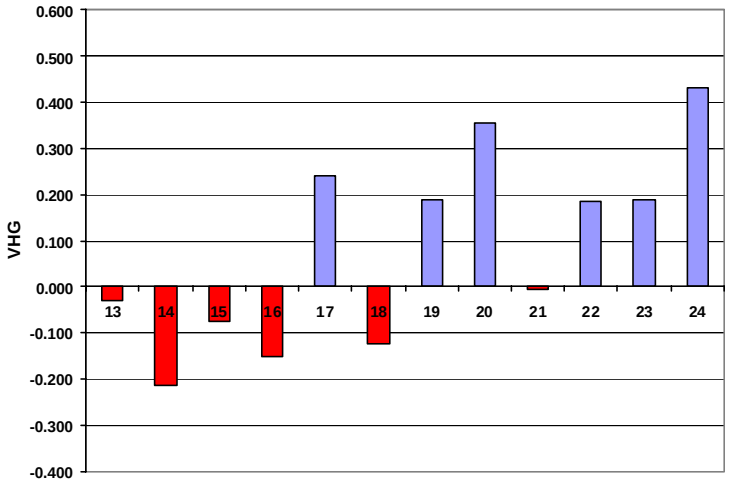

APPENDIX A Figure 6. Georectified aerial photo with piezometer locations on the Fisher Floodplain. Piezometers 25-36 correspond with Area D.

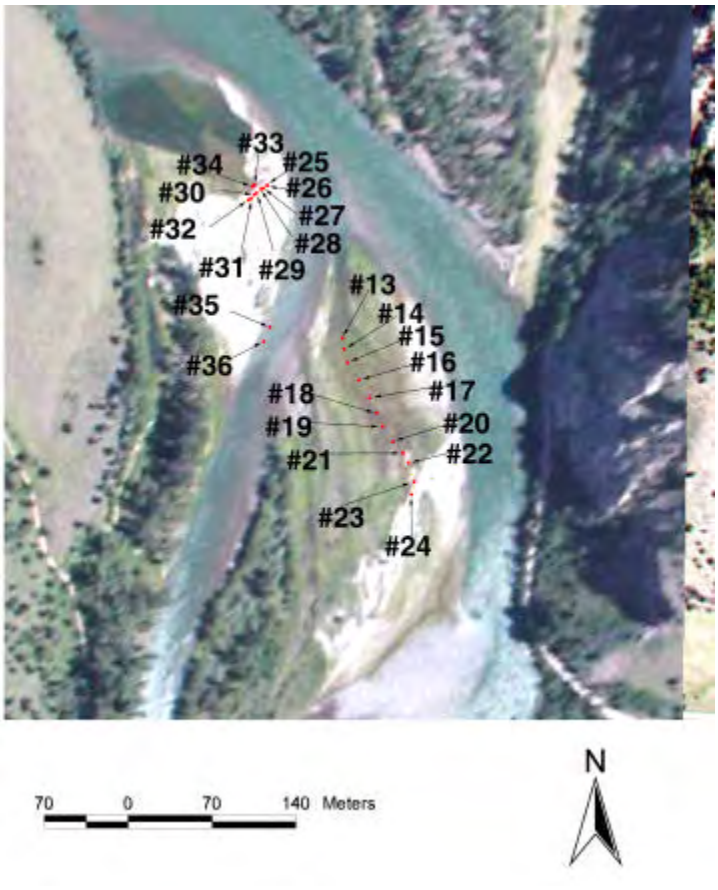

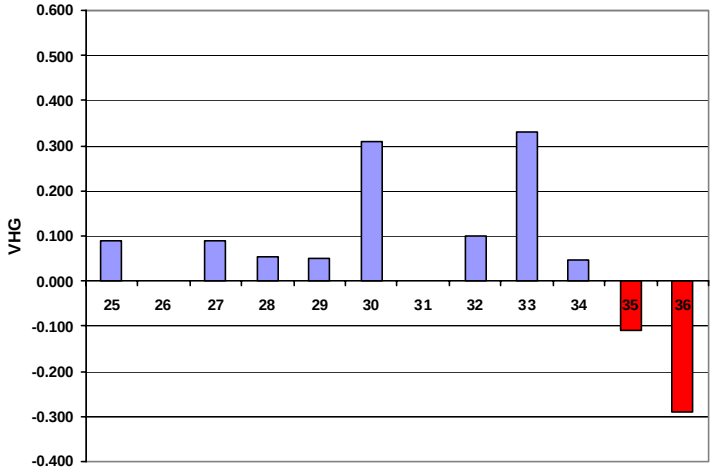

APPENDIX A Figure 7. Georectified aerial photo with piezometer locations on the Fisher Floodplain. Piezometers 37-50 correspond with Area G.

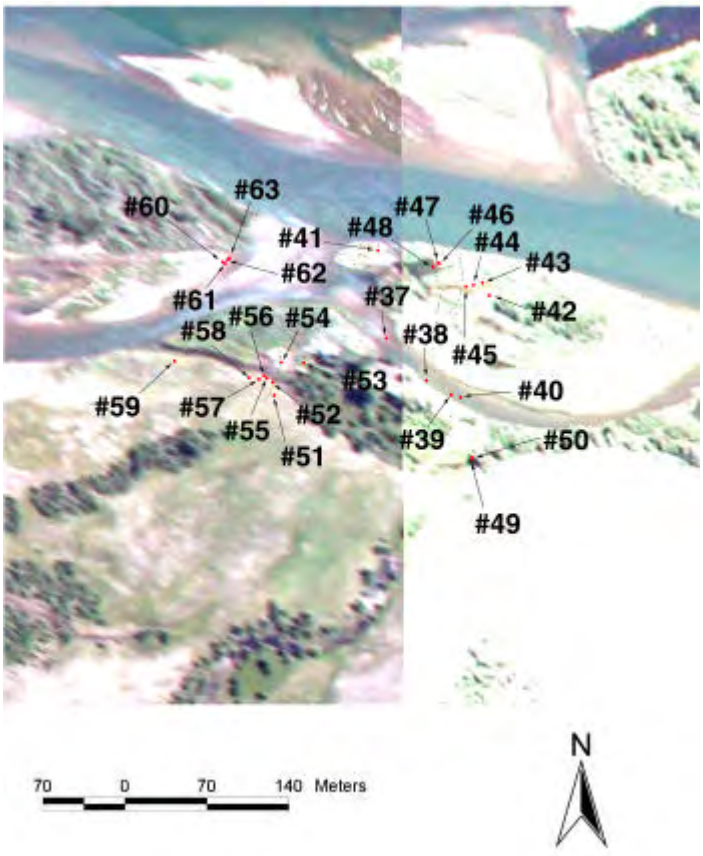

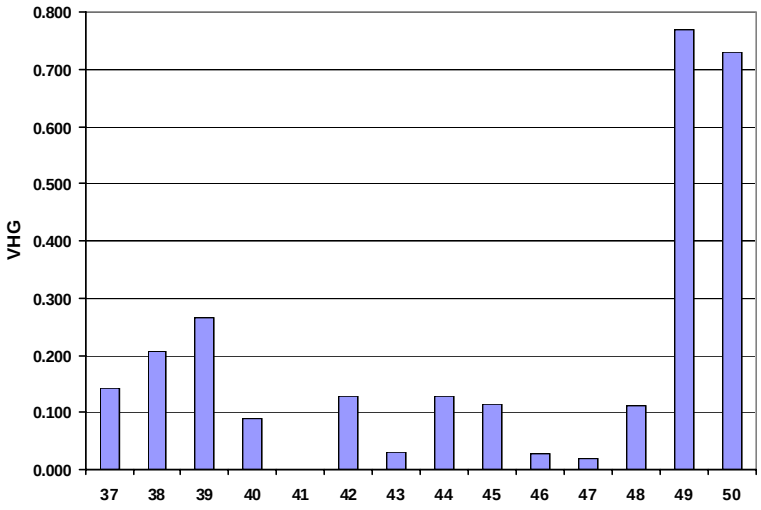

APPENDIX A Figure 8. Georectified aerial photo with piezometer locations on the Fisher Floodplain. Piezometers 51-63 correspond with Area G.

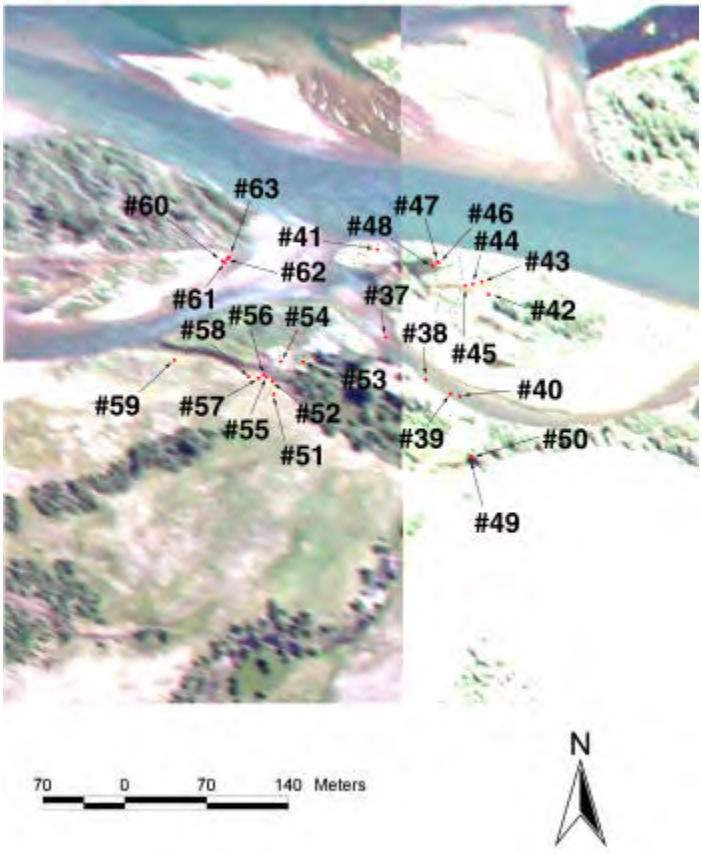

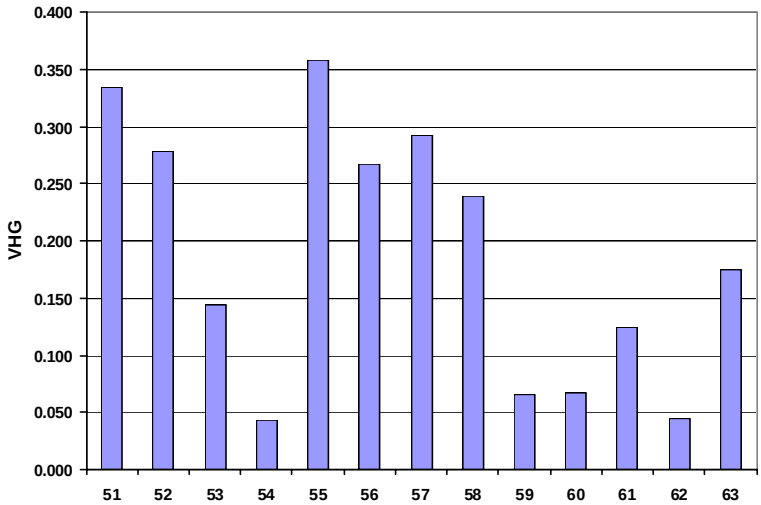

APPENDIX A Figure 9. Georectified aerial photo with piezometer locations on the Fisher Floodplain. Piezometers 64-69 correspond with Area F.

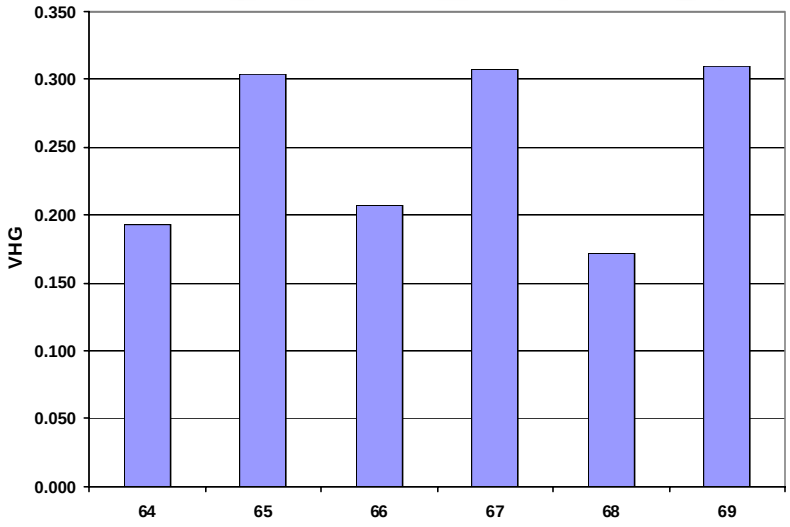

APPENDIX A Figure 10. Georectified aerial photo with piezometer locations on the Fisher Floodplain. Piezometers 70-74 correspond with Area E.

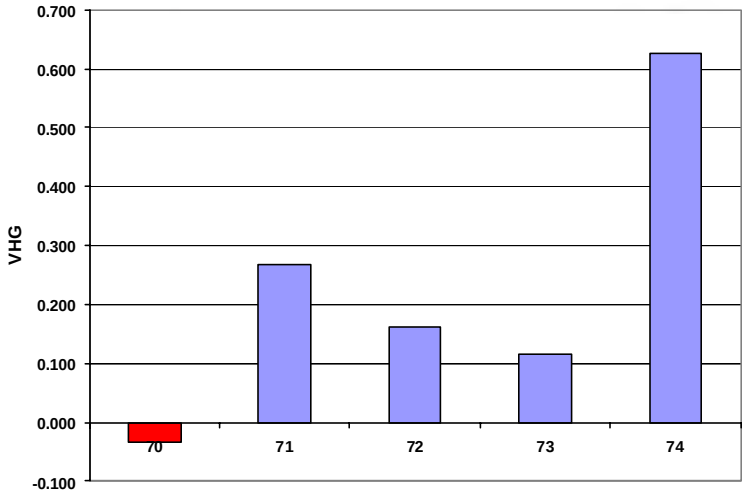

APPENDIX A Figure 11. Georectified aerial photo with piezometer locations on the Fisher Floodplain. Piezometers 75-80 correspond with Area A.

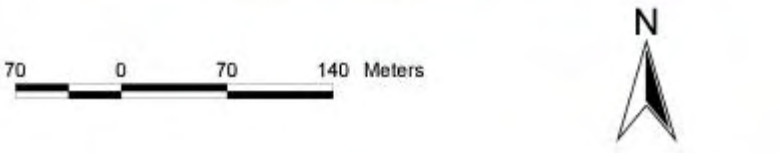

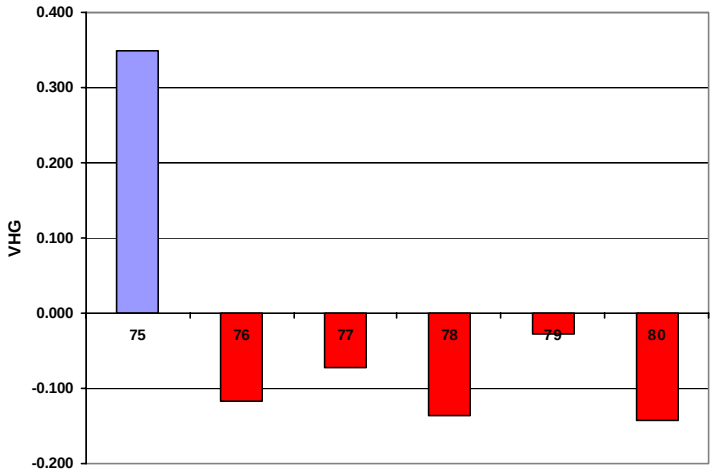

APPENDIX A Figure 12. Georectified aerial photo with piezometer locations on the Fisher Floodplain. Piezometers 81-86 correspond with Area H.

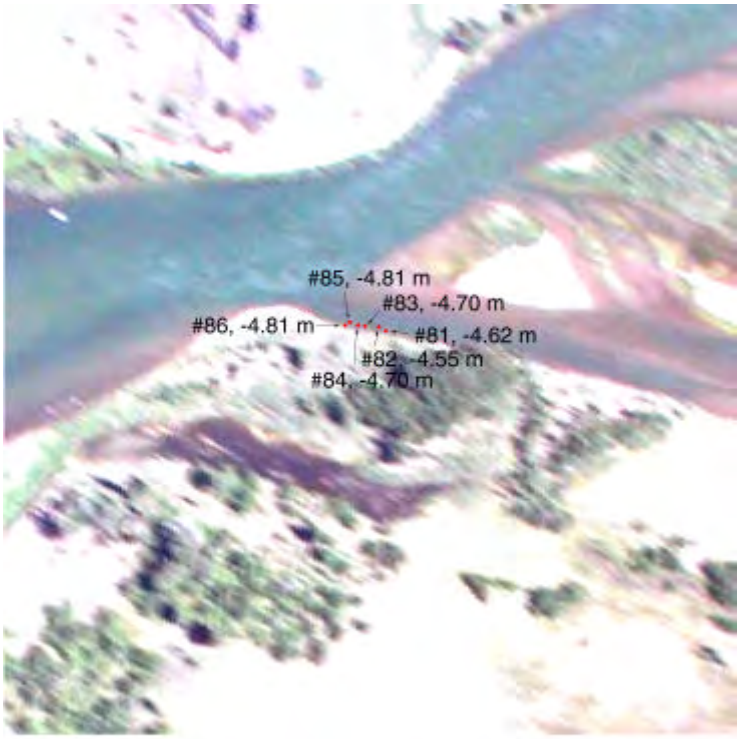

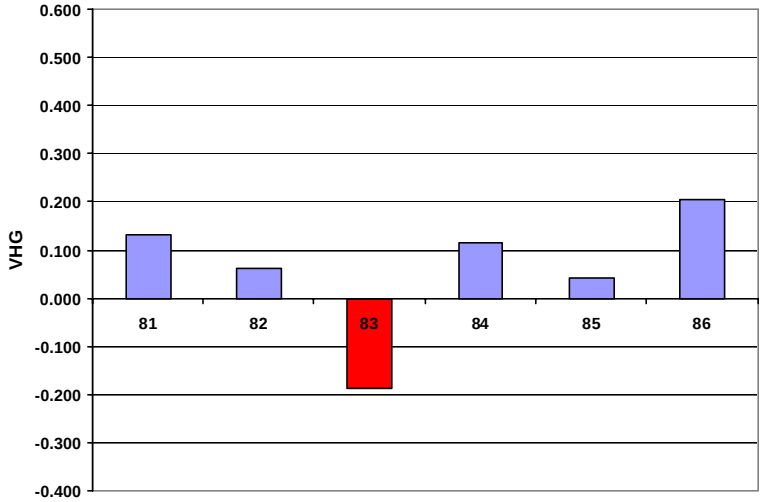

APPENDIX A Figure 13. Georectified hyperspectral image of the Fisher floodplain with locations of Temperature loggers. Temperatures were recorded every two hours for 16 months. Data are displayed in the following figures.

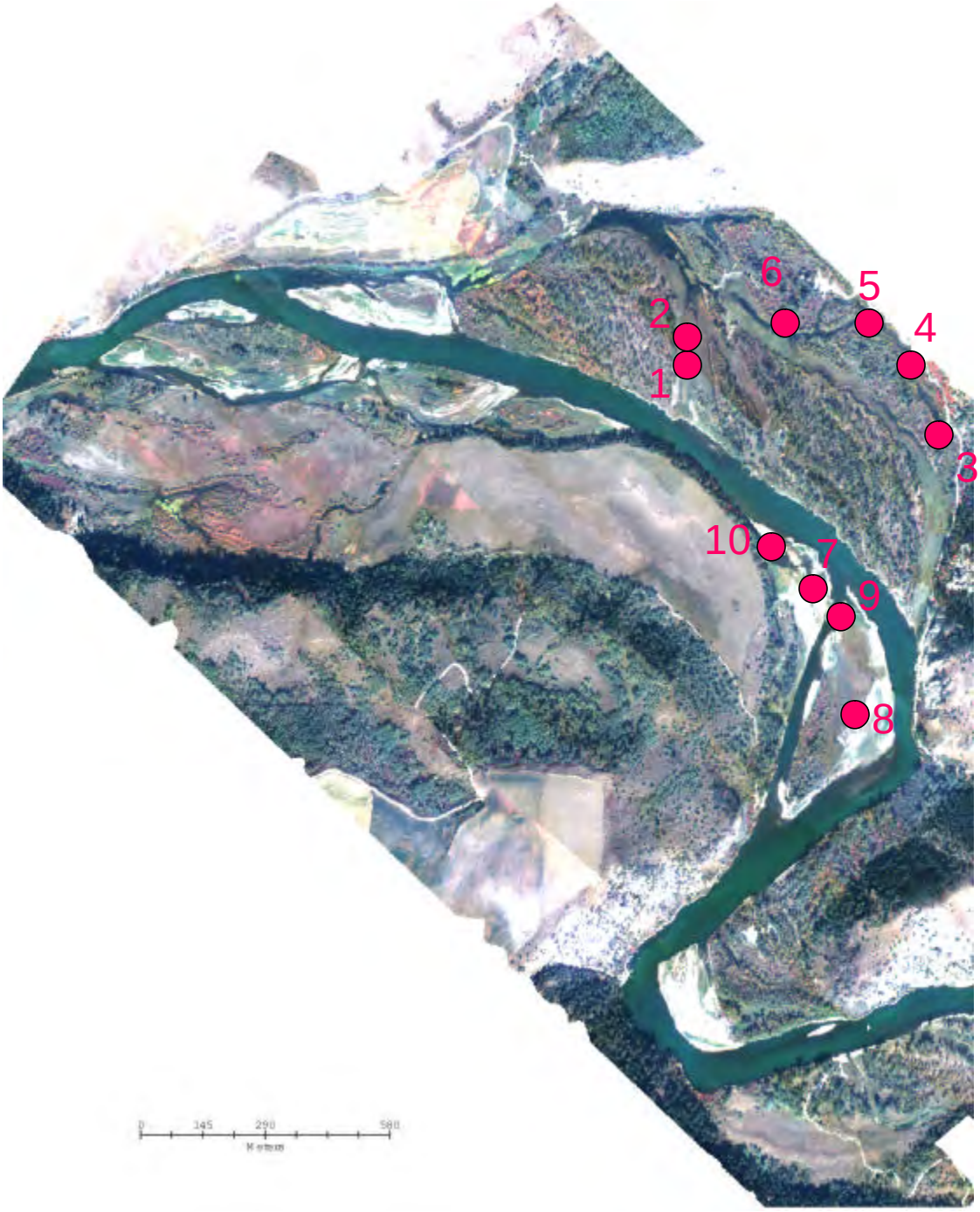

APPENDIX A Figure 14. Temperatures at Thermal Site 1 on the Fisher floodplain Aug 2001 – Nov 2002. Data were recorded every two hours. Circled temperatures were the result of exposure to atmospheric temperatures during low discharge.

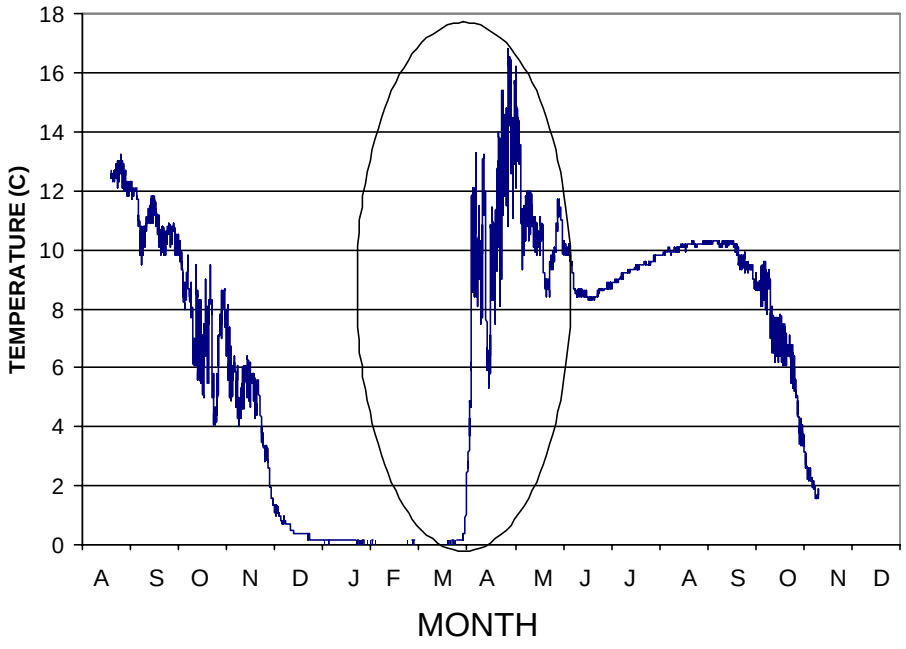

APPENDIX A Figure 15. Temperatures at Thermal Site 2 on the Fisher floodplain Aug 2001 – Nov 2002. Data were recorded every two hours. Circled temperatures were the result of exposure to atmospheric temperatures during low discharge.

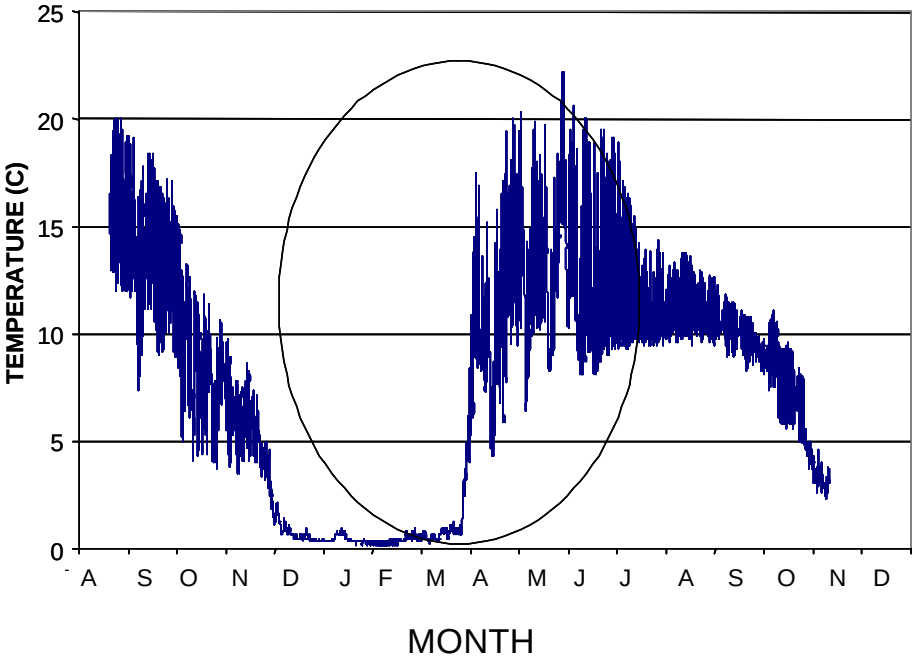

APPENDIX A Figure 16. Temperatures at Thermal Site 3 on the Fisher floodplain Aug 2001 – Nov 2002. Data were recorded every two hours.

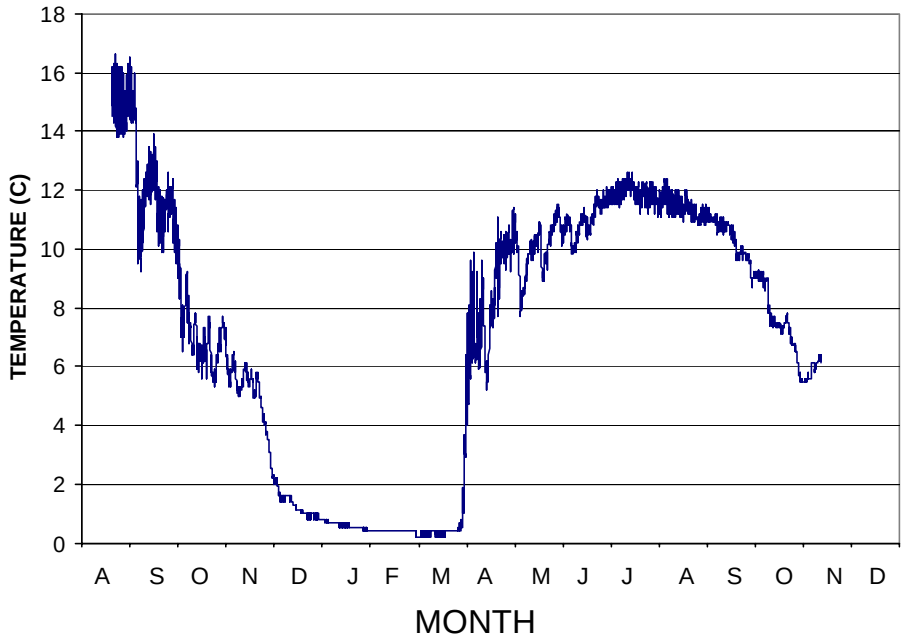

APPENDIX A Figure 17. Temperatures at Thermal Site 4 on the Fisher floodplain Aug 2001 – Nov 2002. Data were recorded every two hours.

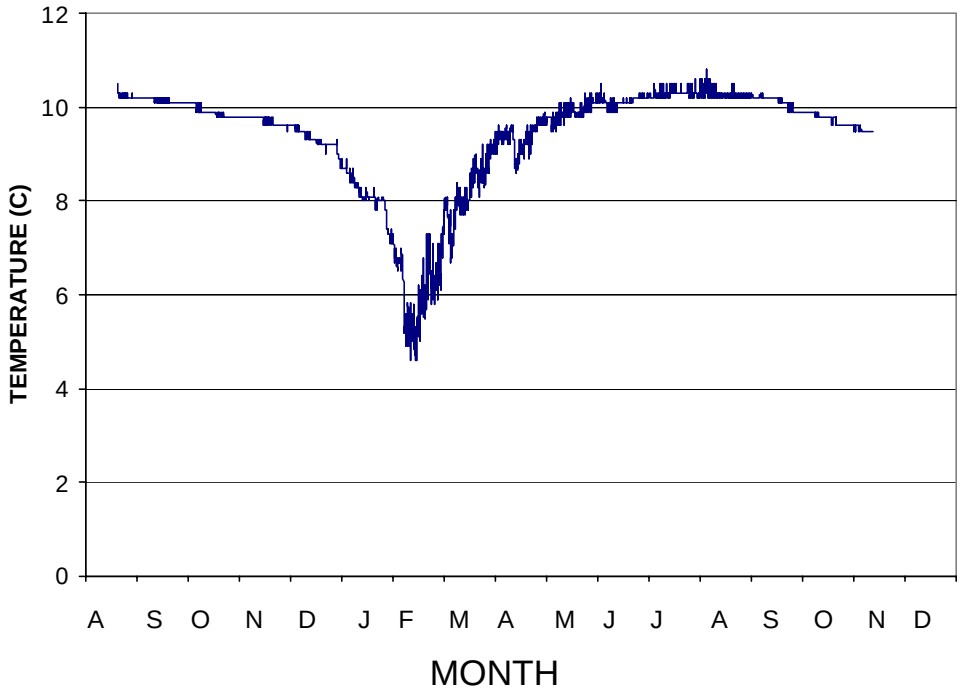

APPENDIX A Figure 18. Temperatures at Thermal Site 5 on the Fisher floodplain Aug 2001 – Nov 2002. Data were recorded every two hours

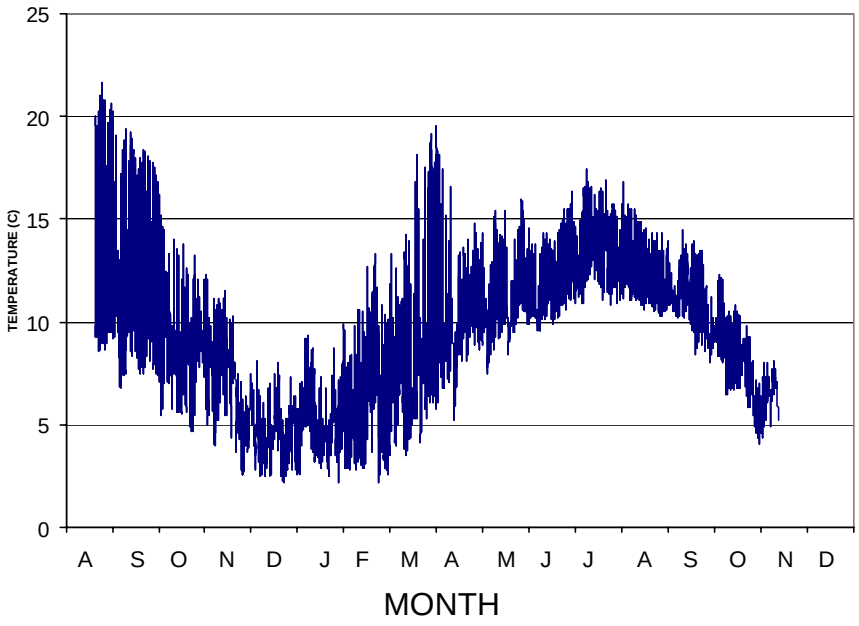

APPENDIX A Figure 19. Temperatures at Thermal Site 6 on the Fisher floodplain Aug 2001 – Nov 2002. Data were recorded every two hours

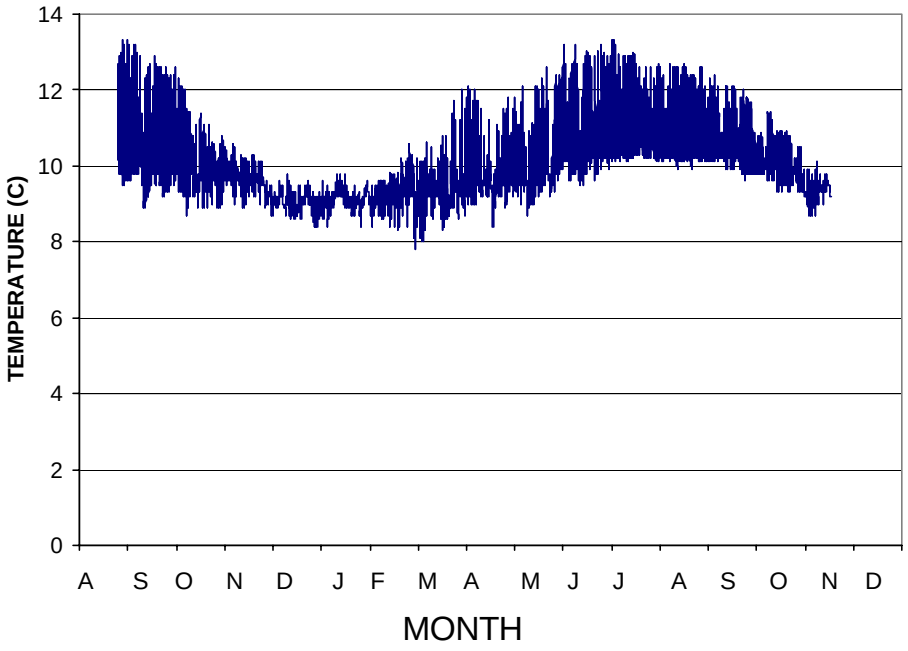

APPENDIX A Figure 20. Temperatures at Thermal Site 7 on the Fisher floodplain Aug 2001 – Nov 2002. Data were recorded every two hours. Circled temperatures were the result of exposure to atmospheric temperatures during low discharge.

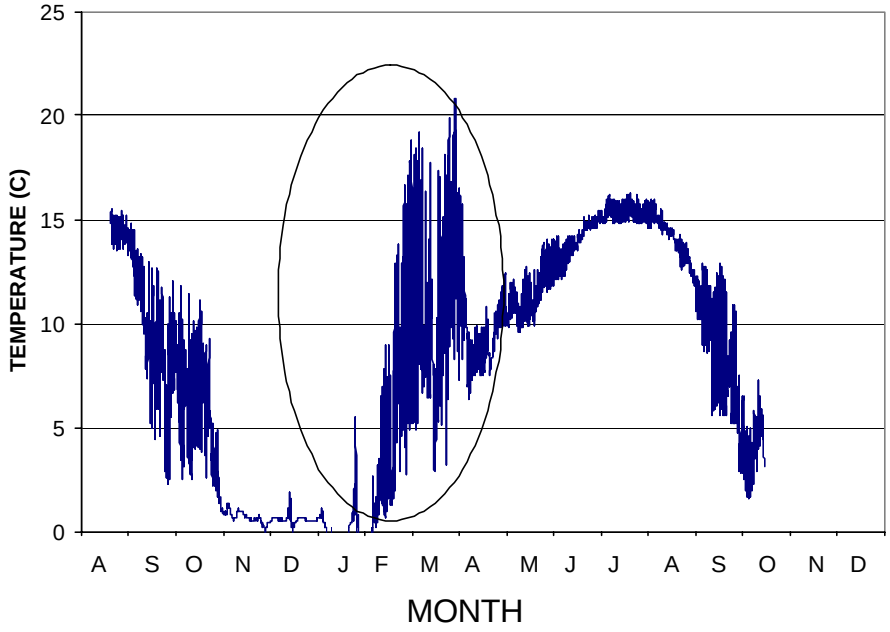

APPENDIX A Figure 21. Temperatures at Thermal Site 8 on the Fisher floodplain Aug 2001 – Nov 2002. Data were recorded every two hours. Circled temperatures were the result of exposure to atmospheric temperatures during low discharge.

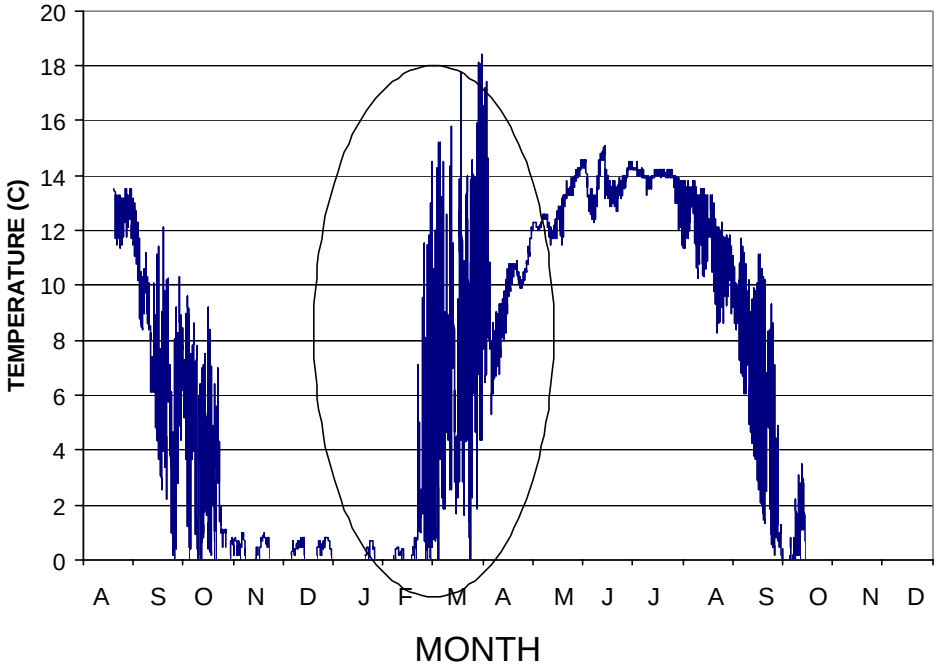

APPENDIX A Figure 22. Temperatures at Thermal Site 9 on the Fisher floodplain Aug 2001 – Nov 2002. Data were recorded every two hours. Circled temperatures were the result of exposure to atmospheric temperatures during low discharge.

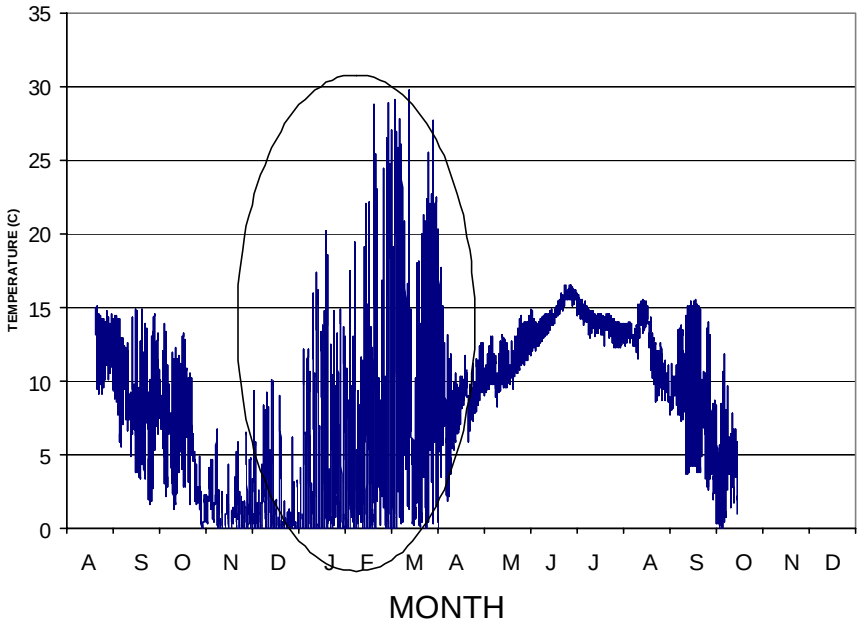

APPENDIX A Figure 23. Temperatures at Thermal Site 10 on the Fisher floodplain Aug 2001 – Nov 2002. Data were recorded every two hours.